Classification of interfacial wetting behavior in binary liquid mixtures

S. Dietrich*
Fachbereich Physik, Bergische Universität Wuppertal, Postfach 10 01 27, D-5600 Wuppertal 1, Federal Republic of Germany

A. Latz
Physik Department, Technische Universität München, Theoretische Physik, James-Franck-Strasse, D-8046 Garching, Federal Republic of Germany
(Received 31 October 1988)

On the basis of both the Blume-Emery-Griffiths model and the Percus-Yevick theory we completely classify the wetting behavior of simple binary liquid mixtures at their liquid-vapor interface. The criteria with respect to the atomic interactions are whether a particular binary liquid mixture fulfills either the sufficient conditions for the absence of a wetting transition, or the necessary conditions for critical wetting, or the necessary conditions either for being wet already at low temperatures or for undergoing a first-order wetting transition upon approaching the critical end point along the triple line. The Percus-Yevick theory enables us to study systematically the dependence of interfacial wetting on the atomic radii of those two types of particles forming the binary liquid mixture. Also as functions of these radii, we determine all those boundaries in the parameter space of the atomic interactions within which the Percus-Yevick theory predicts such bulk phase diagrams as expected for simple binary liquid mixtures.
MS code no. BX3803 1988 PACS number(s): 68.45.Gd, 68.10.−m, 82.65.Dp, 64.10.+h

I. INTRODUCTION

Binary liquid mixtures are formed by two sorts of molecules which we call A and B particles. In the gas phase at high temperatures these particles mix. Upon lowering the temperature, one encounters a phase separation into a gas phase of low density and into a fluid phase of higher density. In both phases the two sorts of molecules remain mixed. A further decrease of temperature finally leads to a phase separation of the fluid into an A-rich- and into a B-rich-liquid phase which can both still coexist with the gas phase.

Figure 1 displays the schematic drawing of the corresponding bulk phase diagram in the space of temperature T and the two chemical potentials μ_A and μ_B of the two sorts of particles. S_1 and S_2 are sheets of first-order phase transitions separating the gas phase from the fluid phase and the A-rich-liquid phase from the B-rich-liquid phase, respectively. S_1 and S_2 are bounded by lines L_1 and L_2, respectively, of second-order phase transitions. S_1 and S_2 intersect at the triple line (TL) of the three-phase coexistence. The intersection between the TL and L_2 forms a critical end point $T_{\rm cep}$.

In general, first-order phase transitions, as they occur, for example, at S_1 and S_2 in the case of binary liquid mixtures, may give rise to *wetting phenomena.* Consider, e.g., the *interface* between the A-rich liquid and the wall of the container enclosing the fluid. Upon approaching S_2 along p_a from the A-rich side by decreasing $\mu_A-\mu_B$ (see Fig. 1), a thin layer of a quasi-B-rich-liquid phase may form at the wall–A-rich-liquid interface. If its thickness diverges by approaching S_2 one has *complete wetting* and the interface is *wet* as soon as S_2 is reached where the B-rich-liquid phase is indeed thermodynamically stable. If a different point of S_2, say at lower temperature, is reached along a different path p_b (see Fig. 1), this thickness may not grow and the wall–A-rich-liquid interface remains *nonwet* on the A-rich side of S_2. Consequently, the A-rich side of S_2 can be divided into a wet and a nonwet region which are separated from each other by a line L_W (see Fig. 1) such that one encounters a *wetting transition* at coexistence, i.e., *on* the A-rich side of S_2, from nonwet to wet by crossing this line along the path p_c (see Fig. 1). If at that wetting transition the thickness of the wetting layer grows continuously to infinity, it is called *critical wetting,* whereas in the case of a discontinuous jump to infinity it is called *first-order wetting.* This discontinuity extends into the one-phase region of the wetting phase by forming a *prewetting line.* A more complete account of the various wetting phenomena is given in Ref. 1, for earlier reviews see Refs. 2–7. An excellent introduction to this subject is given in Ref. 8.

Similarly, one can study the complementary case of the wall–B-rich-liquid interface upon approaching the B-rich side of S_2 or the wall-vapor interface upon approaching S_1 from the vapor side. Thus, binary liquid mixtures offer the opportunities to study the wetting behavior at a wall for different fluid phases of one and the same physical system and to follow the nature of wetting transitions by varying chemical potentials (e.g., along the line L_W in Fig. 1). The general features of these wetting phenomena of binary liquid mixtures at a wall have been discussed in Ref. 9.

Both in theory and experiment, the presence of the wall complicates a precise determination and control of the aforementioned interfacial structures. First, these

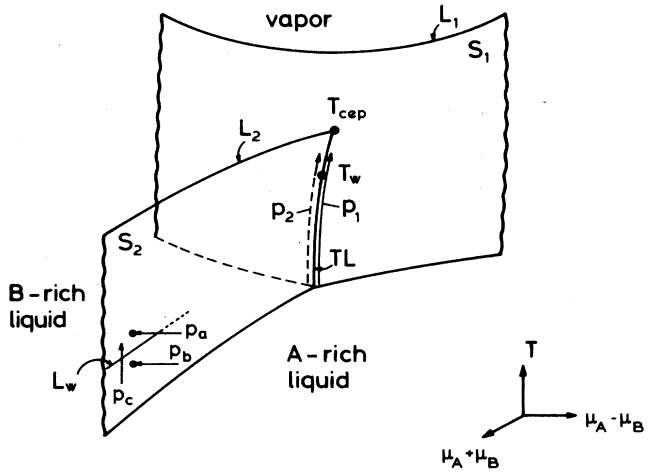

FIG. 1. Schematic bulk phase diagram of a simple binary liquid mixture in the space of temperature T and the chemical potentials μ_A and μ_B of the two sorts of molecules exhibiting the vapor phase and the A-rich- and B-rich-liquid phases which are separated by sheets S_1 and S_2 of first-order phase transitions. Here the solid phase is omitted (see Fig. 2). L_1 and L_2 are lines of second-order phase transitions, TL represents the triple line and T_{cep} is the critical end point. L_W indicates a line of wetting transitions at the container walls, which for reasons of clarity is not continued towards TL. The meaning of the paths p_a, p_b, and p_c is explained in the main text. The path p_1 runs on S_1 along the A-rich side of TL, whereas p_2 runs on S_1 along the B-rich side of TL. For reasons of clarity p_1 and p_2 are taken slightly off TL. T_W indicates an interfacial wetting transition on TL along either p_1 or p_2. If this wetting transition is first order, a prewetting line is attached tangentially to TL at T_W lying on the sheet S_1. Similarly, a prewetting sheet may be attached to L_W. These prewetting singularities are omitted here for reasons of clarity. The interested reader will find them in Fig. 3 of Ref. 9.

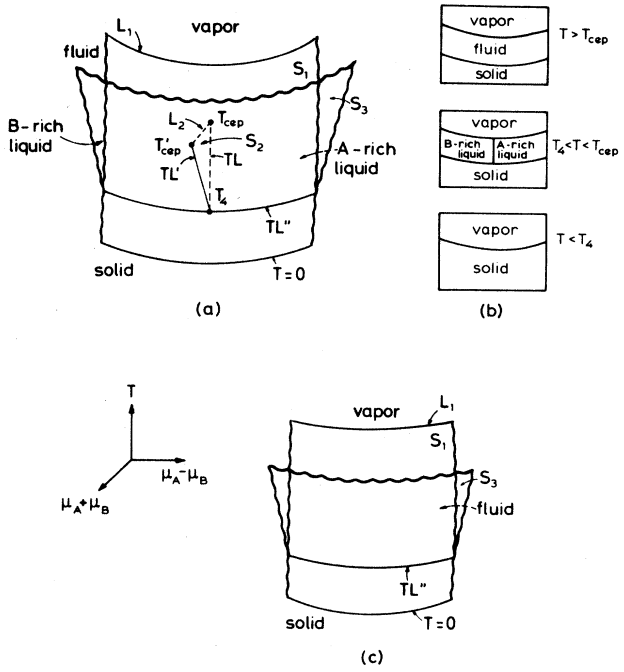

FIG. 2. Schematic bulk phase diagrams of binary liquid mixtures including the solid phase. We use the same notation as in Fig. 1. The presence of the solid phase leads to the melting sheet S_3 which limits the extension of sheet S_2. As a consequence, one finds two additional triple lines: at TL' the A-rich liquid, B-rich liquid, and the solid coexist and along TL'' the liquid, solid, and gas phases coexist. The intersection of TL' and L_2 gives another critical end point T'_{cep}. The intersection of TL and TL' leads to a four-phase coexistence at T_4. (b) represents cuts through the phase diagram (a) at various constant temperatures T. The phase diagram in (c) corresponds to a binary liquid mixture whose sorts of particles differ only slightly so that T_{cep} is so low that it falls below TL''. As a consequence the phase separation into two liquid phases, i.e., S_2, is wiped out. In the limit of identical sorts of particles L_1 and TL'' reduce to straight lines becoming independent of $\mu_A-\mu_B$ and corresponding to the critical point and the triple point, respectively, in a simple one-component system. Wavy boundaries indicate that the corresponding sheets extend beyond them. For reasons of clarity we consider only a single solid phase.

wetting phenomena depend not only on the atomic interactions between the components of the binary liquid mixture, but also on two substrate potentials acting on the A and B particles, respectively.[9] This leads to a substantial enlargement of the relevant parameter space[9] and impedes a detailed comparison between model calculations and experimental data. Second, close to the wall the substrate potentials lead to such a high local pressure (pressure might be associated with $\mu_A+\mu_B$) that one observes density oscillations (for a list of corresponding references see Sec. III B in Ref. 1). These density oscillations signal the formation of a few solidlike layers at the wall. Thus, any realistic calculation should allow for the possibility of solidification—even if one avoids the vicinity of the bulk solid phase (see Fig. 2). However, such theories have only recently started to emerge for simple one-component systems (see Ref. 10 and Sec. VIII A in Ref. 1 for further references). Third, strictly speaking, the wall-liquid interface represents a nonequilibrium situation because the substrate atoms tend to desolve in the liquid. This changes the substrate and it leads to a contamination of the liquid just at the interface of interest.

Recent experiments for wetting of a wall by binary liquid mixtures have been performed by Pohl and Goldburg,[11] Beysens and Estéve,[12] Sigl and Fenzl,[13] and by Franck and co-workers.[14–17] For a discussion of these experiments and further references, see Sec. V E in Ref. 1. There are only a few model calculations for these kinds of wetting phenomena. Most of them deal with short-range atomic interactions,[18–20] which are inappropriate for fluid systems with van der Waals types of interactions. For a discussion of the effect of long-range forces for these wetting transitions see Ref. 9 and Sec. IV C in Ref. 1.

In view of the aforementioned difficulties induced by the presence of a hard wall, it is a particular advantage

that binary liquid mixtures offer the opportunity to study wetting phenomena which involve fluid phases only, i.e., both coexisting bulk phases, which form the interface to be wetted, and the wetting phase itself are fluids. Such wetting phenomena require the coexistence of three fluid phases in the bulk phase diagram, as it is the case along the triple line in Fig. 1. The corresponding spatial structures are displayed in Fig. 3 for a grand canonical ensemble in the absence of gravity. (A discussion of canonical ensembles in the presence of gravity will be given at the end of this introduction.) Although the wetting phenomena depicted in Fig. 3 are conceptually very similar to the wetting of a wall, there are distinct differences.

First, the wetting layer is not formed at a geometrically prescribed boundary but at an *intrinsic* interface, which represents a thermodynamically stable configuration of its own. This gives rise to the notation of *interfacial wetting*.

Second, due to the wetting transition the vapor-fluid interface splits into another vapor-fluid interface and into the liquid-liquid interface [$v|A \rightarrow v|B|A$ in Fig. 3(a)], which *both* exhibit capillary waves. (For comparison the wetting of a wall involves only one fluctuating interface.) Indeed, the location of a first-order wetting transition and its prewetting line are affected by these additional capillary waves. Since fluid mixtures are governed by long-range van der Waals forces, continuous wetting transitions, however, are unaffected by capillary waves. This allows us to treat these interfacial wetting phenomena within mean-field theory (MFT) (see Ref. 21 and Sec. IV C in Ref. 1).

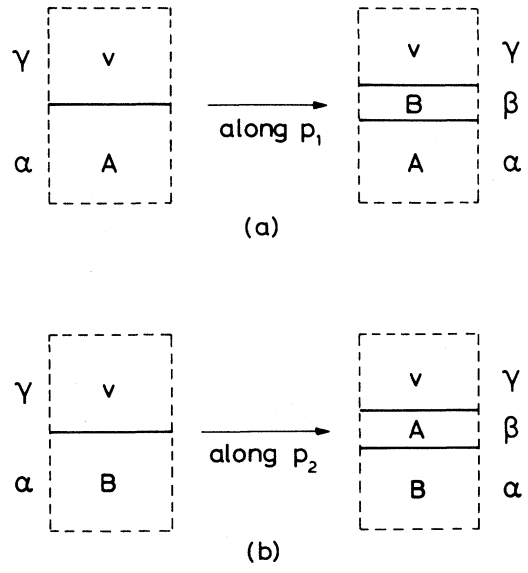

FIG. 3. (a) Interfacial wetting of the vapor–A-rich-liquid interface by the B-rich liquid along the path p_1 given in Fig. 1. (b) Interfacial wetting of the vapor–B-rich-liquid interface by the A-rich liquid along the path p_2 given in Fig. 1. The dashed lines indicate that, as in a grand canonical ensemble, these systems are connected to a reservoir of A and B particles. Thus the spatial location of the $v|A$ and of the $v|B$ interface, respectively, is not fixed. It should be emphasized that, in contrast to many experiments, v denotes the equilibrium vapor phase and not air. The wetted liquid phase is denoted by α, the wetting liquid phase is called β, and the vapor phase is named γ. Along the path p_1 the α phase is A rich and the β phase is B rich, whereas along the path p_2 the α phase is B rich and the β phase is A rich.

Third, the interfacial wetting phenomena only depend on the interactions among the A particles and among the B particles themselves and on the interaction between the A and B particles. Thus, interfacial wetting is characterized by a substantially smaller parameter space than wetting of a wall by a binary liquid mixture, where two additional substrate potentials are relevant. As a consequence, interfacial wetting depends only on those interactions, which determine simultaneously the bulk properties of binary liquid mixtures. Therefore, one might hope that certain features of interfacial wetting phenomena are fixed by the *bulk* properties of the participating phases. Since bulk properties are more easily accessible than surface properties, this would represent an important fact.

First, in experiments there is practically an unlimited number of different binary liquid mixtures. Although there are already numerous experimental studies of interfacial wetting[22–35] (for a discussion of these experiments, see Sec. V D in Ref. 1), they still explore only a very small subset of possible binary liquid mixtures. In order to provide some guidance for a systematic further exploration we classify the possible interfacial wetting behavior of binary liquid mixtures on the basis of their bulk properties. In particular, it would be very interesting to find a system undergoing critical interfacial wetting. Up to now only first-order interfacial wetting transitions have been reported,[23,25,26,28,31,34] but without finding the corresponding prewetting line, which is supposed to be associated with a first-order wetting transition. It should be noted that it was the discovery of an interfacial wetting transition by Moldover and Cahn,[23] which triggered many of the following experimental and theoretical studies of wetting in general; but this particular interfacial wetting transition was induced by adding a third component to a binary liquid mixture and thus occurred, in fact, in a ternary mixture (see Ref. 35). Moreover, one has to keep in mind that in most of the experiments mentioned above, the vapor has been air and not the equilibrium vapor of the binary liquid mixture. Thus, one must be rather cautious by later comparing these experimental data with the case of a pure binary liquid mixture, which is the subject of this paper.

As in the case of the experiments only for a few particular binary liquid mixtures, interfacial wetting has been studied theoretically by seriously taking into account the long-range character of the A-A, A-B, and B-B interactions.[36–38] In these studies both first-order and critical wetting have been found in agreement with general analytic arguments.[9] In all these calculations only the exceptional case of those binary liquid mixtures has been considered, the components of which have equal radii. (There is one study of interfacial wetting with different radii.[39] However, these authors use a square gradient approximation to the free-energy functional, which is inappropriate for systems with van der Waals interactions.)

In this paper we present a systematic study of the influence of different atomic radii on interfacial wetting. This allows us to find general trends for the wetting transition as function of the ratio of the two radii. Since these radii are known rather accurately this presents again some guidance for experimental studies of interfacial wetting. Furthermore, it provides a firm ground for future, more detailed, numerical studies of specific model systems. Here we refrain form such specific calculations in favor of focusing on those properties of interfacial wetting, which can be analyzed for *all* binary liquid mixtures exhibiting a simple bulk phase diagram.

In the present study all explicit calculations for interfacial profiles have been performed for grand canonical ensembles, which correspond to Figs. 1–3. Before we turn to these calculations in the following sections let us comment briefly on how these theoretical results are related to experimental data, which normally stem from closed systems under the influence of gravity.

These systems represent canonical ensembles in which the number of A and B particles, N_A and N_B, the volume V, and temperature T are fixed. The overall densities $\rho_A = N_A/V$ and $\rho_B = N_B/V$ are chosen such that the system is at three-phase coexistence whereby the relative volumina of these phases within V depend on this choice. Upon a change of temperature, these relative volumina are changed but the system remains at three-phase coexistence (unless one phase disappears due to a choice of ρ_A and ρ_B which has not been sufficiently adapted). The bulk values of the densities in the coexisting phases are those which one obtains in a grand canonical ensemble at the triple line in Fig. 1 for that given temperature. Consider now the situation in Fig. 3(a) in which the B-rich liquid wets the vapor–A-rich-liquid interface along the path p_1 in the grand canonical ensemble. Furthermore, suppose now that the mass density of the A-rich liquid is lower than that of the B-rich liquid. In the closed system and below T_W this leads to the configuration in Fig. 4(a). Above T_W the configuration looks like that in Fig. 4(b). Both figures correspond to experimental findings. To the best of our knowledge there are no theoretical calculations which prove that these configurations represent the true thermodynamical equilibrium. Among the questions, which are still unresolved and are not the topic of this paper, are the following: (i) Under which conditions on N_B, V, the shape of the cell, and gravity is the formation of the droplet with a finite contact angle more favorable than a vapor–A-rich-liquid interface only covered by a microscopically thin quasi-B-rich-liquid film? [The latter configuration is supposed to prevail in Fig. 4(a) outside the droplet region of the interface. However, the crossover from the droplet to this microscopically thin B-rich-liquidlike film is unknown.] (ii) Does the vanishing of the contact angle of this droplet signal the wetting transition as obtained by the corresponding grand canonical calculation? This question arises because the thickness l of the wetting layer in Fig. 4(b) is limited by gravity due to the height L, although above T_W l should be infinite. This limitation due to gravity can be described in a grand canonical calculation as a shift of the chemical potentials such that the wetting layer is slightly off the

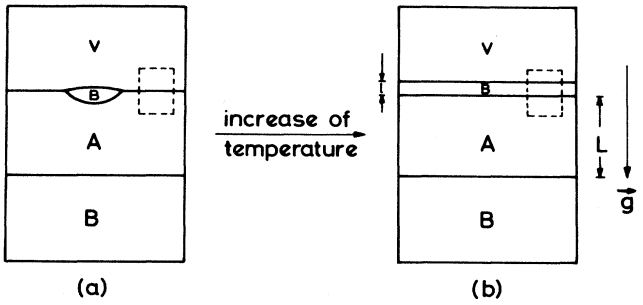

FIG. 4. Interfacial wetting in a closed system with gravity g below (a) and above (b) T_W. Here the wetting phase has the higher mass density. Below T_W a droplet of B-rich liquid with a finite contact angle may be formed at the interface with the vapor, which is not air. Above T_W the contact angle is zero, but the thickness l of the wetting film remains finite due to gravity depending on the height L. After taking into account this effect of gravity by an appropriate shift in the chemical potentials, the local interface structures within the dashed lines are supposed to resemble the corresponding ones in Fig. 3(a) for a grand canonical ensemble without gravity. For further discussions see the main text.

coexistence with the bulk B-rich-liquid phase [see Eq. (3.29) in Ref. 40 and references therein]. Due to this effect the surface tension $\sigma_{v,A}$ between the vapor and the A-rich liquid is less than the sum $\sigma_{v,B}+\sigma_{B,A}$ of the surface tension between the vapor and B-rich liquid and between the two liquid phases. It is unclear how to reconcile this fact with a vanishing contact angle, which requires $\sigma_{v,A}=\sigma_{v,B}+\sigma_{B,A}$.

Furthermore, the thickness l of the wetting layer is limited by the finite number N_B of B particles. This restriction is generic for a canonical system and cannot be described within a grand canonical framework. For L and N_B/V sufficiently large gravity represents the more severe restriction. Since, in this case, gravity can be incorporated into the grand canonical description one can argue that, after taking this correction into account, the interfacial structures, as calculated within a grand canonical ensemble, resemble the local structure of the interface in the canonical system with gravity within the dashed lines in Fig. 4.

If, however, the wetting phase, here taken as to be the B-rich-liquid phase, has the lower mass density, it is more difficult to find the connection between the canonical system with gravity and the grand canonical system without gravity. If the tube of Fig. 4 contains a volume fraction of the B-rich and lighter phase, the equilibrium configuration is given by Fig. 5(a) independent from whether $T<T_W$ or $T>T_W$, because at three-phase coexistence gravity does not allow one to maintain the vapor–A-rich-liquid interface even below T_W. This could only be achieved if the system is always prepared to be just at the boundary of three-phase coexistence but without allowing for the formation of a bulk portion of the B-rich-liquid phase [see Fig. 5(b)] for $T<T_W$. As shown in Fig. 5(c) above T_W a layer of the B-rich-liquid phase forms at the interface with the vapor. Since gravity favors the formation of this layer its thickness is only

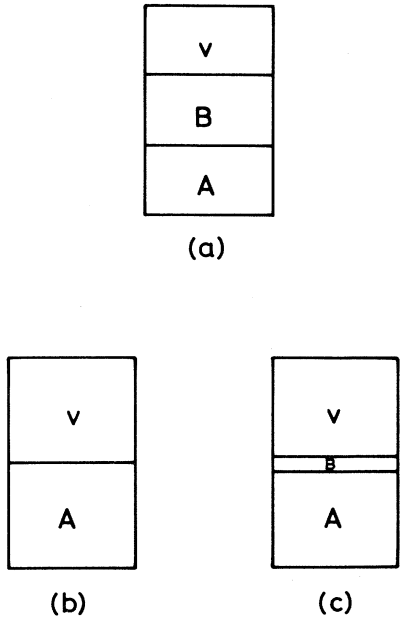

FIG. 5. Interfacial wetting for the case in which in the corresponding grand canonical ensemble the vapor–A-rich-liquid interface is wetted above T_W by the B-rich liquid which happens to be the lighter liquid. The configuration in (a) is independent from T_W, since there is a volume proportional part of the container filled by the B-rich phase. The configurations in (b) and (c) also represent systems at three-phase coexistence but such that there is just no volume part of the B-rich phase in the container. (b) corresponds to $T < T_W$ and in (c) $T > T_W$.

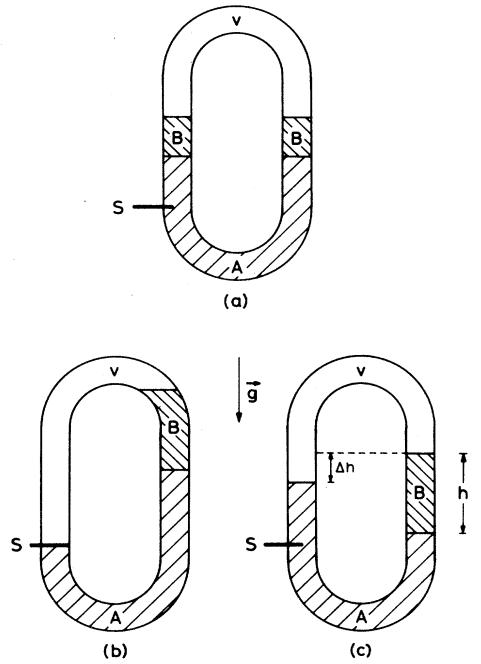

FIG. 6. Binary liquid mixture in a closed U tube at three-phase coexistence (Ref. 41). The A-rich-liquid phase has the higher mass density $\bar{\rho}_A$. The equilibrium configuration is shown in (a). For example, by closing the shutter S and tilting one can prepare the configuration (b). For times less than the diffusion time, which the A and B particles need to restore the configuration (a), (b) represents a new, restricted equilibrium configuration. After opening the shutter S it relaxes to the one in (c). Again, on the time scale mentioned above, this configuration enables one to study the vapor–A-rich-liquid and the vapor–B-rich-liquid interfaces simultaneously. The relative depression is given by $\Delta h/h = 1-\bar{\rho}_B/\bar{\rho}_A$. The potential energy divided by the cross section of the U tube is for (c) higher than for (a) by the amount $g(\bar{\rho}_A-\bar{\rho}_B)h^2\bar{\rho}_B/(4\bar{\rho}_A)$. In order not to lose three-phase coexistence upon a change of temperature, the relative volumina of the liquid phases should roughly correspond to the overall critical composition at T_{cep}. This restriction may cause the A-rich–B-rich-liquid interface to come close to the lower bow of the tube. In such a case the aforementioned gravitational instability leads to a sudden change from (c) to (a). This can be avoided by choosing different cross sections for the right and left wing of the U tube, respectively, which leads back to a (meta)stable configuration similar to that in (c).

limited by the number N_B of B particles. This way one can detect whether the vapor–A-rich-liquid phase undergoes a wetting transition or not, even if the wetting phase is lighter. However, since, in this case, the limiting factor for the thickness of the wetting film is given only by N_B, there is no obvious connection between the details of these interfacial structures and those calculated in a grand canonical ensemble. Finally, let us note here that we do not consider those interfacial structures which are induced by a mass density inversion between the A-rich and the B-rich bulk liquids upon a change of temperature as investigated in Refs. 27 and 30.

Figure 6 shows the possibility to maintain the interface between the vapor and the heavier liquid even in the presence of the lighter liquid by using a closed U tube.[41] This configuration offers the opportunity to study both the vapor–A-rich-liquid and the vapor–B-rich-liquid interface simultaneously. Also in this case, the influence of gravity and of the fixed numbers of A and B particles on the interfacial structures above and below T_W deserve further studies. In addition, the dynamics for building up these equilibrium interfacial structures by diffusion requires a detailed analysis.

It was the purpose of the latter parts of the Introduction to stress the importance of gravity and the fixed number of particles for comparing experimental data with theoretical calculations of interfacial properties in grand canonical ensembles. Let us now turn to these calculations which are prerequisites for solving these aforementioned difficulties.

II. EFFECTIVE INTERFACE POTENTIAL

It is our aim to determine the dependence of interfacial wetting on the details of the microscopic interaction potentials between the A and B particles. For a specific system this question could be addressed by a numerical simulation. Up to now, however, this technique has been applied only either to the wetting of a wall or to simple

model systems with short-range forces (see Ref. 1 for references). But none of these simulations have seriously taken into account the long-range part of the interaction potentials, which are crucial for wetting phenomena in fluid systems.

Here we resort to the density functional theory which has proven to be a successful analytical method for the description of inhomogeneous simple fluids. (For a review see Ref. 42, for applications to wetting phenomena see Refs. 1 and 7.) Within this approach the long-range part of the van der Waals interactions can fully be taken into account and the whole class of possible physical systems can be scanned.

Our starting point is the variational grand canonical free-energy functional (its derivation and status are discussed in Appendix A)

$$\Omega[\rho_i(\mathbf{r});T,\mu_i]=\int d^3r\, f_h(\rho_i(\mathbf{r}),T)+\tfrac{1}{2}\sum_{i,j}\int d^3r\int d^3r'\,\tilde{w}_{ij}(|\mathbf{r}-\mathbf{r}'|)\rho_i(\mathbf{r})\rho_j(\mathbf{r}')-\sum_i \mu_i\int d^3r\,\rho_i(\mathbf{r})\ . \tag{2.1}$$

Ω gives the grand canonical free energy for a given configuration of inhomogeneous densities $\rho_i(\mathbf{r})$ with $i=A$ and B, The equilibrium densities $\rho_{0,i}(\mathbf{r};T,\mu_i)$ minimize Ω and they yield the grand canonical potential $\Omega_0(T,V,\mu_i)$. $f_h(\rho_i,T)$ is a suitably chosen Helmholtz free-energy density for a spatially homogeneous binary liquid mixture (see below and Appendices A and B). In this section its specific form does not matter. $\tilde{w}_{AA}$, $\tilde{w}_{BB}$, and $\tilde{w}_{AB}$ are derived from the pair potentials w_{AA}, w_{BB}, and w_{AB} [see Eqs. (A1) and (A3)] between the particles, which are modified at short distances by suitable reference potentials $w_{r,ij}$ such that the potentials $\tilde{w}_{ij}$ remain finite [see Eq. (A26) and Appendix B]. In accordance with Fig. 3 we impose boundary conditions such that for $z\to+\infty$, $\rho_{0,i}(z)$ approaches the bulk values of the vapor phase. Depending on whether we consider path p_1 or p_2, $\rho_{0,i}(z\to-\infty)$ is given by the bulk values of the A-rich- or B-rich-liquid phase. z denotes the direction orthogonal to the interface.

Equation (2.1) gives a microscopic description of interfacial structures. The interfacial wetting transitions we are concerned with are critical phenomena which connect two and three spatial dimensions. In fluids the long-range van der Waals forces cause the upper critical bulk dimension for the corresponding fluctuations to be less than three.[21] Therefore, Eq. (2.1) will yield reliable results for wetting transitions although it is a mean-field theory. The local-density approximation for the reference free energy is appropriate for interfacial structures between *fluid* phases, because they are monotonic and smooth. This is in contrast to interfacial structures close to a solid wall, where the sharp density variation gives rise to density oscillations which are not captured by the local-density approximation. However, a more serious drawback of this approximation even in our case is that the variational functional in Eq. (2.1) does not allow for the formation of solid phases. Thus, we must modify our results at low temperatures in order to take into account the actual structure of the bulk phase diagram as shown in Fig. 2.

Let us now describe the interfacial wetting behavior depicted in Fig. 3. For density configurations with the aforementioned boundary conditions the free-energy functional in Eq. (2.1) splits into a bulk contribution and into a surface contribution,

$$\Omega[\rho_i(\mathbf{r});T,\mu_i]=V\Omega_b(T,\mu_i)+A\,\Omega_s[\rho_i(\mathbf{r});T,\mu_i]\ . \tag{2.2}$$

Since we are at α-γ coexistence, i.e., on S_1 in Fig. 1, we have

$$\Omega_b(T,\mu_i)=\Omega(\rho_{i,\alpha};T,\mu_i)/V=\Omega(\rho_{i,\gamma};T,\mu_i)/V\ , \tag{2.3}$$

where $\rho_{i,\alpha}$ and $\rho_{i,\gamma}$ are the equilibrium bulk densities in the α and γ phase, respectively. (Here we drop the index 0 which has been used in Appendix A to denote equilibrium values.) In this grand canonical ensemble the position of the interface of area A within the volume V is not fixed; Eq. (2.2) is independent from this interface position.

For the bulk free-energy density we have [see Eq. (2.1)]

$$\Omega(\rho_{i,\kappa};T,\mu_i)/V=f_h(\rho_{i,\kappa},T)-\tfrac{1}{2}\sum_{i,j}\hat{w}_{ij}\rho_{i,\kappa}\rho_{j,\kappa}-\sum_i\mu_i\rho_{i,\kappa}=:\Omega_\kappa\ . \tag{2.4}$$

Along the triple line these functions are equal to each other for $\kappa=\alpha$, β, and γ. But here we always have $\Omega_\alpha=\Omega_\gamma=\Omega_b$. In Eq. (2.4) we have introduced the total strength of the (modified) interaction potentials $\tilde{w}_{ij}$:[43]

$$\hat{w}_{ij}=-\int d^3r\,\tilde{w}_{ij}(\mathbf{r})>0\ . \tag{2.5}$$

The surface tension between the α and γ phase is the minimum value of Ω_s:

$$\sigma_{\alpha,\gamma}(T,\mu_i)=\min_{\rho_i(\mathbf{r})}\Omega_s[\rho_i(\mathbf{r});T,\mu_i]=\min_l\Omega_s(l,T,\mu_i)=\Omega_s(l_0,T,\mu_i)\ . \tag{2.6}$$

Here we have introduced the *effective interface potential* $\Omega_s(l,T,\mu_i)$, which is the surface free energy per area under the restriction that at the α-γ interface a wetting film with thickness l of the β-like phase is formed (see Ref. 1). The actual equilibrium thickness $l_0(T,\mu_i)$ minimizes $\Omega_s(l,T,\mu_i)$. The importance of the effective interface potential is due to the fact that its asymptotic behavior for large l determines the wetting behavior of the corresponding system (see Fig. 3.2 in Ref. 1). In the presence of long-range interactions, as in our case of interfacial wetting in binary liquid mixtures governed by nonretarded van der Waals forces, one finds[1,9,40]

$$\Omega_s(l,T,\mu_i)=l(\Omega_\beta-\Omega_\gamma)+\sigma_{\alpha,\beta}+\sigma_{\beta,\gamma}+\omega(l)\ . \tag{2.7}$$

$\sigma_{\alpha,\beta}$ is the surface tension between the two liquid phases and $\sigma_{\beta,\gamma}$ is the surface tension between the wetting phase

(in the absence of the α phase) and the vapor. In Eq. (2.7) both $\sigma_{\alpha,\beta}$ and $\sigma_{\beta,\gamma}$ are evaluated at the triple line. If the β phase wets the α-γ interface $l_0=\infty$ and

$$\Omega_s(l_0)=\sigma_{\alpha,\gamma}=\sigma_{\alpha,\beta}+\sigma_{\beta,\gamma} ;$$

otherwise $l_0<\infty$ and $\sigma_{\alpha,\gamma}<\sigma_{\alpha,\beta}+\sigma_{\beta,\gamma}$. Due to the first term in Eq. (2.7), which is due to deviations from the triple line on S_1 and which describes complete interfacial wetting (see Sec. III in Ref. 40), it is evident that wetting can only occur on the triple line, where $\Omega_\beta=\Omega_\gamma$. Otherwise,

$$\Omega_\beta(\rho_{i,\beta};T,\mu_i)>\Omega_\gamma ,$$

because $\rho_{i,\beta}$ are taken as those densities of the β phase at the triple line but T and μ_i have values where the β phase is thermodynamically unstable. Here we do not pursue this further (see Ref. 40) but stay on the triple line. There the wetting behavior depends on $\omega(l)$, which is the correction to the surface free energies due to the finite thickness of l. For large l one has[9]

$$\omega(l)=al^{-2}+bl^{-3}+\cdots . \tag{2.8}$$

The coefficient a, which is also known as Hamaker constant,[44] depends only on the temperature, because for a given temperature the chemical potentials are fixed by the condition to be on the triple line. The Hamaker constant can be expressed in terms of experimental data for the dielectric functions of the fluids and thus one can achieve a good fit for the thickness of wetting films. (For the case of wetting a wall by a one-component fluid, see, e.g., Ref. 45, for the case of interfacial wetting see the attempts by Law.[46,47]) Here, however, we strive for a first-principle calculation of the Hamaker constant on the basis of statistical mechanisms which allows us to deduce trends in the wetting behavior as function of the molecular structure of the particles forming the binary liquid mixture. From Ref. 9 we have:

$$\begin{aligned} a(T)=&\tfrac{1}{8}(Q_\alpha-Q_\beta)(Q_\beta-Q_\gamma)\\ &\times[(1+\tilde{\lambda}_{\alpha\beta})(1+\tilde{\lambda}_{\beta\gamma})t_{3,AA}\\ &+(1-\tilde{\lambda}_{\alpha\beta})(1-\tilde{\lambda}_{\beta\gamma})t_{3,BB}+2(1-\tilde{\lambda}_{\alpha\beta}\tilde{\lambda}_{\beta\gamma})t_{3,AB}] \end{aligned} \tag{2.9}$$

with

$$\tilde{\lambda}_{\alpha\beta}=(M_\alpha-M_\beta)/(Q_\alpha-Q_\beta) \tag{2.10}$$

and

$$\tilde{\lambda}_{\beta\gamma}=(M_\beta-M_\gamma)/(Q_\beta-Q_\gamma) . \tag{2.11}$$

Here M_κ and Q_κ are suitable combinations of *bulk* densities for the various phases at the triple line corresponding to the concentration difference and the overall number density

$$M=\rho_A-\rho_B \tag{2.12}$$

and

$$Q=\rho_A+\rho_B . \tag{2.13}$$

The conjugate fields to M and Q are

$$H=\tfrac{1}{2}(\mu_A-\mu_B) \tag{2.14}$$

and

$$\Delta=-\tfrac{1}{2}(\mu_A+\mu_B) , \tag{2.15}$$

respectively. $t_{3,ij}$ are the leading coefficients in the expansion of the partly integrated interaction potentials $\bar{w}_{ij}$:

$$\begin{aligned} t_{ij}(z)&=\int_z^\infty dz'\int d^2r\,\bar{w}_{ij}((r^2+z'^2)^{1/2})\\ &=-(t_{3,ij}z^{-3}+t_{4,ij}z^{-4}+\cdots) . \end{aligned} \tag{2.16}$$

The higher-order coefficients in the effective interface potential [Eq. (2.8)] have, at least approximately, a similar structure (see Refs. 1 and 9).

For the following reason, in this paper, we restrict our discussion to the temperature dependence of $a(T)$. The expression in Eq. (2.9) has been first derived within the so-called sharp-kink approximation in which Eq. (2.1) is minimized in the subspace of piecewise constant density functions.[9] Later it turned out that Eq. (2.9) remains unchanged if one allows for density profiles which vary smoothly on the scale of the bulk correlation lengths at the emerging α-β and β-γ interfaces.[40] There is even evidence that Eq. (2.9) is *exact*,[1] which means it can be derived from Eq. (2.1). Therefore, the precision of our following discussion is *only* limited by the accuracy with which the density functional in Eq. (2.1) predicts the *bulk densities* of binary liquid mixtures for given interaction potentials.

The temperature dependence of $\mathrm{sgn}[a(T)]$ allows us to draw the following conclusions (compare Fig. 3.2 in Ref. 1).

(i) $a(T)<0$ for all T: This means that $l=\infty$ is always at least a local maximum of $\Omega_s(l)$. Thus, it never can be its global minimum. Therefore, in this case, there is no wetting transition at all.

(ii) $a(T)>0$ for all T: This means that $l=\infty$ is always at least a local minimum of $\Omega_s(l)$. If it happens to be its global one for all T, the α-γ interface is wet for all T. Otherwise, due to higher-order terms in $\omega(l)$, there will be a first-order wetting transition at $T_W<T_{\mathrm{cep}}$.

(iii) $a(T)<0$ for low temperatures and $a(T_{\mathrm{cep}})\geq 0$: In this case, the α-γ interface is not wet at low temperatures. Furthermore, there is a temperature $T_W<T_{\mathrm{cep}}$ such that $a(T\geq T_W)\geq 0$, i.e., that $l=\infty$ is at least a local minimum for $T\geq T_W$. This fulfills the necessary conditions for critical wetting. [If $b(T_W)>0$, the sufficient condition for critical wetting is also fulfilled, provided it is not spoiled by terms in $\omega(l)$ of still higher order.] If critical wetting does occur, $a(T_W)=0$ is an exact, implicit equation for the wetting transition temperature.

These are the three classes of interfacial wetting behavior mentioned in the Abstract. In the remaining parts of the paper we determine which binary liquid mixture falls either in class (i), (ii), or (iii).

For that purpose we determine $a(T)$ for low temperatures and close to T_{cep}. [We assume that $a(T)$ has at

most one zero and that all bulk densities decrease monotonically upon an increase of temperature. The latter property is fulfilled for the models we shall consider in Secs. III and IV.] Since $a(T)=a_0(Q_\alpha-Q_\beta)$ vanishes at $T_{\rm cep}$, the necessary condition $a(T_{\rm cep})=0^+$ for wetting depends on the sign of $a_0(T_{\rm cep})\neq 0$ and on the sign of $Q_\alpha-Q_\beta$, which according to our remark above, does *not* depend on temperature. Consequently, we have to distinguish four cases for the condition $a(T_{\rm cep})=0^+$:

$$\text{(I)}\quad Q_\alpha>Q_\beta \text{ and } M_\alpha>M_\beta\text{: } \bar{t}_{3,AA}>E_B\ , \tag{2.17}$$

$$\text{(II)}\quad Q_\alpha<Q_\beta \text{ and } M_\alpha<M_\beta\text{: } \bar{t}_{3,AA}<E_B\ , \tag{2.18}$$

$$\text{(III)}\quad Q_\alpha>Q_\beta \text{ and } M_\alpha<M_\beta\text{: } \bar{t}_{3,BB}>E_A\ , \tag{2.19}$$

$$\text{(IV)}\quad Q_\alpha<Q_\beta \text{ and } M_\alpha>M_\beta\text{: } \bar{t}_{3,BB}<E_A\ . \tag{2.20}$$

Here we have used the notation

$$\bar{t}_{3,ij}=t_{3,ij}/t_{3,AB}\ , \tag{2.21}$$

$$E_B=-[(1+\lambda_{\alpha\beta})(1+\lambda_{\beta\gamma})]^{-1}\times[(1-\lambda_{\alpha\beta})(1-\lambda_{\beta\gamma})\bar{t}_{3,BB}+2(1-\lambda_{\alpha\beta}\lambda_{\beta\gamma})]\ , \tag{2.22a}$$

and

$$E_A=-[(1-\lambda_{\alpha\beta})(1-\lambda_{\beta\gamma})]^{-1}\times[(1+\lambda_{\alpha\beta})(1+\lambda_{\beta\gamma})\bar{t}_{3,AA}+2(1-\lambda_{\alpha\beta}\lambda_{\beta\gamma})]\ . \tag{2.22b}$$

In Eqs. (2.21), (2.22a), and (2.22b) we have evaluated the functions $\tilde{\lambda}_{\kappa\kappa'}$ at $T_{\rm cep}$:

$$\lambda_{\kappa\kappa'}=\tilde{\lambda}_{\kappa\kappa'}(T=T_{\rm cep})\ . \tag{2.23}$$

Similarly, in Eqs. (2.17)–(2.20) the various inequalities between the densities Q_α, Q_β, M_α, and M_β should involve these densities just slightly below $T_{\rm cep}$. However, as already noted above, these inequalities are valid independently from temperature.

Note that $\tilde{\lambda}_{\alpha\beta}=\tilde{\lambda}_{\beta\alpha}$ and that therefore this is the same function both along path p_1 and p_2 (see Fig. 1). $\tilde{\lambda}_{\beta\gamma}$, however, is a different function along p_1 and along p_2. But since at $T_{\rm cep}$ the difference between the A-rich- and B-rich-liquid phase is gone, $\lambda_{\beta\gamma}$ is again independent from the path. Therefore, both E_A and E_B are independent from the path. Only the fact, which of the four cases in Eqs. (2.17)–(2.21) applies, depends on the choice of the path along the triple line.

Finally, let us note that in the derivation of Eqs. (2.17)–(2.20) we have used the fact that $1\pm\lambda_{\beta\gamma}>0$. This is fulfilled due to $\rho_{A,\beta}>\rho_{A,\gamma}$ and $\rho_{B,\beta}>\rho_{B,\gamma}$, because β is a liquid phase and γ the gas phase; similarly $Q_\beta-Q_\gamma>0$. The cases I and II correspond to $\lambda_{\alpha\beta}>0$, whereas the cases III and IV belong to $\lambda_{\alpha\beta}<0$.

If Eqs. (2.17)–(2.20) are fulfilled, the α-γ interface is wet at least close to $T_{\rm cep}$, provided that $l=\infty$ is not only a local but also the global minimum of the effective interface potential. For a wetting transition to occur, $a(T_4)$ must be negative [see Fig. 2(a)]. Within our model [Eq. (2.1)] there is no solid phase. Therefore, we must stop to consider our formulas for $T\le T_4$ without knowing T_4 explicitly. [We assume that $T_{\rm cep}>T_4$, which means that we do not consider the case in Fig. 2(c).] We do know, however, that upon lowering the temperature the concentration of A particles in the B-rich-liquid phase and the concentration of B particles in the A-rich-liquid phase decrease. We now assume that T_4 is sufficiently low so that we have

$$\left.\begin{aligned}&\rho_{A,\alpha}\simeq\rho_A^{(0)},\rho_{B,\alpha}\simeq 0\\&\rho_{A,\beta}\simeq 0,\rho_{B,\beta}\simeq\rho_B^{(0)}\end{aligned}\right\}\ \text{at } T_4 \text{ on } p_1\ , \tag{2.24}$$

$$\left.\begin{aligned}&\rho_{A,\alpha}\simeq 0,\rho_{B,\alpha}\simeq\rho_B^{(0)}\\&\rho_{A,\beta}\simeq\rho_A^{(0)},\rho_{B,\beta}\simeq 0\end{aligned}\right\}\ \text{at } T_4 \text{ on } p_2\ , \tag{2.25}$$

and

$$\rho_{A,\gamma}\simeq 0,\rho_{B,\gamma}\simeq 0 \text{ at } T_4\ . \tag{2.26}$$

$\rho_A^{(0)}$ and $\rho_B^{(0)}$ represent the densities of the one-component A fluid and of the one-component B fluid at their corresponding triple points. Thus, we obtain

$$a(T_4)\simeq-\tfrac{1}{2}\rho_B^{(0)}(\rho_B^{(0)}t_{3,BB}-\rho_A^{(0)}t_{3,AB}) \text{ on } p_1 \tag{2.27}$$

and

$$a(T_4)\simeq-\tfrac{1}{2}\rho_A^{(0)}(\rho_A^{(0)}t_{3,AA}-\rho_B^{(0)}t_{3,AB}) \text{ on } p_2\ . \tag{2.28}$$

$\rho_A^{(0)}$ and $\rho_B^{(0)}$ depend in a complicated way on $\hat{w}_{AA}$ and $\hat{w}_{BB}$, respectively, and on the sizes of the particles. We now assume that in a dense fluid its density is mainly determined by the repulsive part of the interaction potential. This means that the ratio $\rho_A^{(0)}/\rho_B^{(0)}$ depends only weakly on $\hat{w}_{AA}$ and $\hat{w}_{BB}$ so that

$$\rho_A^{(0)}/\rho_B^{(0)}\simeq(R_B^{(0)}/R_A^{(0)})^3\ , \tag{2.29}$$

where $R_A^{(0)}$ and $R_B^{(0)}$ are the diameters (see Appendix B) of the A particles and of the B particles, respectively. Thus the condition $a(T_4)<0$ for the α-β interface to be nonwet at low temperatures takes on the following form:

$$\bar{t}_{3,BB}>r_0^3 \text{ along } p_1 \tag{2.30}$$

and

$$\bar{t}_{3,AA}>r_0^{-3} \text{ along } p_2\ . \tag{2.31}$$

$r_0=R_B^{(0)}/R_A^{(0)}$ denotes the ratio of the diameters.

Equations (2.17)–(2.22) and Eqs. (2.30) and (2.31) show that the various wetting properties (i)–(iii) depend on $\bar{t}_{3,AA}$, $\bar{t}_{3,BB}$, r_0, $\lambda_{\alpha\beta}$, and $\lambda_{\beta\gamma}$. Since $\lambda_{\alpha\beta}$ and $\lambda_{\beta\gamma}$ are ratios of bulk densities evaluated at $T_{\rm cep}$, they depend only on the following arguments (see below):

$$\lambda_{\kappa\kappa'}=\lambda_{\kappa\kappa'}(\bar{w}_{AA},\bar{w}_{BB},r_0)\ , \tag{2.32}$$

where

$$\bar{w}_{ij}=\hat{w}_{ij}/\hat{w}_{AB}\ . \tag{2.33}$$

Therefore, we are left with a five-dimensional parameter space spanned by $\bar{t}_{3,AA}$, $\bar{t}_{3,BB}$, $\bar{w}_{AA}$, $\bar{w}_{BB}$, and r_0. Strictly speaking, these quantities are independent from each oth-

er. In practice, however, they are correlated with each other. A typical form for $\bar{w}_{ij}(\mathbf{r})$ is (see Appendix B)

$$\bar{w}_{ij}(\mathbf{r})=\begin{cases}4\epsilon_{ij}[(\sigma_{ij}/r)^{12}-(\sigma_{ij}/r)^{6}] & \text{for } r/\sigma_{ij}\geq 2^{1/6}\ ,\\ -\epsilon_{ij} & \text{for } r/\sigma_{ij}\leq 2^{1/6}\ ,\end{cases} \tag{2.34}$$

where $\sigma_{AA}=:R_A^{(0)}$, $\sigma_{BB}=:R_B^{(0)}$, and $\sigma_{AB}=(\sigma_{AA}+\sigma_{BB})/2$. With this form one finds[9]

$$\bar{t}_{3,AA}=\frac{8}{(1+r_0)^3}\bar{w}_{AA} \tag{2.35}$$

and

$$\bar{t}_{3,BB}=\frac{8r_0^3}{(1+r_0)^3}\bar{w}_{BB}\ . \tag{2.36}$$

With these two relations the relevant parameter space is reduced from five to three dimensions: $\bar{w}_{AA}$, $\bar{w}_{BB}$, and r_0. On the other hand, the bulk quantities depend on $\hat{w}_{AA}$, $\hat{w}_{BB}$, $\hat{w}_{AB}$, $R_A^{(0)}$, and $R_B^{(0)}$. However, once one has used, say, $\hat{w}_{AB}$ as scale for the temperature and the two chemical potentials and, say, $R_A^{(0)}$ as scale for the two number densities, one is left with the identical parameter space $\bar{w}_{AA}$, $\bar{w}_{BB}$, and r_0 as above. [These arguments already entered into Eq. (2.32).]

Thus, our considerations show that, within our (reasonable) approximations, those three parameters, which characterize the bulk quantities of a given binary liquid mixture, determine via a complicated, implicit relationship uniquely its wetting behavior with respect to the categories (i)–(iii) given above. In other words, the bulk properties of binary liquid mixtures allow one to categorize their interfacial wetting behavior. This surprising result can only hold for *interfacial wetting*. In the case of wetting at a wall, there is no chance to eliminate the substrate potential as a relevant parameter in favor of characteristics of the adsorbate-adsorbate interactions.

Thus, the procedure we shall pursue in the following sections is obvious. After choosing a particular form of the reference free energy f_h [Eq. (2.1)] we first explore all those parts of this three-dimensional parameter space, in which the corresponding binary liquid mixtures exhibit a simple bulk phase diagram. Second, we use Eqs. (2.17)–(2.22), (2.30) and (2.31) in conjunction with Eqs. (2.35) and (2.36) in order to categorize within this parameter space the corresponding interfacial wetting behavior.

This wetting behavior depends, of course, on the path along which $T_{\rm cep}$ is reached. Along the path p_1 (see Fig. 1) the α phase is A rich and the β phase is B rich. Consequently, $M_\alpha=\rho_{A,\alpha}-\rho_{B,\alpha}$ is positive and $M_\beta=\rho_{A,\beta}-\rho_{B,\beta}$ is negative so that $M_\alpha>M_\beta$. Similarly along p_2 we have $M_\alpha<M_\beta$. This means that along p_1 we have to consider only cases I and IV [Eqs. (2.17) and (2.20)], whereas along p_2 only cases II and III [Eqs. (2.18) and (2.19)] are relevant. This means that along p_1, $\lambda_{\alpha\beta}\gtrless 0$ corresponds to $Q_\alpha\gtrless Q_\beta$, whereas along p_2, $\lambda_{\alpha\beta}\gtrless 0$ corresponds to $Q_\alpha\lessgtr Q_\beta$.

III. INTERFACIAL WETTING IN THE BLUME-EMERY-GRIFFITHS (BEG) MODEL

In this section we consider binary liquid mixtures which consist of particles having all the same size. As the reference free energy we choose [see Eqs. (2.1), (2.12), and (2.13)]

$$f_h(\rho_i,T)=\sqrt{2}R_A^{-3}k_BT\left[\tfrac{1}{2}(\bar{Q}+\bar{M})\ln[(\bar{Q}+\bar{M})/2]+\tfrac{1}{2}(\bar{Q}-\bar{M})\ln[(\bar{Q}-\bar{M})/2]\right.$$
$$\left.+(1-\bar{Q})\ln(1-\bar{Q})+\tfrac{3}{2}\bar{Q}\ln(2^{1/3}R_A^{-2}\Lambda_A\Lambda_B)+\tfrac{3}{4}\bar{M}\ln\frac{m_B}{m_A}\right] \tag{3.1}$$

with

$$\bar{Q}=2^{-1/2}R_A^3(\rho_A+\rho_B) \tag{3.2}$$

and

$$\bar{M}=2^{-1/2}R_A^3(\rho_A-\rho_B)\ . \tag{3.3}$$

R_A is a known function of $R_A^{(0)}$ $(=R_B^{(0)})$ [see Eq. (2.34) and Appendix B], and thus represents the effective diameter of the particles. R_A (which here is equal to R_B) depends weakly on temperature and density (see Appendix B). For reasons of simplicity we disregard this density dependence. m_A and m_B are the masses of the two particles and

$$\Lambda_i=h(2\pi m_i k_B T)^{-1/2} \tag{3.4}$$

is the thermal de Broglie wavelength. Equation (3.1) is the simplest choice of the reference free energy which, on the one hand, reduces in the low-density limit to the free energy of an ideal mixture of monoatomic gases

$$f_h(\rho_i\to 0,T)=k_BT\sum_i\rho_i[\ln(\rho_i\Lambda_i^3)-1]\ , \tag{3.5}$$

and which, on the other hand, takes into account that the overall density of spheres with diameter R cannot exceed the density of a close-packed structure

$$(\rho_A+\rho_B)_{\max}=\sqrt{2}/R^3\ , \tag{3.6}$$

so that

$$\bar{Q}\leq 1,\quad |\bar{M}|\leq\bar{Q}\ . \tag{3.7}$$

Combining Eqs. (2.4), (2.14), (2.15), and (3.1) one obtains for the total free-energy density $f=\Omega(\rho_i,T,\mu_i)/V$:

$$f=\sqrt{2}R_A^{-3}\left\{k_BT\left[\frac{\bar{Q}+\bar{M}}{2}\ln\left[\frac{\bar{Q}+\bar{M}}{2}\right]+\frac{\bar{Q}-\bar{M}}{2}\ln\left[\frac{\bar{Q}-\bar{M}}{2}\right]+(1-\bar{Q})\ln(1-\bar{Q})\right]\right.$$
$$\left.-\tfrac{1}{2}(\hat{J}\bar{M}^2+\hat{K}\bar{Q}^2+2\hat{C}\bar{Q}\bar{M})-H\bar{M}+\Delta\bar{Q}\right\}, \tag{3.8}$$

where

$$\hat{J}=\tfrac{1}{4}(\hat{w}_{AA}-2\hat{w}_{AB}+\hat{w}_{BB})\sqrt{2}R_A^{-3}, \tag{3.9}$$

$$\hat{K}=\tfrac{1}{4}(\hat{w}_{AA}+2\hat{w}_{AB}+\hat{w}_{BB})\sqrt{2}R_A^{-3}, \tag{3.10}$$

and

$$\hat{C}=\tfrac{1}{4}(\hat{w}_{AA}-\hat{w}_{BB})\sqrt{2}R_A^{-3}. \tag{3.11}$$

In Eq. (3.8) we have omitted the last two terms from Eq. (3.1), because they are linear in the density variables and therefore irrelevant for determining phase equilibria and number densities. Equation (3.8) is identical to the mean-field expression for the free-energy density of the Blume-Emery-Griffiths model.[48–50] Note that according to our approach the parameters and variables in Eq. (3.8) are precisely specified by the characteristics of binary liquid mixtures. If one uses $\hat{J}>0$ as the energy scale, f depends on the reduced variables $\bar{T}=k_BT/\hat{J}$, $\bar{H}=H/\hat{J}$, $\bar{\Delta}=\Delta/\hat{J}$, and on the two parameters $\bar{K}=\hat{K}/\hat{J}$ and $\bar{C}=\hat{C}/\hat{J}$.

Although Eq. (3.8) does not represent a quantatively reliable description of binary liquid mixtures, it nonetheless gives all the qualitative features expected for them, e.g., the phase diagram in Fig. 1. Thus the BEG model is the simplest model to pursue completely the procedure we outlined at the end of Sec. II. The symmetries of the BEG model allow us to obtain a particular transparent, qualitative picture of the possible interfacial wetting behaviors in binary liquid mixtures. This eases our corresponding discussion of the Percus-Yevick (PY) model in Sec. IV, which is a more realistic model but which is also more complicated. In addition, there are considerable efforts to understand the statistical mechanics for interfacial wetting in the BEG model with short-range forces as well as for the closely related Blume-Capel model,[51–57] so that our study of the BEG model represents an interesting theoretical problem of its own.

The bulk phase diagram belonging to Eq. (3.8) depends on the two parameters (see Appendix C; recall that there all bars are omitted)

$$\bar{K}=(\bar{w}_{AA}+\bar{w}_{BB}+2)/(\bar{w}_{AA}+\bar{w}_{BB}-2), \tag{3.12}$$

$$\bar{C}=(\bar{w}_{AA}-\bar{w}_{BB})/(\bar{w}_{AA}+\bar{w}_{BB}-2), \tag{3.13}$$

or equivalently on

$$\bar{w}_{AA}=(\bar{K}+2\bar{C}+1)/(\bar{K}-1), \tag{3.14}$$

$$\bar{w}_{BB}=(\bar{K}-2\bar{C}+1)/(\bar{K}-1). \tag{3.15}$$

Our *first* task is to locate that region in $(\bar{K},\bar{C})$ space, where the corresponding bulk phase diagrams resemble those of simple binary liquid mixtures (Fig. 1). On the basis of Ref. 50, this problem has been solved in Ref. 9. For the convenience of the reader these results are shown in Fig. 7. They reflect the symmetry of the grand canonical free energy with respect to the transformation $C\rightarrow -C$, which corresponds to the interchange of A and B particles.

The various boundaries of the enclosed area follow from the following properties. Those systems lying on the lines $\overline{A_2D_a}$ or $\overline{A_1D_b}$ have a critical end point T_{cep} which touches L_1 (see Fig. 1). In the phase diagram of those systems which are beyond the boundaries $\overline{D_aA_4}$ or $\overline{D_bA_3}$ the line L_1 of critical points develops a tricritical point, which finally splits into a lower and an upper criti-

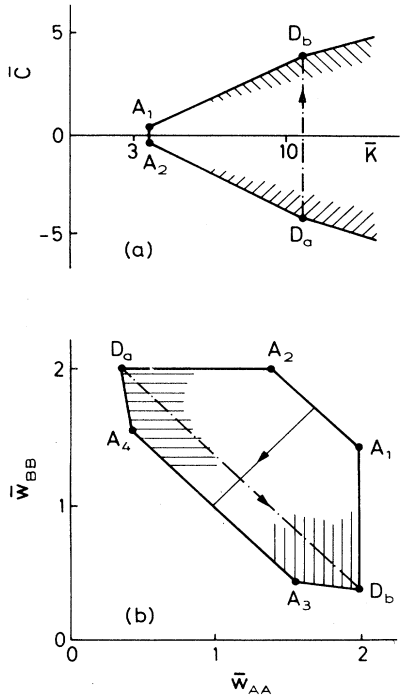

FIG. 7. Within the enclosed region in the $(\bar{K},\bar{C})$ plane (a) and in the $(\bar{w}_{AA},\bar{w}_{BB})$ plane (b), respectively, Eq. (3.8) yields bulk phase diagrams of the type shown in Fig. 1. In (a) the region is unbound towards $\bar{K}=\infty$. For more details see Fig. 2 in Ref. 9. Here we adopt the same notation as in Refs. 50 and 9. The lines in (a) and (b) correspond to each other; the arrows indicate the direction of increasing values of $\bar{K}$ and $\bar{C}$, respectively. Those systems located in the hatched areas have the property that their critical fluid at T_{cep}, which coexists with its vapor, is rich with those particles which have the weaker interaction strength among themselves. For a discussion of this effect see the main text. (The hatched areas, in particular for large values of K, have not been determined systematically so that here their extension is not precisely specified.)

cal end point by forming another triple line which involves a fourth phase. Beyond the boundary A_1A_2, T_{cep} becomes tricritical and a fourth phase can emerge.

Now we concentrate on the interfacial behavior. In the *second* step we analyze $a(T)$ for low temperatures [Eq. (2.9)]. In accordance with Ref. 9, Eqs. (2.30), (2.31), (2.35), and (2.36) lead to the conclusion that the α-γ interface is nonwet at low temperatures under the following conditions (here $r_0=1$):

$$\bar{w}_{BB}>1 \quad \text{along } p_1 \ , \tag{3.16}$$

and

$$\bar{w}_{AA}>1 \quad \text{along } p_2 \ . \tag{3.17}$$

If the inequalities in Eqs. (3.16) and (3.17) are reversed, $l=\infty$ is at low temperatures at least a local minimum of the effective interface potential.

In the *third* step we focus on the condition $a(T_{cep})=0^+$, i.e., that at least at T_{cep} $l=\infty$ is a minimum of the effective interface potential. For that purpose we have to consider Eqs. (2.17)–(2.22), (2.35) and (2.36) and the remarks at the end of Sec. II. The key quantities are the functions $\lambda_{\alpha\beta}(\bar{K},\bar{C})$ and $\lambda_{\beta\gamma}(\bar{K},\bar{C})$. Their calculation is described in detail in Appendix B. Their behavior for constant $\bar{K}$ as function of $\bar{C}$ is shown in Fig. 8. Both are antisymmetric around $\bar{C}=0$ [compare Eqs. (C25) and (C26)] and $\lambda_{\alpha\beta}=+1$ and -1 on A_1D_b and A_2D_a, respectively [see Eq. (C30)].

Now we have to check Eqs. (2.17)–(2.20). Which of the four inequalities we have to use depends on $\mathrm{sgn}(\bar{C})$ because within the BEG model we have

$$\bar{C}\gtrless 0 \Longleftrightarrow Q_A \gtrless Q_B \ . \tag{3.18}$$

Along the *path* p_1 α is the A-rich liquid and β the B-rich liquid so that, according to the remarks at the end of Sec. II, for $\bar{C}>0$ case (I) must be considered, whereas for $\bar{C}<0$ it is case (IV). Along the *path* p_2 for $\bar{C}>0$ case (II) applies, whereas for $\bar{C}<0$ it is case (III).

As an example let us consider the systems with $\bar{C}>0$ along p_1. For $\bar{C}$ close to the boundary A_1D_b both $\lambda_{\alpha\beta}$ and $\lambda_{\beta\gamma}$ approach $+1$ (see Fig. 8) so that E_B vanishes [Eq. (2.22a)]. Since $\bar{t}_{3,AA}$ is positive the condition in Eq. (2.17) is definitely fulfilled for these large values of $\bar{C}$. On the other hand for $\bar{C}\to 0^+$ E_B tends towards $\bar{t}_{3,BB}$ [see Eq. (2.22a) and Fig. 8]. According to Eqs. (2.36) and (3.15) $\bar{t}_{3,BB}$ $(\bar{C}=0)=(\bar{K}+1)/(\bar{K}-1)$, which is equal to $\bar{t}_{3,AA}$ $(\bar{C}=0)$ due to Eqs. (2.35) and (3.14). Thus, for $\bar{C}\to 0^+$ the condition in Eq. (2.17) starts to fail. The other cases can be discussed similarly.

In addition these properties of E_A and E_B allow us to draw conclusions about the value of the wetting transition temperature T_W in the case of critical wetting in which T_W is given by $a(T=T_W)=0$ [see Eq. (2.8) and the discussion in the second paragraph following Eq. (2.16)]. For $\bar{C}\to 0$ the inequalities in Eqs. (2.17)–(2.20) turn into equalities which means that for these values of $\bar{C}$ the curly bracket in Eq. (2.9) vanishes at $T=T_{cep}$. On the other hand, by definition, this curly bracket also vanishes at T_W. Since $a(T)$ is a monotonic and continuous function of temperature, we can therefore conclude that

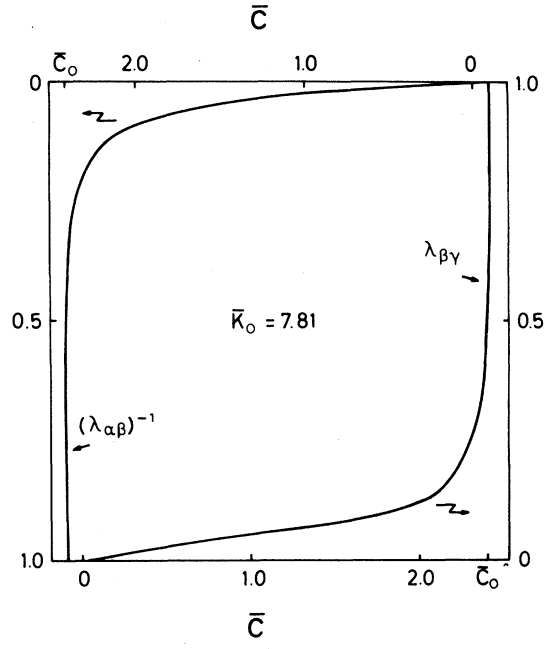

FIG. 8. Typical behavior of $\lambda_{\alpha\beta}(\bar{K},\bar{C})$ and $\lambda_{\beta\gamma}(\bar{K},\bar{C})$ for the BEG model as function of $\bar{C}$ with constant $\bar{K}=\bar{K}_0=7.81$. $\bar{C}_0=\bar{C}_0(\bar{K}_0)=2.405$ corresponds to a point on the boundary A_1D_b. Towards that point both functions rapidly approach 1. $\lambda_{\beta\gamma}$ vanishes at $\bar{C}=0$ whereas $\lambda_{\alpha\beta}$ diverges at $\bar{C}=0$. The behavior of the functions for negative values of $\bar{C}$ follows from $\lambda_{\alpha\beta}(\bar{C})=-\lambda_{\alpha\beta}(-\bar{C})$ and $\lambda_{\beta\gamma}(\bar{C})=-\lambda_{\beta\gamma}(-\bar{C})$. $\bar{C}_0(\bar{K}_0)$ is an increasing function of $\bar{K}_0$. As one can infer from this figure, the curves $\lambda_{\beta\gamma}$ and $\lambda_{\alpha\beta}$ join smoothly and with a common vertical tangent at $\bar{C}=\bar{C}_0$ where their value is 1. However, for values of $\bar{K}$ which are larger than those belonging to D_a and D_b (see Fig. 7) there is a gap between the curves $\lambda_{\alpha\beta}$ and $\lambda_{\beta\gamma}$ at the corresponding boundaries $\bar{C}_0(\bar{K})$. This gap widens for larger values of $\bar{K}$.

T_W approaches T_{cep} for $\bar{C}\to 0$. On the other hand, close to the boundaries A_1D_b and A_2D_a, the differences $\bar{t}_{3,ii}-E_j$ are largest so that according to Eq. (2.9) and due to the monotonic behavior of $a(T)$ the difference $T_{cep}-T_W$ is also largest. For $\bar{w}_{BB}=1$ along p_1 and $\bar{w}_{AA}=1$ along p_2, respectively [see Eqs. (2.30) and (2.31)] T_W reaches T_4 (see Fig. 2).

If these results are combined with those for low temperatures as obtained in the previous second step we arrive at our final conclusions. They are summarized in Fig. 9. The different hatchings give for all bulk systems a complete classification with respect to the three wetting behaviors (i)–(iii) which we have listed in the second paragraph after Eq. (2.16). The wetting behavior along the two paths p_1 and p_2 (see Fig. 1) are, of course, complementary: If wetting can occur along one of them, it cannot occur along the other.

A detailed discussion of these results will follow in Sec. V which will include our findings from the more realistic model analyzed in Sec. IV. Nonetheless, we want to briefly list the main conclusions which can be drawn from Fig. 9. Those with an asterisk are at least partly specific for the BEG model.

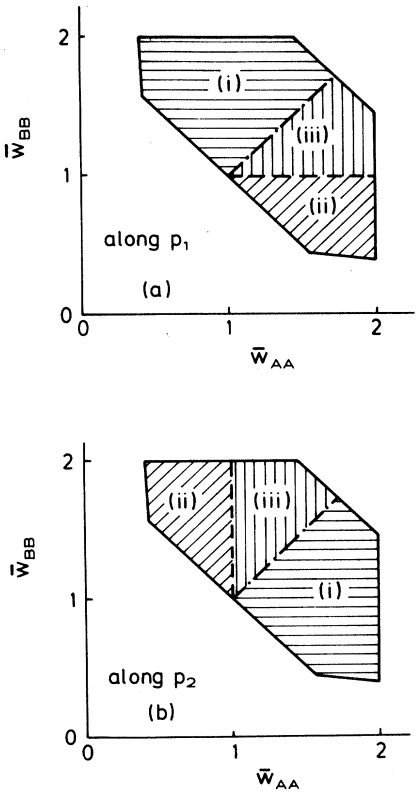

FIG. 9. Classification of binary liquid mixtures with respect to three different interfacial wetting behaviors (i)–(iii) along path p_1 (a) and along path $p_2^{(b)}$, (b) respectively (see Fig. 1). In accordance with the main text [see second paragraph after Eq. (2.16)] one has (i) no wetting transition at the α-γ interface, (ii) either the α-γ interface is wet for all temperatures or there is a first-order wetting transition, (iii) critical wetting is possible. For the behavior of the wetting transition temperature in case (iii) see Fig. 10.

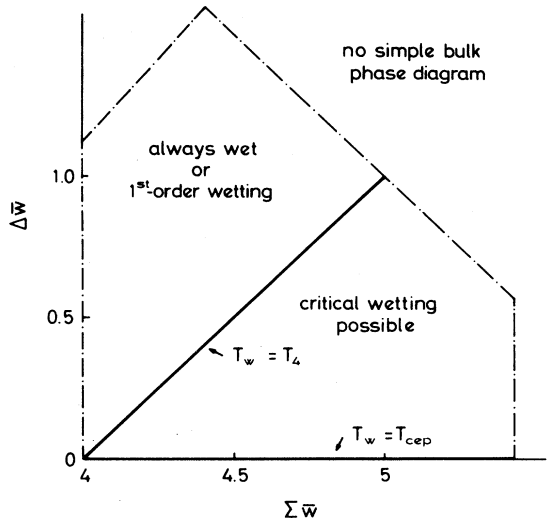

FIG. 10. Size of the region where critical wetting is possible. $\Sigma\bar{w}=(\hat{w}_{AA}+\hat{w}_{BB}+2\hat{w}_{AB})/\hat{w}_{AB}$ is the total strength of all three interactions. $\Delta\bar{w}=(\hat{w}_{BB}-\hat{w}_{AA})/\hat{w}_{AB}$ along path p_2 and $\Delta\bar{w}=(\hat{w}_{AA}-\hat{w}_{BB})/\hat{w}_{AB}$ along path p_1, respectively, measure the difference of the interaction strengths among the particles themselves. For critical wetting to be possible $\Delta\bar{w}$ must be sufficiently small and $\Sigma\bar{w}$ must be sufficiently large. The optimum value is achieved for $\hat{w}_{AA}+\hat{w}_{BB}=3\hat{w}_{AB}$. The transition temperature T_W for critical wetting increases towards T_{cep} for decreasing values of $\Delta\bar{w}$.

(1) There is no indication that there are binary liquid mixtures whose liquid-vapor interface does not become wet at least at the critical end point along either side of the triple line. However, this does not prove Cahn's statement,[58] which is based on a model with purely short-range forces, that wetting has to occur necessarily. In the case of wetting of a wall, it is known that the competition between short-range and long-range forces may prevent wetting at all[59–63,13–17] (see also Fig. 9.1 in Ref. 1). Such a behavior cannot be inferred from our present study since we focus only on the leading term in the effective interface potential.

(2*) The wetting behavior is symmetric about the diagonal $\bar{w}_{AA}=\bar{w}_{BB}$ if the paths p_1 and p_2 are interchanged accordingly.

(3*) The liquid phase with the higher number density never wets the liquid-vapor interface [see Eq. (3.18) and Figs. 8 and 9].

(4*) Along one side of the triple line, one-half of the system displays no interfacial wetting. From the other half, 51% may undergo critical wetting and 49% are either wet at all temperatures or undergo first-order wetting. This also means that 51% of all binary liquid mixtures may exhibit critical wetting along one or the other side of the triple line.

(5*) Critical wetting can only occur for such binary liquid mixtures in which the values of the interaction strengths among the A particles and among the B particles are sufficiently close to each other (see Fig. 10). This is the case if at low temperatures the number densities of the pure A and B liquid are similar.

(6*) The region in which critical wetting can occur shrinks rapidly to zero if the total strength of all interactions together becomes too small.

(7*) The transition temperature for critical wetting increases towards the critical end point if the number densities of the pure A and of the pure B liquids become similar.

The statistical statement in conclusion (4) assumes that the binary liquid mixtures as found in nature are distributed homogeneously over the enclosed area in Figs. 8 and 9. In general, however, $\hat{w}_{AB}$ is not independent from $\hat{w}_{AA}$ and $\hat{w}_{BB}$ so that, in fact, physical systems will be concentrated around a certain line $\bar{w}_{BB}(\bar{w}_{AA})$. As a consequence probabilities are no longer given as ratios of areas but as ratios of line segments of the curve $\bar{w}_{BB}(\bar{w}_{AA})$. This will be discussed in more detail in Sec. V.

At the end of this section we would like to remark that in Ref. 9 some of those above conclusions, which involve the densities at T_{cep}, were attempted without being able

to resort to the quantitative results derived here. Those limited conclusions in Ref. 9 were based *inter alia* on the assumption that $\mathrm{sgn}(M_\alpha(T_{\mathrm{cep}}))=\mathrm{sgn}(C)$. Our actual calculations show, however, that even within the BEG model with its special symmetry around $C=0$, not all binary liquid mixtures fulfill the above equation. Instead there are mixtures in which the critical fluid at T_{cep}, which is coexisting with its noncritical vapor, is richer in those particles which have the weaker interaction among themselves. Those systems are indicated in Fig. 7 by a hatching.

This effect can be understood as follows. The vapor should be dominated by the less attractive particles, i.e., $\mathrm{sgn}(M_\gamma(T_{\mathrm{cep}}))=-\mathrm{sgn}(C)$. Upon approaching the boundaries $\overline{A_1D_b}$ or $\overline{A_2D_a}$ the difference between the fluid and the vapor phase vanishes because T_{cep} touches L_1 [see Fig. 1 and the second paragraph after Eq. (3.15)]. Therefore, $M_\alpha(T_{\mathrm{cep}})-M_\gamma(T_{\mathrm{cep}})\to 0$ close to $\overline{A_1D_b}$ or $\overline{A_2D_a}$. Since, however, neither $M_\alpha(T_{\mathrm{cep}})$ nor $M_\gamma(T_{\mathrm{cep}})$ vanish on these boundaries, $M_\alpha(T_{\mathrm{cep}})$ must take on the sign of $M_\gamma(T_{\mathrm{cep}})$, which is opposite to that of C (see above). What remains true is that the density of the more attractive particles is larger in the fluid phase than in the vapor phase so that

$$\mathrm{sgn}(M_\alpha(T_{\mathrm{cep}})-M_\gamma(T_{\mathrm{cep}}))=\mathrm{sgn}(C)\ .$$

IV. INTERFACIAL WETTING IN THE PERCUS-YEVICK MODEL

The discussion of the BEG model in the previous section allowed us to find several important results for the interfacial wetting behavior in binary liquid mixtures, which also will serve us as a guide in the present section. However, Eq. (3.1) represents an approximation for the free-energy density of a mixture of hard spheres, which is valid only for small values of the number densities (see Appendix D). At larger values of the number densities, for example, the different size of the two types of particles will start to become important. This aspect is not contained in Eq. (3.1). The following choice represents a more accurate expression for the reference-free-energy density (we use the same notation as in Sec. III):

$$f_h(\rho_i,T)=\sqrt{2}R_A^{-3}k_BT\left[\bar{f}_h(\bar{\rho}_i)+3\sum_i\bar{\rho}_i\ln(\Lambda_i/R_A)\right]\ , \tag{4.1}$$

with $\bar{\rho}_i=2^{-1/2}R_A^3\rho_i$ and

$$\bar{f}_h(\bar{\rho}_i)=-\bar{p}_h(\bar{\rho}_i)+\sum_i\bar{\rho}_i\bar{\mu}_{h,i}(\bar{\rho}_i)\ . \tag{4.2}$$

$\bar{p}_h$ and $\bar{\mu}_{h,i}$ are the dimensionless pressure and chemical potentials, respectively, of the hard-sphere-fluid mixture

$$p_h(\rho_i,T)=\sqrt{2}R_A^{-3}k_BT\bar{p}_h(\bar{\rho}_i) \tag{4.3}$$

and

$$\mu_{h,i}(\rho_i,T)=k_BT\bar{\mu}_{h,i}(\bar{\rho}_i)\ . \tag{4.4}$$

$\bar{p}_h$ and $\bar{\mu}_{h,i}$ are given as

$$\bar{p}_h(\bar{\rho}_i)=\left[(1+d_3+d_3^2)\left[\sum_i\bar{\rho}_i\right]-\frac{\pi}{\sqrt{2}}\bar{\rho}_A\bar{\rho}_B(1-r)^2(1+r+d_2r)\right](1-d_3)^{-3} \tag{4.5}$$

and

$$\bar{\mu}_{h,i}(\bar{\rho}_i)=\ln(\bar{\rho}_i/(1+d_3))+3\bar{R}_id_2/(1-d_3)+\tfrac{9}{2}\bar{R}_i^2d_2^2/(1-d_3)^2+3\bar{R}_i^2d_1/(1-d_3)+\frac{\pi}{3\sqrt{2}}\bar{R}_i^3\bar{p}_h(\bar{\rho}_i)\ . \tag{4.6}$$

Here $\bar{R}_A=1$, $\bar{R}_B=r=R_B/R_A$ [see Eq. (B18)], and

$$d_k=\frac{\pi}{3\sqrt{2}}\sum_i\bar{R}_i^k\bar{\rho}_i,\quad i=A,B,\quad k=1,2,3\ . \tag{4.7}$$

Whereas Eqs. (4.1)–(4.4) are exact, Eqs. (4.5)–(4.7) are the approximate expressions of pressure and chemical potentials of the reference system as obtained from the exact solution of the generalized Percus-Yevick equation for a mixture of hard spheres with diameters R_A and R_B, respectively.[64–67] [Equations (4.5)–(4.7) correct misprints in Refs. 66 and 67.]

In this section we proceed along the same lines as in Sec. III. The only difference is that we replace Eq. (3.1) by Eq. (4.1). [Again we can omit the second term in Eq. (4.1), which is identical with the last two terms in Eq. (3.1) and which is irrelevant for determining phase equilibria.] The corresponding changes are presented explicitly in Appendix D.

Before we turn to these details let us note that we can restrict our analysis to the case $r\le 1$. Because the free-energy density is invariant with respect to the interchange of the A and B particles the properties of the systems with $r\ge 1$ follow from those with $r\le 1$ whose parameters have been changed according to following rules:

$$\begin{aligned}&p\to p,\quad \mu_A\leftrightarrow\mu_B,\quad T\to T,\quad H\to -H,\quad \Delta\to\Delta\ ,\\ &\bar{K}\to\bar{K},\quad \bar{C}\to-\bar{C},\quad \bar{t}_{3,AA}\leftrightarrow\bar{t}_{3,BB},\quad \bar{w}_{AA}\leftrightarrow\bar{w}_{BB}\ .\end{aligned} \tag{4.8}$$

Correspondingly one has to change $M\to -M$, $Q\to Q$. In addition, the two paths p_1 and p_2 have to be interchanged.

First, as we did in Sec. III, we have now to determine for each r those values of $\bar{K}$ and $\bar{C}$ or $\bar{w}_{AA}$ and $\bar{w}_{BB}$ for which the corresponding bulk phase diagrams have the structure shown in Fig. 1. As in the BEG model the PY model does not contain the formation of a solid phase. Therefore, the structure of the bulk phase diagram at low temperatures (Fig. 2) has to be incorporated by hand [see Eqs. (2.24), (2.25), and (2.29)]. From the numerical treatment of the PY model we find that Eq. (2.29) is fulfilled with an accuracy better than 99% for temperatures T less than about $0.7T_{\mathrm{cep}}$. Therefore, our treatment of the behavior at low temperature should be correct unless T_4/T_{cep} happens to be significantly larger than 0.7.

To the best of our knowledge the analog of Fig. 7,

which holds for the BEG model, has not yet been determined for the PY model, in particular with r as a third axis. Therefore, we performed for the PY model and for a range of r values the same kind of calculation as Furman, Dattagupta, and Griffiths[50] did for the BEG model. However, this analysis of the PY model is significantly more difficult than of the BEG model, because the BEG model exhibits several symmetry properties [see Eqs. (C27)–(C30)] which go beyond that one which is due to the invariance with respect to interchanging A and B. This latter one is the only one which is also present in the PY model.

The various boundaries in Fig. 7 are mainly due to the appearance of tricritical points [see the second paragraph after Eq. (3.15)]. The same is true for the PY model. In extension of Eq. (C10) these points are characterized by

$$\partial^n \bar{H}(\bar{M},\bar{\Delta},\bar{T})/\partial \bar{M}^{\,n}=0, \quad n=1,\ldots,4 ,$$
$$\partial^5 \bar{H}(\bar{M},\bar{\Delta},\bar{T})/\partial \bar{M}^{\,5}>0 . \tag{4.9}$$

As in Eqs. (C14)–(C17) these derivatives must be obtained from the functions $\bar{H}(\bar{M},\bar{Q},\bar{T})$ and $\bar{\Delta}(\bar{M},\bar{Q},\bar{T})$ given explicitly in Eqs. (D5) and (D6). Due to the complicated form of these functions the analytical calculations become readily prohibitive, in particular for $n=3,4$. [For comparison, in the case $n=2$ see Eq. (C17) following from Eqs. (C2) and (C3), which is still simple compared with Eqs. (D5) and (D6).] Thus, we had to resort to algebraic computer calculations in order to keep track of the numerous terms. For selected examples we checked these results numerically and by plotting the variational functional from Eqs. (2.4) and (4.1) and by directly following the coalescence of its minima.

Once the above system of equations [Eq. (4.9)] is obtained explicitly it must be solved numerically. (This is also in contrast to the BEG model where the solutions can be obtained analytically.) Due to the numerical problem of small differences between large numbers it becomes increasingly difficult to find these solutions for large values of $\bar{K}$ and for the upper boundary in the $(\bar{K},\bar{C})$ diagram in the case of $r\le 1$, which corresponds to the line A_1D_b in Fig. 7. (There are no numerical problems along the lower boundary.) In order to overcome these difficulties we augmented the requirements for a system to exhibit a simple bulk phase diagram by the following conditions:

$$\left[\frac{\bar{\rho}_A}{\bar{\rho}_A+\bar{\rho}_B}\right]_{\text{vapor},\,T=T_{\text{cep}}} > 5\times 10^{-3} \tag{4.10}$$

and

$$(\bar{\rho}_A+\bar{\rho}_B)_{\text{vapor},\,T=T_{\text{cep}}} > 5\times 10^{-5} . \tag{4.11}$$

Our rule is that we discard all those systems which along a path of constant $\bar{K}=\bar{K}_0$ fail to fulfill either Eq. (4.10) or (4.11) within a distance of $\delta\bar{C}=0.02$ from that tricritical point which corresponds to this value $\bar{K}_0$. Our conditions in Eqs. (4.10) and (4.11) are motivated by the observation that such small values of the partial and total density of the vapor are accompanied by values of the reduced pressure $\bar{p}$ in the order of 10^{-4} and by a substantial decrease of T_{cep} so that we have already reached the limits of applicability of the PY model where solidification sets in. In addition to Eqs. (4.10) and (4.11) we do not consider systems with $\bar{K}>100$. According to these rules we scan the $(\bar{K},\bar{C})$ plane with a mesh ($\delta\bar{K}=0.02$, $\delta\bar{C}=0.02$). [We use the same mesh to check the wetting conditions in Eqs. (2.17)–(2.22).]

Our results for $r=1$ are displayed in Fig. 11. As one can see the allowed region as obtained within the PY model is considerably smaller than within the BEG model. The results for $r\neq 1$ will be displayed later together with our findings for the various wetting behaviors within the allowed regions.

At this stage it is very instructive to follow, as a function of $\bar{C}$ throughout the allowed regions and for selected values of r, the behavior of $\bar{T}_{\text{cep}}$ and of the concentration x_B^* of B particles in the critical fluid at T_{cep}, $x^*_{B,\alpha}=x^*_{B,\beta}$, and of the coexisting gas phase, $x^*_{B,\gamma}$; here $x_B=\rho_B/(\rho_A+\rho_B)$. Our results are shown in Fig. 12. $\bar{T}_{\text{cep}}$ ($\bar{K}=$const, $\bar{C}$, $r=1$) is symmetric around $\bar{C}=0$, where it takes on its minimum value. The maximum values are reached at the lower and upper bounds of the allowed region [compare Fig. 11(a)]. The minimum of $\bar{T}_{\text{cep}}$ coincides with that value of $\bar{C}$ where $Q_\alpha=Q_\beta$; for $r=1$ this is $\bar{C}=0$, but it remains true for $r<1$ where the minimum is shifted to larger values of $\bar{C}$. [Recall that

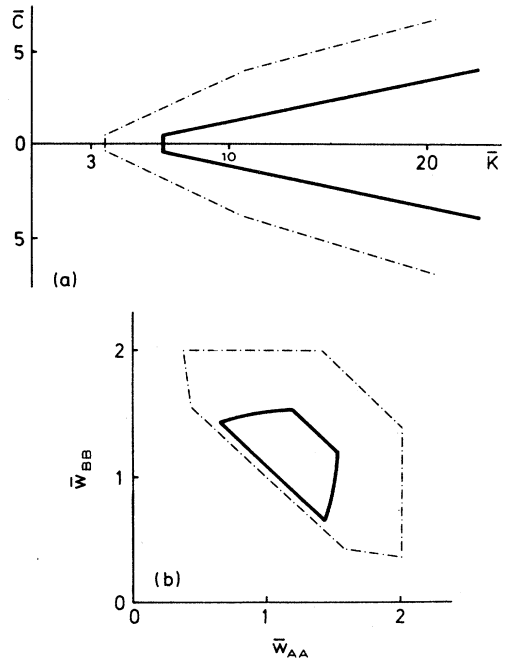

FIG. 11. Within the enclosed region in the $(\bar{K},\bar{C})$ plane (a) and in the $(\bar{w}_{AA},\bar{w}_{BB})$ plane (b), respectively, the PY model with $r=1$ (solid lines) yields bulk phase diagrams of the type shown in Fig. 1. For comparison the dash-dotted lines indicate the corresponding results for the BEG model (see Fig. 7). In (b) the gap between the lower left solid and dash-dotted lines arises due to the fact that within the PY model we consider only systems with $\bar{K}<100$. In any case $\bar{K}$ must be larger than 6.55 compared with 3.80 for the BEG model.

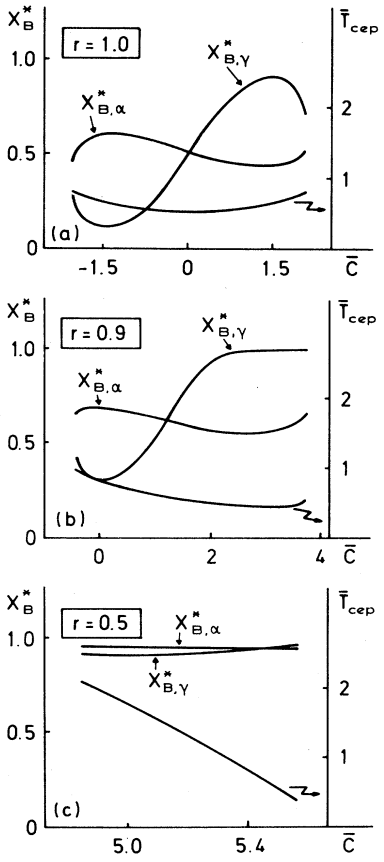

FIG. 12. Reduced critical end-point temperature $\bar{T}_{cep} = k_B T_{cep}/\hat{J}$ and concentration $x_B^* = x_B(T = T_{cep})$ of B particles in the critical fluid $\alpha = \beta$ and in the coexisting vapor γ $[x_B = \rho_B/(\rho_A + \rho_B)]$ as function of $\bar{C}$ for $\bar{K} = 13.335$ and for (a) $r = 1.0$, (b) $r = 0.9$, and (c) $r = 0.5$. The curves end at the boundaries of the corresponding $\bar{C}$ intervals within which the bulk phase diagram is simple. A discussion of these results of the PY model is given in the main text.

$\mathrm{sgn}(Q_\alpha - Q_\beta)$ is independent from temperature.] For $r < 0.72$ $\mathrm{sgn}(Q_\alpha - Q_\beta)$ cannot change sign as a function of $\bar{C}$ so that in Fig. 12(c) $\bar{T}_{cep}$ reaches its minimum value at the upper boundary of the allowed $\bar{C}$ interval. At fixed values of $\bar{C}$, $\bar{T}_{cep}$ increases as a function of $\bar{K}$. For $r = 1$ the two concentrations $x_{B,\alpha}^*$ and $x_{B,\gamma}^*$ are antisymmetric functions of $\bar{C}$ around ($\bar{C} = 0$, $x_B^* = 0.5$). This symmetry is gone for $r \neq 1$. Close to its turning points both $x_{B,\alpha}^*$ and $x_{B,\gamma}^*$ behave as expected: If the strength of the interaction between the B particles is increased, i.e., if $\bar{C}$ becomes smaller, x_B^* increases in the fluid phase and decreases in the vapor phase. However, close to the boundaries of the allowed $\bar{C}$ intervals and for not too small values of r this behavior is reversed. This is due to the increase of $\bar{T}_{cep}$, which towards the boundaries approaches the line L_1 (Fig. 1). But before $\bar{T}_{cep}$ reaches L_1 where it would form a tricritical point, at which $x_{B,\alpha}^*$ and $x_{B,\gamma}^*$ would merge, another tricritical point is formed on L_1 which leads to the determination of this $\bar{C}$ interval. Upon a further increase (or decrease on the other side) this latter tricritical point would split into an upper and lower critical end point by forming a fourth phase. Due to this preemption $x_{B,\alpha}^*$ and $x_{B,\gamma}^*$ remain distinct at the boundaries of the allowed $\bar{C}$ interval. This behavior has to be contrasted with the BEG model, where this mechanism occurs beyond the lines $D_a A_4$ and $D_b A_3$ in Fig. 7; along $A_1 D_b$ and $A_2 D_a$, however, T_{cep} does manage to reach the critical line L_1 and forms a tricritical point between the fluid and the vapor. This does not occur in the PY model. The boundary at small values of $\bar{K}$ in Fig. 11(a) arises due to the same mechanism as in the corresponding case in the BEG model: for too small values of $\bar{K}$, $\bar{T}_{cep}$ becomes tricritical due to the formation of a fourth phase.

Now that in the first step we have determined those regions in parameter space where the PY model exhibits simple bulk phase diagrams we can turn to the discussion of the wetting behavior. In the second step, from Eqs. (2.30), (2.31), (2.35), and (2.36) we find that the α-γ interface is nonwet at low temperatures if

$$\bar{w}_{BB} > \tfrac{1}{8}(1+r)^3 \quad \text{along } p_1 \tag{4.12}$$

and

$$\bar{w}_{AA} > \frac{1}{8}\frac{(1+r)^3}{r^3} \quad \text{along } p_2 \ . \tag{4.13}$$

If the inequalities in Eqs. (4.12) and (4.13) are reversed, $l = \infty$ is at low temperatures at least a local minimum of the effective interface potential.

In the third step we focus on the wetting behavior close to T_{cep}. As in Sec. III we have to consider Eqs. (2.17)–(2.22), (2.35), and (2.36) and the last paragraph in Sec. II. These conditions are determined by the functions $\lambda_{\alpha\beta}(\bar{K},\bar{C},r)$ and $\lambda_{\beta\gamma}(\bar{K},\bar{C},r)$ which are plotted in Fig. 13 for $\bar{K}$ fixed and for two values of r. Note that for $r = 1$ these curves are antisymmetric around $\bar{C} = \bar{C}_1 = \bar{C}_2 = 0$ as in the BEG model. For $r \neq 1$, however, $\lambda_{\alpha\beta}$ diverges at $\bar{C}_1$ and $\lambda_{\beta\gamma}$ vanishes at $\bar{C}_2$ with $\bar{C}_1$ and $\bar{C}_2$ different from each other and from zero. Therefore, $\lambda_{\alpha\beta}$ and $\lambda_{\beta\gamma}$ are no longer antisymmetric around a certain value of $\bar{C}$. In addition, $|\lambda_{\beta\gamma}|$ remains strictly less than 1 even at the boundaries of the corresponding $\bar{C}$ intervals. There $\lambda_{\alpha\beta}$ no longer joins $\lambda_{\beta\gamma}$ continuously if $\bar{K}$ is too large. This gap widens for increasing value of $\bar{K}$. Recall that $\lambda_{\alpha\beta}$ (and $\lambda_{\beta\gamma}$) are independent from the fact whether α or β is the A-rich-liquid phase at $T < T_{cep}$. Since $\mathrm{sgn}(\tilde{\lambda}_{\alpha\beta}) = \mathrm{sgn}(\lambda_{\alpha\beta})$ [see Eqs. (2.10) and (2.23)] we can conclude that for those values of $\bar{C}$ for which $\lambda_{\alpha\beta}$ is positive, i.e., for $\bar{C}_2 < \bar{C} < \bar{C}_0^+$, $Q_A > Q_B$ whereas negative values of $\lambda_{\alpha\beta}$, i.e., for $\bar{C}_0^- < \bar{C} < C_2$, correspond to $Q_A < Q_B$. Thus, Fig. 13 is in accordance with the intuitive argument that, say, the number density of the A-rich liquid increases with the interaction strength of the A particles and decreases with their size. If both particles have the same size the number density is higher for that liquid phase, which is rich in that particles with the larger interaction strength. If the A particles are larger than the B particles, i.e., $r < 1$ as in Fig. 13, the A-rich-liquid phase remains the phase with the higher number density only if the interaction strength between the larger A particles is

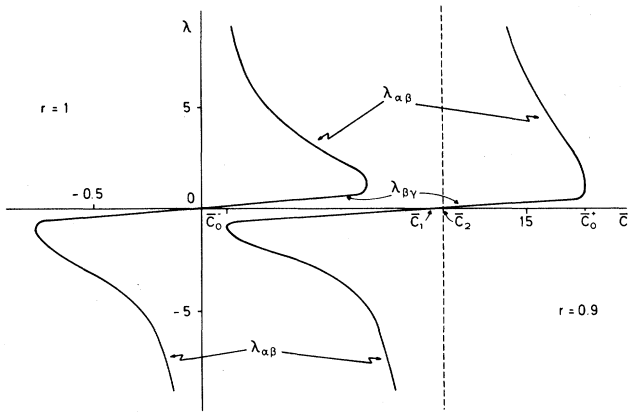

FIG. 13. Typical behavior of $\lambda_{\alpha\beta}(\bar{K},\bar{C},r)$ and $\lambda_{\beta\gamma}(\bar{K},\bar{C},r)$ in the PY model as a function of $\bar{C}$ for constant $\bar{K}=\bar{K}_0=7.81$. The left curves are for $r=1$ and the right ones for $r=0.9$. $\lambda_{\alpha\beta}$ has a negative slope whereas the slope of $\lambda_{\beta\gamma}$ is positive. For this particular value of $\bar{K}$ $\bar{C}$ varies between $\bar{C}_0^-=-0.76$ and $\bar{C}_0^+=+0.76$ in the case of $r=1$ and between $\bar{C}_0^-=+0.12$ and $\bar{C}_0^+=+1.78$ in the case of $r=0.9$. In the latter case $\lambda_{\alpha\beta}$ diverges at $\bar{C}=\bar{C}_1\simeq 1.11$, whereas $\lambda_{\beta\gamma}$ has a zero at $\bar{C}=\bar{C}_2\simeq 1.06$. But for smaller values of r one finds $\bar{C}_1>\bar{C}_2$. For $r=1$ both curves are antisymmetric around $\bar{C}=0$; they join smoothly at a value $\lambda_0=0.95$. (In the BEG model this occurred at $\lambda_0=1$, see Fig. 8.) λ_0 decreases further for larger values of $\bar{K}$. As in the BEG model, gaps open up between $\lambda_{\alpha\beta}$ and $\lambda_{\beta\gamma}$ for even larger values of $\bar{K}$ and for all values of r at the boundaries $\bar{C}_0^-$ and $\bar{C}_0^+$, respectively. The difference $\bar{C}_0^+-\bar{C}_2$ decreases for smaller values of r and vanishes at $r\simeq 0.72$. Thus, for $r<0.72$, the positive branch of $\lambda_{\alpha\beta}$ is missing. For the interpretation of Fig. 13, in terms of $\mathrm{sgn}(Q_A-Q_B)$, see the main text.

sufficiently large, i.e., $\bar{C}>\bar{C}_2$. With growing size of the A particles this is more difficult to achieve. Indeed, the difference $\bar{C}_0^+-\bar{C}_2$ decreases for smaller values of r and vanishes at about $r=0.72$. Consequently, the positive branch of $\lambda_{\alpha\beta}$ is missing for $r<0.72$. In these cases the growing size of the A particles cannot be longer compensated by a larger interaction strength between the A particles in order to keep Q_A larger than Q_B. (This case of $\bar{C}_0^+$ preempting $\bar{C}_2$ is not shown explicitly in Fig. 13.) For the following discussion, we keep in mind that in the parameter space $(\bar{C},\bar{K},r)$ the two-dimensional manifold $\bar{C}=\bar{C}_2(\bar{K},r)$ represents the separatrix between $Q_A>Q_B$ and $Q_A<Q_B$; simultaneously $\lambda_{\alpha\beta}$ changes its sign there, too.

Now we are in the position to check the condition $a(T_{\mathrm{cep}})=0^+$ given by Eqs. (2.17)–(2.20). For that purpose we define the two functions [see Eq. (2.22)]

$$E:=\begin{cases} E_A & \text{for } \bar{C}<\bar{C}_2\ , \\ E_B & \text{for } \bar{C}>\bar{C}_2\ , \end{cases} \tag{4.14}$$

and

$$t:=\begin{cases} \bar{t}_{3,BB} & \text{for } \bar{C}<\bar{C}_2\ , \\ \bar{t}_{3,AA} & \text{for } \bar{C}>\bar{C}_2\ . \end{cases} \tag{4.15}$$

$\bar{t}_{3,BB}$ and $\bar{t}_{3,AA}$ are given in terms of $\bar{K}$, $\bar{C}$, and r by Eqs. (2.35), (2.36), (3.14), and (3.15). For various values of $\bar{K}$ and r, the functions E and t are plotted in Fig. 14 as function of $\bar{C}$.

According to our results in Sec. II a particular binary liquid mixture exhibits for $T\to T_{\mathrm{cep}}$ at $l=\infty$ a minimum of its effective interface potential along the path p_1 (see Fig. 1) if $t<E$ for $\bar{C}<\bar{C}_2$ and $t>E$ for $\bar{C}>\bar{C}_2$, respectively, and along the path p_2 if $t>E$ for $\bar{C}<\bar{C}_2$ and $t<E$ for $\bar{C}>\bar{C}_2$, respectively. Otherwise $l=\infty$ is a maximum of the effective interface potential.

For $r=1$ both E and t are symmetric around $\bar{C}=0$ and continuous at $\bar{C}=0=\bar{C}_2$. The wetting condition $a(T_{\mathrm{cep}})=0^+$ is fulfilled along path p_1 for $\bar{C}>0$ and along

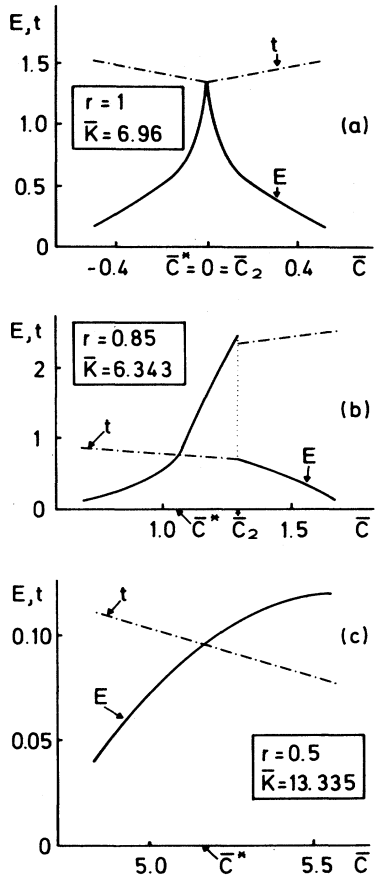

FIG. 14. The functions $E(\bar{C})$ and $t(\bar{C})$ [see Eqs. (4.14) and (4.15)] (a) for $r=1$, (b) $r=0.85$, and (c) $r=0.5$ and for selected values of $\bar{K}$. E corresponds to the solid curves and t to the dash-dotted curves; they end at the boundaries of the corresponding allowed $\bar{C}$ intervals. E and t intersect at $\bar{C}=\bar{C}^*$. For $0.7<r<1$ both E and t are discontinuous at $\bar{C}=\bar{C}_2$, which is indicated in (b) by dots. For $\bar{C}\lesssim\bar{C}_2$, $\lambda_{\alpha\beta}\lesssim 0$ and $Q_A\lesssim Q_B$, whereby the A-rich liquid is rich in the large particles. In (c) $\bar{C}_2$ is preempted by the end of the allowed $\bar{C}$ interval. Along p_1 the wetting condition $a(T_{\mathrm{cep}})=0^+$ is fulfilled for $\bar{C}>C^*$ and along p_2 for $\bar{C}<\bar{C}^*$. In case of critical wetting $t-E$ is proportional to $T_{\mathrm{cep}}-T_W$, which vanishes at $\bar{C}^*$. $\bar{C}^*$ and $\bar{C}_2$ coincide only for $r=1$. A more detailed discussion is given in the main text.

path p_2 for $\bar{C}<0$ [see Fig. 14(a)]. Therefore, in this case, the separatrix $\bar{C}=\bar{C}^*(\bar{K},r)$ which distinguishes between the behavior $a(T_{cep})=0^+$ and $a(T_{cep})=0^-$, coincides with the separatrix $\bar{C}_2(\bar{K},r)$, which distinguishes between $Q_A<Q_B$ and $Q_A>Q_B$. Thus, for $r=1$ we find in the PY model the same structure as in the BEG model (compare Fig. 9).

This is no longer true for $r<1$ [see Fig. 14(b)]. Due to the lack of symmetry both E and t are discontinuous at $\bar{C}=\bar{C}_2$. Along path p_1 (i.e., one considers the possibility of wetting by the liquid rich in small particles) the wetting condition is fulfilled for $\bar{C}>\bar{C}^*$ and along p_2 (i.e., one considers the possibility of wetting by the liquid rich in large particles) the wetting condition is fulfilled for $\bar{C}<\bar{C}^*$. According to Figs. 3 and 14(b) we obtain, therefore, the following conclusions.

First, consider the possibility of wetting by the liquid rich in small particles. In this case all liquids of this type with the lower number density do wet (along p_1 and $\bar{C}>\bar{C}_2$). However, it is also possible that wetting occurs by a liquid of this type but which has a higher number density than the wetted liquid (along p_1 and $\bar{C}^*<\bar{C}<\bar{C}_2$).

Second, consider the possibility of wetting a liquid rich in small particles by a liquid rich in large particles. In this case, wetting can occur only if the wetting liquid has a lower number density than the wetted liquid (along p_2 and $\bar{C}<\bar{C}^*$). However, not all liquids of this type and with the lower number density do wet the liquid with the higher number density (along p_2 and $\bar{C}^*<\bar{C}<\bar{C}_2$).

Finally, if the ratio between the sizes of the particles becomes too small, the liquid rich in large particles has always a lower number density than the liquid rich in small particles [Fig. 14(c)], so that $E=E_A$ and $t=\bar{t}_{3,BB}$ throughout the allowed $\bar{C}$ interval. According to Fig. 14(c) the wetting condition is fulfilled along path p_1 for all $\bar{C}>\bar{C}^*$ and along path p_2 for all $\bar{C}<\bar{C}^*$. Therefore, if in this case wetting occurs by the liquid rich in small particles (it does so for $\bar{C}>\bar{C}^*$ along p_1), the wetting phase has always a higher number density than the wetted phase, which is rich in large particles. On the other hand, if in this case wetting occurs by the liquid rich in large particles (it does so for $\bar{C}<\bar{C}^*$ along p_2), the wetting phase has always a lower number density than the wetted phase, which is rich in small particles.

If the wetting condition $a(T_{cep})=0^+$ and Eqs. (4.12) and (4.13) are fulfilled so that critical wetting can occur, the difference $t-E$ is proportional to $T_{cep}-T_W$ [see our discussion in the second paragraph after Eq. (3.18)]. Since $t(\bar{C})$ and $E(\bar{C})$ intersect at $\bar{C}=\bar{C}^*$, the separatrix $\bar{C}^*(\bar{K},r)$ is also the locus of those binary liquid mixtures whose wetting transition temperature in the case of critical wetting coincides with the critical end-point temperature. Along the path p_1 T_W decreases for larger values of $\bar{C}$, whereas along the path p_2, it decreases for smaller values of $\bar{C}$.

We have performed this kind of analysis, as described above and in Fig. 14, throughout those parts of the $(\bar{K},\bar{C})$ parameter space, which is accessible according to our restrictions for the bulk phase diagram, and for 15 different values of r. These results are summarized in Figs. 15–18.

First, these figures show the dependence of the allowed region in the $(\bar{K},\bar{C})$ plane as function of r. Only for $r=1$ this region is symmetric around the diagonal $\bar{w}_{AA}=\bar{w}_{BB}$. In this case, as for $r\neq 1$, the upper-right and lower-left boundaries are straight lines given by

$$\bar{w}_{BB}=-\bar{w}_{AA}+2(\bar{K}+1)/(\bar{K}-1)$$

[see Eq. (3.12)]. For $r=1$ the upper boundary corresponds to $\bar{K}=6.55$ and the lower to $\bar{K}=100$. The latter one is parallel and close to the line corresponding to

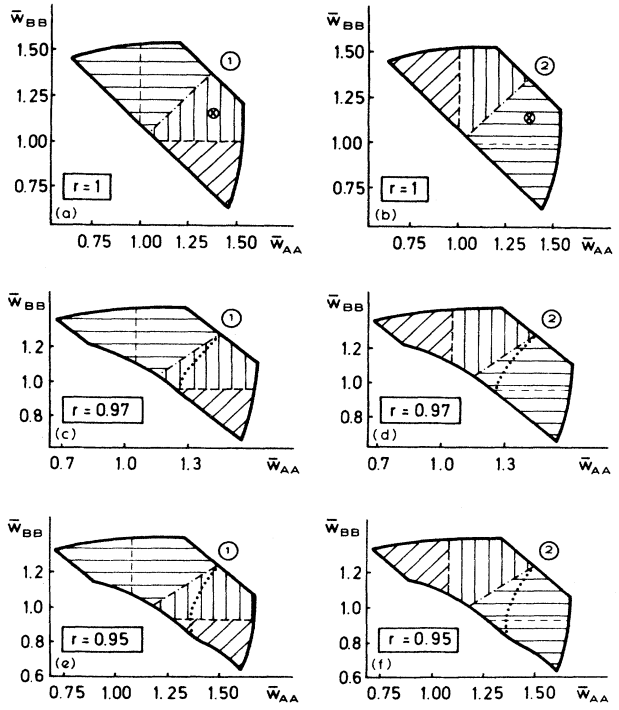

FIG. 15. Allowed parameter space within which the PY model predicts a simple bulk phase diagram of binary liquid mixtures for (a) and (b) $r=1$, (c) and (d) $r=0.97$, and (e) and (f) $r=0.95$. The corresponding wetting behavior along path 1 and path 2 (see Fig. 1) is indicated by the same hatchings as in Fig. 9. Horizontal hatching indicates the absence of interfacial wetting; diagonal hatching with positive slope stands for systems which are either wet at all temperatures or which undergo a first-order wetting transition; vertical hatching indicates candidates for critical wetting. The straight dashed lines are related to the wetting behavior at low temperatures whereas the dash-dotted curve represents those systems with $T_W=T_{cep}$. On the right-hand side of the dotted line lie those systems whose liquid phase being rich in large particles has nonetheless the higher number density. The dotted and the dash-dotted curves coincide only for $r=1$. As it must be, the comparison between paths 1 and 2 shows that wetting can occur only along one side of the triple line. Further explanations and a detailed discussion are given in the main text. The encircled crosses in (a) and (b) indicate the locus of the calculations performed in Refs. 36–38. For their discussion see Sec. V.

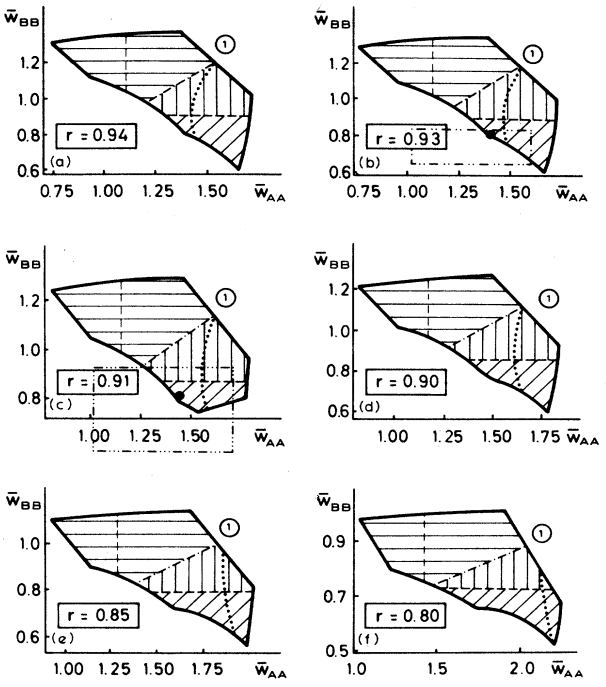

FIG. 16. As in Fig. 15 for (a) $r=0.94$, (b) $r=0.93$, (c) $r=0.91$, (d) $r=0.90$, (e) $r=0.85$, and (f) $r=0.80$. Here we show only the wetting behavior along p_1. The corresponding behavior along p_2 can be inferred from (a)–(f) because one has the same stucture of the hatching as in Figs. 15(b), 15(d), and 15(f). The mixture Ar/Kr is expected to lie within the dash-double-dotted rectangle in (b) and the mixture Kr/Xe within the dash-three-times-dotted rectangle in (c) (see Table I in Sec. V and the discussion of it).

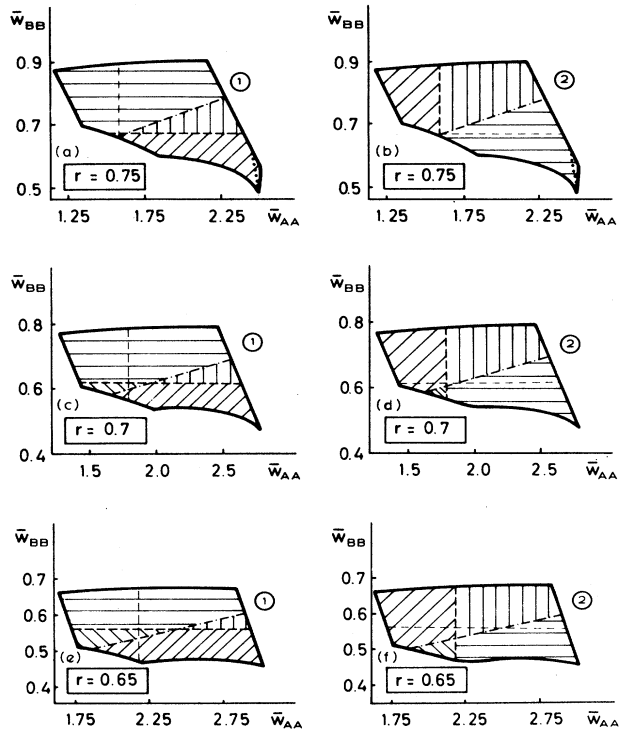

FIG. 17. As in Figs. 15 and 16 for (a) and (b) $r=0.75$, (c) and (d) $r=0.7$, and (e) and (f) $r=0.65$. The dotted line disappears for $r \leq 0.7$. For $r \leq 0.75$ a fourth category of wetting behavior comes into existence which we characterize by a diagonal hatching with negative slope. For those systems at low temperatures $l=\infty$ is (at least) a local minimum of the effective interface potential whereas it is a maximum at T_{cep}. Within the triangle formed by the two dashed lines and the dash-dotted line lie candidates for a dewetting transition along p_1. Since the wetting behavior along p_2 does not follow as easily as before from that along p_1 we show both possibilities. More explanations are given in the main text.

$\bar{K}=\infty$ so that by discarding systems with $\bar{K}>100$ we omit only a small portion of the whole allowed region. For $r=1$ the other two constraints [Eqs. (4.10) and (4.11)] are not yet effective, but they become so for $r<1$. This is apparent in the comparison between Figs. 15(c) and (15e) with 15(a). For $r<1$ only the left part of the lower boundary remains a straight line corresponding to the condition $\bar{K}<100$, whereas for larger values of $\bar{w}_{AA}$ two crossover regions occur on that boundary which signal the onset of the condition in Eqs. (4.10) and (4.11), respectively. (For $r=0.91$ [see Fig. 16(c)] and $r=0.92$ (which is not shown) the lower boundary develops additional structures. This exceptional behavior deserves further studies.) The lower-right and the upper-left boundaries are curved; they are due to the occurrence of tricritical points (compare the discussion of Figs. 7, 11, and 12). The lower-right boundary disappears for $r<0.75$. For $r \leq 0.7$ the right part of the allowed region is bound by the upper-right and lower-left boundary alone. Note the progressive change of scale on the $\bar{w}_{AA}$ and $\bar{w}_{BB}$ axes for decreasing values of r. For that reason the curves $\bar{K}=$const, i.e., the upper-right and the left part of the lower boundary, appear to become more and more vertical although their slope remains constant and equal to -1. The curvature of the upper-left boundary decreases for smaller values of r.

The dotted curves in Figs. 15, 16, 17(a), and 17(b) are the loci of the points $\bar{C}_2$ as discussed in Fig. 14. Thus on its left-hand side, all those binary liquid mixtures lie whose liquid phase being rich in large particles has, at least close to T_{cep}, the lower number density. [According to our findings $\mathrm{sgn}(Q_A-Q_B)$ is temperature independent so that this statement should hold for all temperatures.] This separatrix disappears for $r<0.72$. It means that if the sizes of the two particles are sufficiently different, the liquid phase being rich in small particles always has the higher number density. This can no longer be compensated by a strong interaction between the large particles.

The second purpose of Figs. 15–18 is to display the various wetting properties along the path p_1 and p_2, respectively (see Fig. 1). The different hatchings have the same meaning as in Fig. 9. The horizontal hatching indicates the absence of any wetting transition, independent from its order. The diagonal hatching with positive slope means that the corresponding systems are either wet at all temperatures or that they undergo a first-order wetting transition. The vertical hatching indicates the possibility of critical wetting. For $r \leq 0.75$ an additional

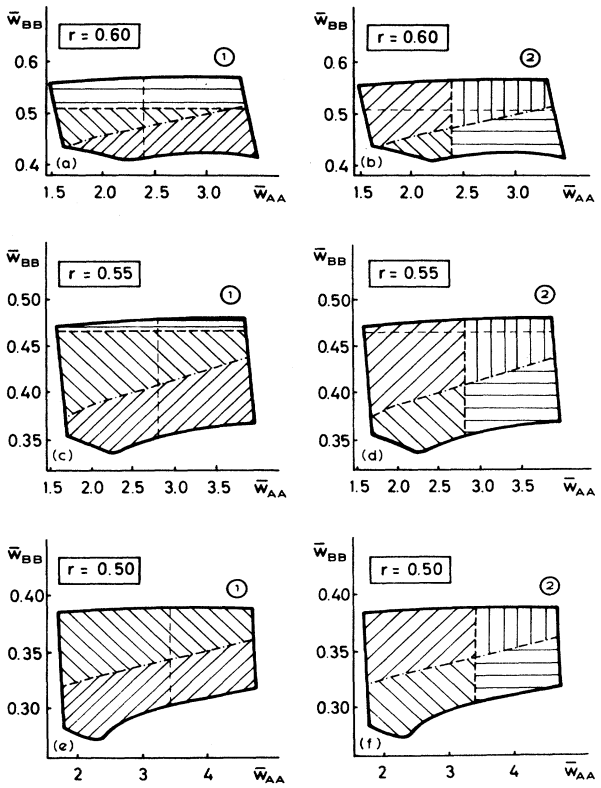

FIG. 18. As in Figs. 15–17 for (a) and (b) $r=0.60$, (c) and (d) $r=0.55$, and (e) and (f) $r=0.50$. For $r<0.6$ there is no possibility for critical wetting along p_1; for r somewhat smaller than 0.5 this possibility is expected to also disappear along p_2. Again, for further discussions, see the main text.

fourth wetting category comes into existence, which we denoted by a diagonal hatching with negative slope. Those systems have the property that at $l=\infty$ their effective interface potentials exhibit at least a local minimum for $T=T_4$ but a maximum at T_{cep}. [This effect occurs because for decreasing values of r the left part of the dash-dotted line falls below the horizontal dashed line and the vertical dashed line moves to the right (see below).] At T_{cep} these systems exhibit the same behavior as those which lie within the horizontally hatched regions. However, at low temperatures $l=\infty$ is a minimum in one case and a maximum in the other. At first glance, one could surmise that those systems of the fourth category might undergo a dewetting transition from wet to nonwet upon an increase of temperature. However, one has to keep in mind that those systems of the fourth category, which lie on the left-hand side of the vertical dashed curve, are characterized by having a (local) minimum at $l=\infty$ and $T=T_4$ both along p_1 and p_2 [see, e.g., Figs. 18(a) and 18(b)]. Since the system cannot be wet at $T=T_4$ both along p_1 and p_2, one of the two minima cannot be the global one. (Wetting along p_1 requires to remain nonwet along p_2. This is in agreement with all the Figs. 15–18.) This does not rule out of the possibility of dewetting. But it can well be that the systems belonging to the fourth category have two minima, one at $l=\infty$ and one at $l=l_0<\infty$, which is the global one. Both minima are then separated by an activation barrier in the effective interface potential. Our results indicate then that towards T_{cep} this activation barrier disappears turning $l=\infty$ from a local minimum into a maximum.

These arguments concern those systems of the fourth category which are on the left-hand side of the vertical dashed line [see Figs. 18(a) and 18(b)]. It is interesting to consider those systems which belong both to the diagonally hatched region with negative slope along p_1 and to the vertically hatched region along p_2. They lie within the triangle formed by the two dashed lines and the dash-dotted line [see, e.g., Figs. 18(a) and 18(b)]. For these systems the possibility of a dewetting transition along p_1 is *not* doomed by the fact that at T_4 $l=\infty$ is also a minimum along p_2. On the contrary, for them $l=\infty$ is a maximum at T_4 along p_2. Thus for $r\leq 0.7$, these systems of the fourth category are indeed candidates for a dewetting transition along p_1. Along p_2 the same systems are candidates for critical wetting [see Figs. 18(a) and 18(b)]. These circumstances are no longer given if p_1 and p_2 are interchanged. Those systems which belong to the fourth category along p_2 have again the aforementioned problem that $l=\infty$ is a minimum at T_4 also along p_1 [see Figs. 17(e) and 17(f)], which impedes—as discussed before—the possibility of a dewetting transition along p_2.

For $r\geq 0.75$ we find three and for $0.60\leq r<0.75$ we find four wetting categories both along p_1 and p_2. A further decrease of r leads to a loss of wetting possibilities. For $r\leq 0.55$ critical wetting is no longer possible along p_1 and for $r\leq 0.50$ there is no possibility any more to avoid that $l=\infty$ is a minimum of the effective interface potential at low temperatures along p_1. For even smaller values of r the vertical dashed line will also disappear [extrapolate Figs. 18(e) and 18(f)]. Consequently, for such small values of r there will be only the possibility of first-order wetting transitions.

These dashed lines are given by $\bar{w}_{AA}=\frac{1}{8}(1+r^{-1})^3$ and $\bar{w}_{BB}=\frac{1}{8}(1+r)^3$, respectively [see Eqs. (2.30), (2.31), (2.35), and (2.36)]. They govern the wetting behavior at low temperatures. For decreasing values of r the vertical dashed line moves to the right, whereas the horizontal dashed line moves downwards. Since the upper-left boundary moves downwards even more rapidly the horizontal dashed line leaves the allowed region for $r<0.55$ [see Figs. 18(c)–18(f)]. The vertical dashed line probably also leaves the allowed region for even smaller values of r.

Finally the dash-dotted line, whose curvature becomes visible on our scale only for $r\leq 0.6$, represents the loci of the points $\bar{C}^*$ which we discussed in Fig. 14. Only for $r=1$ the dotted and the dash-dotted curve coincide [see Figs. 15(a) and 15(b)]. In the case of critical wetting, this line represents those binary liquid mixtures whose wetting transition temperatures coincide with T_{cep}. Along p_1 T_W increases from $T_W=T_4$ at the horizontal dashed line towards $T_W=T_{cep}$ at the dash-dotted curve. Along p_2 this increase occurs from $T_W=T_4$ at the vertical

dashed line.

Before we draw additional conclusions from our data in the discussion following in Sec. V, let us summarize our main findings for the PY model (compare the corresponding summary for the BEG model at the end of the previous section).

(1) As a function of r we have determined which binary liquid mixtures exhibit a simple bulk phase diagram within the PY model.

(2) For $r=1$ we obtain the same qualitative results as for the BEG model (see the end of Sec. III). There are only quantitative differences.

(3) As in the BEG model wetting does occur only along one or the other side of the triple line. However, there are systems whose wetting transition temperatures coincide with T_{cep}; in general, these systems are not those whose number densities of the two liquid phases are equal.

(4) The only remaining symmetry is the one which results from the interchange of the A and B particles.

(5) For equal sizes of the two particles critical wetting is found for those systems whose interactions between like particles are similar. For different sizes of the particles the interaction between the smaller particles must be decreased and between larger particles it must be increased in order to obtain critical wetting.

(6) It is possible that the liquid phase with the higher number density wets the liquid-vapor interface. (This disproves an opposite statement by Lipowsky[68] and consequently some of his conclusions.) This requires the wetting phase to be rich in small particles. In this case and for $r<0.75$ wetting occurs only by the liquid phase with the higher number density.

(7) If the wetting phase is rich in large particles it always has the lower number density.

(8) For $r\leq 0.7$, and if the wetting layer is rich in small particles, there is a possibility for a dewetting transition.

(9) For $r\leq 0.55$ critical wetting is no longer possible by the liquid phase being rich in small particles.

(10) If the sizes of the particles are very different only first-order wetting transitions can occur.

V. DISCUSSION AND CONCLUSION

First let us recall that, as stated in the Introduction, to the best of our knowledge there are only three theoretical studies of interfacial wetting phenomena in binary liquid mixtures, which fully take into account the long-range character of all three interaction potentials.[36–38] These authors explicitly solved the full mean-field equations which result from minimizing the density functional in Eq. (2.1). Since they used the PY model for the reference free energy their results can be compared directly with ours obtained in Sec. IV. They monitored the interfacial profiles of the α-β, α-γ, and β-γ interface (see Fig. 3) along the triple line for the special case $r=1$ and detected interfacial wetting transitions. These authors followed the order of this wetting transition by changing the detailed form of the interaction potentials $\bar{w}_{ij}(r)$ but without changing their integrated strengths $\hat{w}_{ij}$. Therefore, within mean-field theory, all these calculations correspond to a *single* bulk phase diagram, which is completely fixed by $\bar{w}_{AA}$ and $\bar{w}_{BB}$. The locus of these calculations is indicated in Figs. 15(a) and 15(b) which correspond to $r=1$. According to this location, we conclude that wetting can occur only by that liquid phase, which is rich in the less attractive particles. (This corresponds to path p_1 according to our arbitrary choice of denoting those particles with the larger interaction potentials as A particles. The opposite choice would bring the locus on the other side of the diagonal and the role of p_1 and p_2 would be interchanged.) This conclusion is in full agreement with the numerical results in Refs. 36–38. Furthermore, we conclude from Fig. 15(a) that the wetting transition is second order, provided that the next-to-leading-order term in the effective interface potential, i.e., b in Eq. (2.8), is positive. Indeed the authors of Ref. 36 found critical wetting transitions for those interaction potentials which lead to $b(T_W)>0$. [If $b(T_W)$ happens to be negative due to a different choice of the form of the interaction potentials, the wetting transition becomes first order. This has been analyzed in detail in Appendix A of Ref. 9.] Thus, we can conclude that our results are in full agreement with all numerical data of realistic model calculations available at present. Nonetheless Figs. 15–18 demonstrate that such detailed calculations can cover only a vanishing small subset of the possible binary liquid mixtures. Thus, our results relieve one from this dearth.

The comparison between our results and the present available relevant body of experimental data is less straightforward. Until recently there have been only two binary liquid mixtures for which interfacial wetting transitions have been found and which were first order: methanol-cyclohexane (CH_3OH-C_6H_{12}) (Refs. 23–25, and 29) and isopropanol-perfluoromethylcyclohexane (C_3H_7OH-C_7F_{14}) (Refs. 26, 28, and 31). For the first mixture, the wetting transition has been observed only in the presence of small amounts of water, so that one has effectively a ternary mixture (see Ref. 35). Such systems are not covered by our present study. Recently, the data for the second mixture have been augmented by determining the wetting transitions of a series of five other normal alcohols ($C_nH_{2n+1}OH$, $n=0,1,2,4,6$; $n=3$, see above; $n=0$ corresponds to water) mixed with C_7F_{14}.[34] In all these mixtures first-order wetting transitions have been found. This study by Schmidt[34] is particularly valuable because it describes for the first time the dependence of interfacial wetting on systematically changing the molecular properties of one of the particles making up the mixture. This allows one, for example, to follow the ratio of $(T_{cep}-T_W)/T_W$ as function of these systematic changes. Nonetheless, for following reasons, we refrain from comparing our theoretical results with these experimental findings. Besides the problems of (i) purity (see above), as well as of (ii) gravity, and of (iii) the finite number of particles (see the detailed discussion thereof in the Introduction), the following issues play an important role: (iv) The experiments are performed with air as the vapor phase. This raises not only the question of purity but it means in particular that the systems are off the triple line, where our study applies. (v) Furthermore, even if the systems would fulfill these requirements one must

be especially careful to obtain wetting films which are in the thermodynamic equilibrium. If during the experiment a thick wetting layer has been formed, but which is not the equilibrium configuration, it may take very long times until it thins to its equilibrium[69] (see Sec. XII in Ref. 1). However, these problems can be overcome by taking care that during the experiment no wetting films are formed whose thickness is larger than its equilibrium value: the thickening of a thin film is much faster than the thinning of a macroscopicly thick film. Thus, the three-phase coexistence regions must be avoided and the experimental paths should be as indicated in Fig. 1, i.e., slightly of the triple line (see Sec. XII in Ref. 1). (vi) Finally, our theoretical results apply to structureless, spherical particles which interact only via van der Waals forces. Therefore, our model is supposed to work best for mixtures of rare gases. However, such experiments are not yet performed. Obviously, there is a considerable demand of such investigations. But the mixtures used at present consist of particles with a pronounced molecular structure and they are polar. Given the delicate dependence of interfactual properties on microscopic details[1] we therefore adopt the conservative point of view that due to (i)–(vi) the present theory would be stretched too far if we would try a quantitative comparison with these experimental data.

What our results allow us, however, is to draw important conclusions about the trends of the wetting behavior as function of r, which is the ratio of the sizes of the particles B and A. For that purpose we adopt the hypothesis that the ratio between the areas of the various hatched regions in Figs. 15–18 and the area $A_{\rm tot}$ of the whole allowed region gives us the probability $p(r)$ to find the corresponding interfacial wetting behavior in all those binary liquid mixtures which are characterized by that given value of r. These probabilities are displayed in Fig. 19 and give rise to following conclusions.

(1) The chances to find critical wetting are best for $r=0.93$ where they are 64%. It is more likely to find it at the interface between the liquid rich in small particles and the vapor; there the chances are best for $r=0.80$, where they are 40%. For small values of r critical wetting becomes very unlikely [see Fig. 19(c)].

(2) The overall chances to find a first-order wetting transition are complementary to those for critical wetting, because every binary liquid mixture can undergo a wetting transition along one of the two sides of the triple line. Only for small values of r it is more likely to find a first-order wetting transition at the interface between the liquid rich in large particles and the vapor than at the interface with the liquid rich in small particles [see Fig. 19(d)].

(3) For $r \geq 0.6$ it is more likely that the interface between the vapor and the liquid rich in large particles exhibits no wetting transition than the interface involving the liquid rich in small particles. For $r<0.6$ the situation is reversed. Here the absence of a wetting transition means that the effective interface potential $\omega(l)$ has a maximum at $l=\infty$ for all temperatures [see Fig. 19(e)].

(4) Along both sides of the triple line for $r \leq 0.75$ there is an increasing probability for the situation that $l=\infty$ is a minimum of $\omega(l)$ at low temperatures but a maximum close to $T_{\rm cep}$. This is a particular case of nonwetting, which is more likely to occur at the interface between the vapor and the liquid rich in large particles [see Fig. 19(f)].

(5) For $r \leq 0.7$ there is an increasing possibility for a dewetting transition. But this behavior occurs only at the interface between the vapor and the liquid rich in large particles [see Fig. 19(b)].

On the basis of the same hypothesis, Figs. 15–18 also give us some information about the number density of that liquid phase which wets the interface under con-

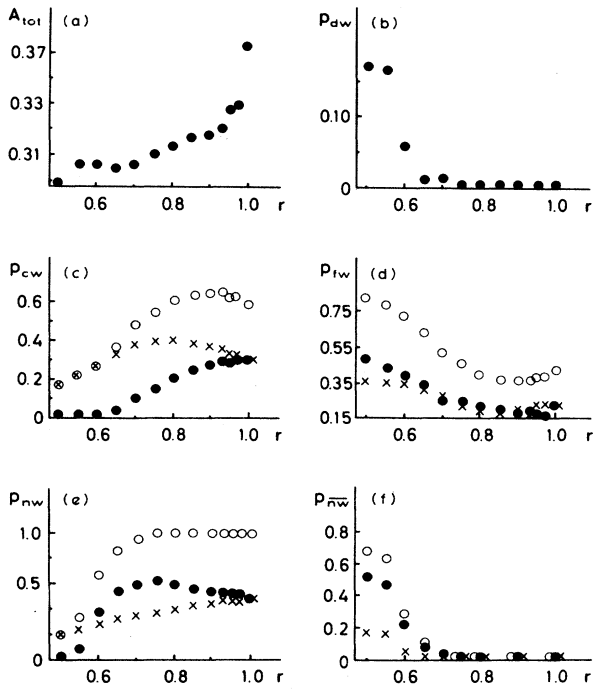

FIG. 19. (a) The total area $A_{\rm tot}$ of the allowed regions shown in Figs. 15–18 shrinks for small values of r. $p=A/A_{\rm tot}$ where A is the area of the various hatched regions in Figs. 15–18. (b) $p_{\rm dw}$ is the probability for dewetting. In this case, A is vertically hatched along path 2 and diagonally with negative slope along path 1 [see Figs. 17(c)–17(f) and 18]. (c) $p_{\rm cw}$ denotes the probability for critical wetting which is indicated by the vertical hatching. (d) First-order wetting with diagonal hatching with positive slope belongs to $p_{\rm fw}$. (e) The horizontal hatching means nonwetting and its probability is denoted as $p_{\rm nw}$. (f) Those systems whose effective interface potential has a minimum at low temperatures but a maximum close to $T_{\rm cep}$ exhibit a particular kind of nonwetting. The probability of their occurrence is denoted as $p_{\overline{\rm nw}}$. The dots correspond to path 1 which describes the interface between the vapor and the liquid phase rich in large particles. The crosses belong to path 2 which corresponds to the interface between the vapor and the liquid phase rich in small particles. The circles give the sum of these two probabilities. Therefore, they indicate the probability that the corresponding wetting behavior (dw, cw, fw, nw, $\overline{\rm nw}$) occurs along either side of the triple line.

sideration. Using the probabilities shown in Fig. 20 we obtain the following additional conclusions.

(6) For all values of r the probability is largest that wetting occurs only by the liquid with the lower number density, which is rich in large particles (see p_{-+} in Fig. 20).

(7) For smaller values of r there is an increasing probability that wetting occurs only by the liquid phase with the higher number density, which is rich in small particles (see p_{+-} in Fig. 20).

(8) For r close to 1 there is the possibility that wetting occurs only by the liquid phase with the lower number density, but which is rich in small particles. This probability vanishes for $r \leq 0.7$ (see p_{--} in Fig. 20).

Our hypothesis for defining the above probabilities is based on the assumption that for a given value of r the possible binary liquid mixtures are homogeneously distributed over the whole allowed region. This requires that $\bar{w}_{AA}$ and $\bar{w}_{BB}$ are independent from each other. However, in the literature one finds several so-called combining rules. These rules express the interaction parameters between unlike particles, i.e., ϵ_{AB} and σ_{AB} [see Eq. (2.34)], in terms of the corresponding ones between like particles, i.e., ϵ_{AA}, σ_{AA}, ϵ_{BB} and σ_{BB}. Besides the very common Lorentz rule for $\sigma_{AB}=(\sigma_{AA}+\sigma_{BB})/2$, various rules for ϵ_{AB} have been suggested:[70,71]

$$\text{(I)}\quad \epsilon_{AB}=\xi(\epsilon_{AA}\epsilon_{BB})^{1/2},\quad 0<\xi\leq 1\ , \tag{5.1a}$$

$$\text{(II)}\quad \epsilon_{AB}=\frac{1}{\sigma_{AB}^6}(\epsilon_{AA}\sigma_{AA}^6\epsilon_{BB}\sigma_{BB}^6)^{1/2}\ , \tag{5.1b}$$

$$\text{(III)}\quad \epsilon_{AB}=2\epsilon_{AA}\epsilon_{BB}/(\epsilon_{AA}+\epsilon_{BB})\ . \tag{5.1c}$$

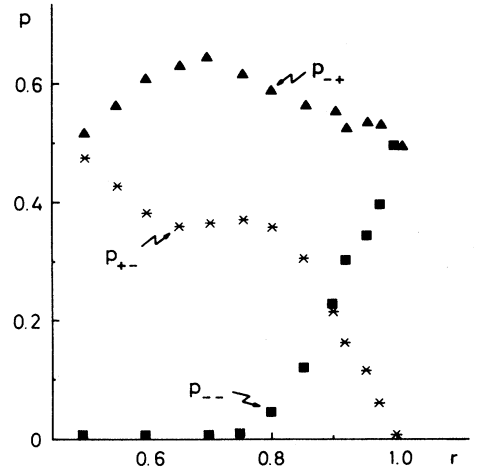

FIG. 20. The probabilities p are defined as ratios of areas: $p_{-+}=A_{-+}/A_{\text{tot}}$ (triangles), $p_{--}=A_{--}/A_{\text{tot}}$ (squares), $p_{+-}=A_{+-}/A_{\text{tot}}$ (stars) [see Fig. 19(a)]. A_{-+} is the area of the region on the left of or above the dash-dotted curve in Figs. 15–18. A_{--} is the area of the region on the right of the dotted curve in Figs. 15–17(b). A_{+-} is the area of the region on the right of or below the dash-dotted curve minus the area A_{--} in Figs. 15–18.

TABLE I. Estimates for the interaction parameters of rare gases taken from Refs. 70, 71, 73, and 77–85. In the lower-left and in the diagonal elements of the table, the first row gives the range of values for ϵ_{ij}/k_B as one finds them in the aforementioned references. The value following the semicolon is the one which we picked as the best one on the basis of these references. The second row gives the range of values for σ_{ij}/Å. Again, after the semicolon stands the apparently most reliable value. The number in parentheses corresponds to $\sigma_{ij}=(\sigma_{ii}+\sigma_{jj})/2$ as obtained from the diagonal. As one can see this combining rule is reliable with the exception of the mixtures with He. In the elements of the table above its diagonal, the first row gives the value of $r=\sigma_{BB}/\sigma_{AA}$, whereas the numbers in the second row give the coordinates $(\bar{w}_{AA},\bar{w}_{BB})$ of the corresponding mixture. For the particularly interesting mixtures Ar/Kr and Kr/Xe [see Figs. 16(b) and 16(c)] we added the error bars on the basis of the scattering of those values given in the diagonal and below. Additional data can be found in Tables 9.12–9.14 of Ref. 75.

Rare gas	He	Ne	Ar	Kr	Xe
He	10–11;11 2.56–2.70;2.65	0.96 (3.19;0.74)	0.79 (8.31;0.32)	0.74 (12.30;0.27)	0.68 (18.75;0.23)
Ne	14 2.87(2.70)	36–43;42 2.74–2.78;2.76	0.82 (2.88;0.47)	0.77 (3.93;0.38)	0.70 (6.16;0.32)
Ar	20–34;24 3.08–3.16;3.12(3.00)	60–72;66 3.05–3.30;3.10(3.06)	119–153;143 3.28–3.42;3.35	$0.93^{+0.03}_{-0.04}$ $(1.39^{+0.21}_{-0.37},0.80^{+0.05}_{-0.14})$	0.85 (1.76,0.55)
Kr	24.7 3.35(3.05)	71.5–74.5;73.5 3.20–3.21;3.21(3.18)	150–170;160 3.39–3.52;3.45(3.47)	163–202;200 3.58–3.70;3.60	$0.92^{+0.03}_{-0.02}$ $(1.44^{+0.27}_{-0.42},0.80^{+0.13}_{-0.21})$
Xe	25.2 3.71(3.15)	73–75;74 3.35–3.46;3.40(3.34)	174–212;200 3.52–3.69;3.62(3.63)	201–233;220 3.57–3.80;3.75(3.76)	220–294;280 3.88–3.98;3.92

For $\xi=1$ Eq. (5.1a) is known as the Berthelot rule. But in most cases $\xi<1$. Equation (5.1c) is called the Fender and Halsey rule.[72] Equation (5.1) implies the following possible relationship between $\overline{w}_{BB}$ and $\overline{w}_{AA}$:

$$\text{(I)}\quad \overline{w}_{BB}=\frac{64}{\xi^2}\frac{r^3}{(1+r)^6}\frac{1}{\overline{w}_{AA}}\ , \tag{5.2a}$$

$$\text{(II)}\quad \overline{w}_{BB}=\frac{(1+r)^6}{64r^3}\frac{1}{\overline{w}_{AA}}\ , \tag{5.2b}$$

$$\text{(III)}\quad \overline{w}_{BB}=\frac{4r^3\overline{w}_{AA}}{(1+r)^3\overline{w}_{AA}-4}\ . \tag{5.2c}$$

Thus, the probability for finding binary liquid mixtures within the allowed region should be enhanced in the vicinity of a hyperbolia $\overline{w}_{BB}(\overline{w}_{AA})$, which may be described by one of the formulas in Eq. (5.2). Thus, in principle, the probabilities should be given not as the ratio of areas but as the ratio of the various line segments along which this hyperbolia intersects the various regions. However, the numerical values of the various formulas in Eq. (5.2) differ from each other considerably and the various calculated and fitted values for ϵ_{AB} scatter significantly around their predicted values in Eq. (5.1). These uncertainties are *inter alia* due to the attempt to parameterize each interaction potential by only two numbers, i.e., ϵ and σ. But the interaction potentials have a more complex structure and therefore require a more detailed description. We refrain to embark into this complicated subject and refer to the ample corresponding literature (see, for example, Refs. 73–76 and references therein). We interpret this scattering of the values of ϵ_{AB} as an indication that the possibilities are not narrowly peaked around such a hyperbolia. Therefore, because the hyperbolia intersects—if it does so at all—the allowed region in a more or less diagonal way from the upper left to the lower right, the ratios between areas and the rations between segments should not differ too much. Thus, the numerical values of the probabilities shown in Figs. 19(b)–19(f) and 20 should not be taken too serious, but their qualitative behavior as function of r is expected to be more reliable.

As already pointed out, our calculations should be most reliable for simple particles like, e.g., the rare gases. On the basis of our estimates for their interaction parameters (see Refs. 70, 71, 73, and 77–85) as given in Table I and according to Figs. 15–18, we conclude that the Ar/Kr and the Kr/Xe mixture might be candidates for interfacial wetting [see Figs. 16(b) and 16(c)] provided that their bulk phase diagram looks like the one in Fig. 2(a) and not as in Fig. 2(c)—which cannot be decided on the basis of the PY model. These mixtures should lie on the left-hand side of the dotted line in Figs. 16(b) and (c), because $\rho_{\mathrm{Xe}}^{(0)}<\rho_{\mathrm{Kr}}^{(0)}<\rho_{\mathrm{Ar}}^{(0)}$. According to Figs. 16(b) and 16(c) we would expect that in the Ar/Kr mixture the Ar-rich-liquid–vapor interface is not wetted by the Kr-rich-liquid phase, and that in the Kr/Xe mixture the Xe-rich-liquid phase does not wet the Kr-rich-liquid–vapor interface. However, wetting should occur by the Ar-rich liquid in the Ar/Kr mixture and by the Kr-rich liquid in the Kr/Xe mixture. Thus, in both cases, the wetting phase has the higher number density and is rich in the smaller particles. Consequently, the wetting film has the lower mass density and its observation would require a setup as described in Fig. 6. [Note that in the model calculation by Tarazona *et al.*[36,37] (see also Figs. 15(a) and 15(b)], which was confined to $r=1$, the authors were able to produce gravity-thinned wetting layers having a lower number density but a higher mass density only by assuming that the particles with the stronger mutual attraction have the smaller mass. But this is not possible for rare gases for which both the size and the interaction strength scale with the mass. For that reason mixtures of rare gases have the property $\overline{w}_{AA}>\overline{w}_{BB}$ (see Table I).] The Kr/Xe mixture might be a candidate for critical wetting, whereas in the Ar/Kr mixture the wetting transition would probably be first order. But since the horizontal dashed line in Fig. 16, which describes the separatrix between first-order and critical wetting, is only obtained by a crude approximation of the behavior of the system at low temperatures [see Eq. (2.30)], its own error bars may well overlap with the rectangle in Fig. 16(b) so that the possibility of a critical wetting transition would not be ruled out completely even for the Ar/Kr mixture.

The experimental data check with our theoretical predictions for the bulk properties. First, the bulk phase diagram of the Ar/Kr mixture turns out to be of the type shown in Fig. 2(c),[86,87] which has been called type I in the nomenclature of Scott and Konynenburg[88,89,86] (see Fig. 21). According to Fig. 16(b) the Ar/Kr mixture lies either within the allowed region—these corresponding phase diagrams have been called type II (Refs. 88, 89, and 86) (see Fig. 21)—or below. In the latter case one expects indeed type I phase diagrams according to Fig. 22. (Although Fig. 22 holds only for $r=1$ we expect this to remain true also for $r=0.93$.) But we cannot expect that a theory, which does not contain the melting transition—like the PY or the van der Waals equation of state—predicts correctly the separatrix between type-I and type-II phase diagrams. Within these limitations we are therefore pleased to see that the PY model predicts correctly that the bulk phase diagram of the Ar/Kr mixture is either of type I or II. The experimental fact that it is of type I means that due to the missing triple line no interfacial wetting with all phases being fluid can occur for this mixture.

Second, the mixtures He/Xe (Refs. 90 and 86), Ne/Ar (Refs. 91, 92, and 86), Ne/Kr (Refs. 93 and 86), and Ne/Xe (Refs. 94–97) have been found to exhibit type-III bulk phase diagrams (see Fig. 21). According to the entries in Table I all these systems lie far to the right of the allowed region of type-II mixtures in Figs. 16 and 17, where, on the basis of Fig. 22, indeed type-III systems are expected to lie. These systems do have a triple line where fluid phases meet and where interfacial wetting phenomena can occur. But in these systems at T_{cep} the difference between the vapor and one liquid phase vanishes, whereas we have focused in this paper on the situation in which at T_{cep} the difference between the two liquid phases vanishes. The study of interfacial wetting phenomena of type-III mixtures would be a natural extension of our present work.

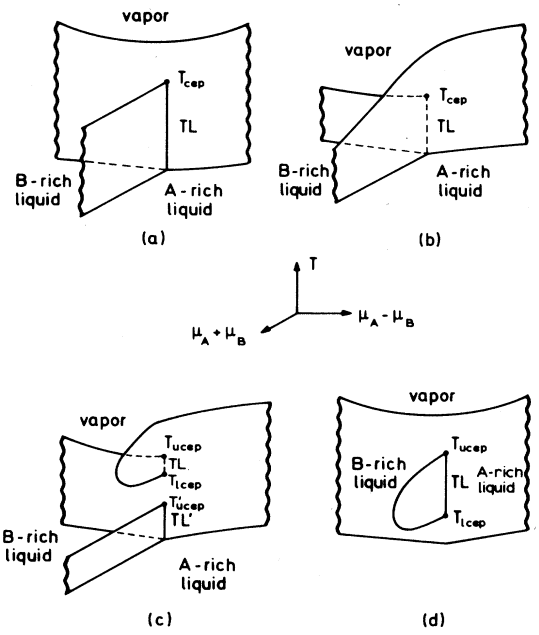

FIG. 21. According to Refs. 88, 89, 50, and 86, there are six main types of bulk phase diagrams for binary liquid mixtures which are denoted as I–IV. (Additional types are mentioned in Fig. 22.) (a) represents I and II. In type I the phase separation between the two liquid phases is missing. Here we have focused on type II (see Fig. 2). If the critical end point T_{cep} in the diagram of type III, (b), is approached along the triple line TL, the interface between the vapor and the B-rich liquid vanishes with the A-rich liquid acting as the spectator phase. (Correspondingly, in type II the vapor acts as a spectator phase.) In the phase diagram of type IV, (c), the critical line of the coexistence sheet between the vapor phase and the A-rich liquid does not extend to arbitrary large values of $\mu_A+\mu_B$ [as it does in (b)] but bends back to form a lower critical end point T_{lcep} at the triple line TL which in turn ends at an upper critical end point T_{ucep}. In addition, at lower temperatures there is a coexistence sheet between the A-rich and B-rich liquid [as in (a)] leading to a second triple line TL′ and a second upper critical end point T'_{ucep}. In phase diagrams of type V this latter coexistence sheet is missing. In binary liquid mixtures of type VI, (d), the two liquid phases are immiscible only for $T_{lcep}<T<T_{ucep}$ and for finite values of $\mu_A+\mu_B$. Such systems are characterized by hydrogen bonds and cannot be described by van der Waals type of theories. If the critical line between the vapor phase and the A-rich liquid has a global maximum as a function of temperature for finite values of μ_A and μ_B (i.e., above the critical points of both the pure A and B liquid), it is said that these systems exhibit gas-gas immiscibility of the first or second kind for (b) and of the third kind for (a). The distinction between types I and II and between types IV and V, respectively, is obtained by extending the van der Waals equation of state down to $T=0$ without taking into account the possibility of solidification. However, on the basis of Fig. 2 one has to expect that many binary liquid mixtures termed as type II or type IV, respectively, are in fact of type I or type V, respectively, because T_{cep} or T'_{ucep} can be preempted by the formation of a solid phase. Since we are interested in the interfacial wetting behavior along the triple line of a simple binary liquid mixture we confined our analysis to type II.

Figure 21 gives us the opportunity to make contact with the work by Scott and van Konynenburg[88,89] and Furman and Griffiths[98] who explored the possible phase diagrams of binary liquid mixtures for the special case $r=1$ by applying the van der Waals (vdW) equation of state. Figure 22 compares our results, which were obtained by using the PY model, with their vdW findings for the case $r=1$ where comparison is possible. Scott and

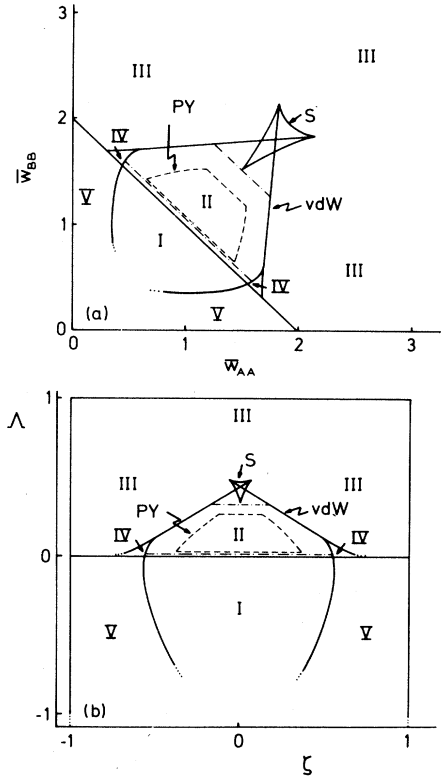

FIG. 22. Regions in parameter space $(\bar{w}_{AA},\bar{w}_{BB})$, (a), and (ζ,Λ), (b), which, in the case of equal core radii $r=1$, correspond to the type of phase diagrams I–V shown in Figs. 1, 2, and 21. Types I and II correspond to those shown in Figs. 2(a) and 2(c), respectively. In the shield region S the change from type II to type III occurs via a series of minor variants of types II and III interpolated between the two main types (Ref. 98). The type IV* is omitted, which occurs in negligible small regions close to the points where II, III, and IV meet (Refs. 86 and 98). Type VI is not found for van der Waals systems. Such phase diagrams require highly nonspherical molecules involving hydrogen bonds. The solid lines are obtained from the solution of the generalized van der Waals equation of state (Refs. 88, 89, 98, and 86). The dashed lines give the boundaries of the region corresponding to the type II which we obtained by using the PY theory [see Fig. 15(a)]. We focused on type II and followed the dashed lines as a function of r (see Figs. 15–18). The upper dash-dotted line indicates the implementation of our rule to avoid the shield region S, here applied to the van der Waals equation of state. Between the lower dash-dotted line and the boundary between I and II systems lie with $\bar{K}>100$, which we discarded for numerical reasons. The PY theory predicts a considerably smaller region of type-II phase diagrams than the van der Waals (vdW) theory and, *a fortiori*, than the BEG model [see Fig. 11(b)] does.

van Koynenburg used the parameters

$$\zeta=(\bar{w}_{BB}-\bar{w}_{AA})/(\bar{w}_{AA}+\bar{w}_{BB})$$

and

$$\Lambda=(\bar{w}_{AA}+\bar{w}_{BB}-2)/(\bar{w}_{AA}+\bar{w}_{BB}) ,$$

which vary between -1 and $+1$ and $-\infty$ and $+1$, respectively. In terms of our variables

$$\bar{w}_{AA}=(1-\zeta)/(1-\Lambda)$$

and

$$\bar{w}_{BB}=(1+\zeta)/(1-\Lambda)$$

we have $\zeta=-2\bar{C}/(\bar{K}+1)$, $\Lambda=2/(\bar{K}+1)$, $\bar{C}=-\zeta/\Lambda$, and $\bar{K}=-1+2/\Lambda$. Our analysis is restricted to $\hat{J}>0$, which means $\Lambda>0$. Figure 22 shows that the PY model predicts a significantly smaller region for type-II mixtures than the vdW model does. Figures 15–18 show how this region evolves as a function of r.

At the end of this section we want to make some remarks about the role of the capillary waves which occur at the α-β and at the β-γ interface. As already stated in the Introduction, their entropic contribution to the effective interface potential is, as function of l, exponentially small and can be neglected in systems with long-range forces. However, due to the hydrodynamic motion the dispersion relation of the capillary waves depends on the thickness of the wetting layer. If one calculates the free energy of these capillary waves of a thin film by treating them as a noninteracting Bose gas[99,100] one obtains, in the case of a wetting film on a wall, a negative contribution of the capillary waves to the Hamaker constant, which tends to thin the wetting film.[101] At low temperatures this contribution is negligible small compared with the Hamaker constant and one can ignore it. However, in contrast to the Hamaker constant, this additional term has been claimed not to vanish at the critical point and thus to become dominant close to T_c.[101] By using the dispersion relations for a wetting film with two fluid interfaces[102] one could extend this analysis in Refs. 100 and 101 to the case of interfacial wetting as considered here. But from a quantitative analysis,[103] it turns out that this predicted contribution of the capillary waves to the effective interface potential close to the critical point is already in direct conflict with the experimental results for the wetting of a wall.[45] Thus, we note that this aspect of the capillary waves deserves further investigations. In particular, one has to study to which extent the capillary waves can still be treated as a noninteracting Bose gas even close to the critical point where the damping diverges due to divergence of the viscosity. Another open question is to what extent one is allowed to simply add these contributions of the capillary waves to the effective interface potential as calculated here (see below). In any case we note that, apart from these subtleties close to the critical point, the numerical contributions due to the capillary waves would be negligible small.

At this point we take the opportunity to state some general remarks concerning the effective interface potential $\omega(l)$ [see Eq. (2.7)]. The usual approach is to calculate it within MFT in a first step. In the case of long-range forces this is a rather demanding task. In a subsequent second step one tries to incorporate at least some of those fluctuations ignored by the MFT used in the first step. This includes basically two types of fluctuations: (i) those which are typical for bulk systems and which cause the bulk properties to deviate from their MFT approximates; (ii) fluctuations of the interface around its planar form assumed within MFT. The influence of (i) on $\omega(l)$ has not been studied thoroughly. One reason is that these fluctuations are important only in a relatively small neighborhood of T_c, where the drumhead model for the interface is starting to break down anyway due to the formation of bubbles and overhangs. As long as the wetting phenomena do not interfere strongly with these bulk critical phenomena one can surmise that the main effects of the bulk fluctuations may be taken into account by replacing the MFT values of the bulk densities entering $\omega(l)$ by their actual values. Since, in three spatial dimensions and in the absence of gravity, fluid interfaces are always rough, the fluctuations of type (ii) must be taken into account seriously even away from T_c. There are basically two lines of attack which can be followed to accomplish this.

The first one is that one devises a solid-on-solid model such that the interface fluctuates under the action of the effective interface potential as obtained from MFT. By applying renormalization-group techniques the solution of this statistical model yields a renormalized effective interface potential $\omega_R(l)$ which now includes the fluctuations of the interface known as capillary waves. In the presence of long-range forces and in three bulk spatial dimensions it turns out that $\omega(l)-\omega_R(l)\sim\exp(-l/\xi_b)$, where ξ_b is the bulk correlation length, thus leaving the power-law terms in $\omega(l)$ unchanged by the capillary waves.[104,21,105] Therefore, within this approach,[106] which is based solely on statistical mechanics and which is completely independent from the dynamic laws of motion behind it, the expression of the coefficient a we used here appears to be exact.

The second line of attack to include the interface fluctuations is to use explicitly the laws of motion, here hydrodynamics, in order to obtain the dynamic Green's function for those collective modes which are considered to be the relevant ones, here the capillary waves. The general rule to calculate, including damping, the free energy from the dynamic Green's function can be found in Ref. 107 and in the references therein. It is this approach which has been taken by Mikheev[101] and Chatterjee *et al.*,[100] although they did not apply the formula given in Ref. 107, which guarantees certain consistency properties which are not fulfilled otherwise. If one denotes $\omega_R'(l)$ as the effective interface potential as obtained along this dynamic route (and disregarding the ignorance of the damping by these authors), one finds $\omega(l)-\omega_R'(l)\sim l^{-2}$ in sharp contrast to the results quoted above.

One has to say that, in general, the improvements of MFT along these two lines of attack, i.e., $\omega_R(l)$ and $\omega_R'(l)$, cannot be expected to be consistent and that *a priori* it is not clear which of the two is the better one. However, it is known that the predictions of the dynamic

approach are poor for the free energy unless there is a particular pronounced peak structure in the frequency spectrum of the Green's function. Another worrisome feature of the dynamic approach in its simplest version, as applied in Refs. 100 and 101, is that it predicts power-law contributions to $\omega_R(l)$ irrespective of whether the liquid obeying the hydrodynamic equations is formed by molecules interacting via short-range or via long-range forces. Within the static approach it is known that this difference is of crucial importance for the wetting behavior.

Let us close by recalling that our main findings and conclusions are summarized at the end of Secs. III and IV and by the remarks (1)–(8) in this section.

Note added in proof. It is a pleasure for us to quote the paper by E. J. Ding and E. H. Hauge, Physica **A155**, 189 (1989), whose manuscript we received after submission of our present paper. In their paper Ding and Hauge strive for a systematic and analytic study of interfacial wetting properties in binary liquid mixtures governed by short-range forces.

ACKNOWLEDGMENTS

We are particularly indebted to Professor H. Wagner for numerous fruitful discussions and helpful comments. Major parts of this work have been performed in the stimulating atmosphere of his group in the Physics Department of the University of Munich. We are also grateful for discussions with Dr. W. Fenzl, who pointed out to us several references, Professor H. Frisch, and Dr. U. Seifert.

APPENDIX A: DENSITY FUNCTIONAL

The binary mixture is described by the position variables $\{\mathbf{r}_{A,1},\ldots,\mathbf{r}_{A,N_A};\mathbf{r}_{B,1},\ldots,\mathbf{r}_{B,N_B}\}$ and the momenta $\{\mathbf{p}_{A,1},\ldots,\mathbf{p}_{A,N_A};\mathbf{p}_{B,1},\ldots,\mathbf{p}_{B,N_B}\}$. The corresponding Hamiltonian $\mathcal{H}$ is given by

$$\mathcal{H}=\mathcal{T}+\mathcal{U}+\mathcal{V} . \tag{A1}$$

With $i=A,B$ the kinetic energy is

$$\mathcal{T}=\sum_i \sum_{k=1}^{N_i} p_{i,k}^2/(2m_i) . \tag{A2}$$

We assume that the potential energy $\mathcal{U}$ is the sum of pair potentials $w_{AA}(\mathbf{r}_A-\mathbf{r}'_A)$, $w_{BB}(\mathbf{r}_B-\mathbf{r}'_B)$, and $w_{AB}(\mathbf{r}_A-\mathbf{r}_B)$ with $w_{ij}(\mathbf{r}_i-\mathbf{r}_j)=w(\mathbf{r}_j-\mathbf{r}_i)$:

$$\mathcal{U}=\tfrac{1}{2}\sum_{i,j}\sum_{k=1}^{N_i}{\sum_{l=1}^{N_j}}' w_{ij}(\mathbf{r}_{i,k}-\mathbf{r}_{j,l}) . \tag{A3}$$

The sum in (A3) is restricted so that $k\neq l$ if $i=j$. It should be noted that for certain aspects three-body contributions must be taken into account (see, e.g., Refs. 75 and 108–110); here we disregard them. The last term in Eq. (A1) represents an external potential acting on the fluid. It may stem from the container walls of the fluid,

$$\mathcal{V}=\sum_i \sum_{k=1}^{N_i} V_i^{\text{ext}}(\mathbf{r}_{i,k}) , \tag{A4}$$

and leads to nonuniform, equilibrium density configurations

$$\rho_{0,i}(\mathbf{r})=\mathrm{Tr}\{f_0\hat{\rho}_i(\mathbf{r})\}=\langle\hat{\rho}_i(\mathbf{r})\rangle , \tag{A5}$$

where

$$\hat{\rho}_i(\mathbf{r})=\sum_{k=1}^{N_i}\delta(\mathbf{r}-\mathbf{r}_{i,k}) , \tag{A6}$$

and where Tr is the classical grand canonical trace

$$\mathrm{Tr}=\sum_{N_A=0}^{\infty}\sum_{N_B=0}^{\infty}[h^{3(N_A+N_B)}N_A!N_B!]^{-1}\times\int\prod_{k=1}^{N_A}d^3r_{A,k}\,d^3p_{A,k}\times\int\prod_{l=1}^{N_B}d^3r_{B,l}\,d^3p_{B,l} . \tag{A7}$$

f_0 is the equilibrium probability density for N_A A particles and N_B B particles in a system of volume V at temperature T exposed to the chemical potential μ_A and μ_B, respectively [$\beta=(k_BT)^{-1}$]:

$$f_0=\mathcal{Z}^{-1}\exp\left[-\beta\left[\mathcal{H}-\sum_i\mu_iN_i\right]\right] . \tag{A8}$$

$\mathcal{Z}$ is the grand canonical partition function,

$$\mathcal{Z}=\mathrm{Tr}\exp\left[-\beta\left[\mathcal{H}-\sum_i\mu_iN_i\right]\right] , \tag{A9}$$

so that $\mathrm{Tr}f_0=1$ and

$$\Omega_0=-k_BT\ln\mathcal{Z}=\Omega_0(T,V,\mu_A,\mu_B) \tag{A10}$$

is the grand canonical potential. Following Evans[42] one now considers the functional

$$\Omega[f]:=\mathrm{Tr}\left[f\left[\mathcal{H}-\sum_i\mu_iN_i+\beta^{-1}\ln f\right]\right] , \tag{A11}$$

where f is any probability density with $\mathrm{Tr}f=1$. One has[42]

$$\Omega_0=\min_f\Omega[f] . \tag{A12}$$

$f_0[V_i^{\text{ext}}(\mathbf{r})]$ is a unique functional of $V_i^{\text{ext}}(\mathbf{r})$ [see Eqs. (A1), (A4), (A8), and (A9)]. To each pair of external potentials $V_i^{\text{ext}}(\mathbf{r})$ corresponds one and only one pair of density profiles $\rho_{0,i}(\mathbf{r},[V_i^{\text{ext}}(\mathbf{r})])$ [see Eq. (A5)], so that this relationship can be inverted: V_i^{ext} can be expressed in terms of $\rho_{0,i}$ which we denote as

$$V_i^{\text{ext}}(\mathbf{r})=W_i(\mathbf{r},[\rho_{0,i}(\mathbf{r})]) .$$

Thus,

$$f_0[V_i^{\text{ext}}(\mathbf{r})]=f_0[W_i(\mathbf{r},[\rho_{0,i}(\mathbf{r})])]$$

can be expressed as functional of the equilibrium density profiles: $f_0=f_0[\rho_{0,i}(\mathbf{r})]$. This enables us to define a new quantity

$$\mathcal{F}[\rho_i]:=\mathrm{Tr}\{f_0[\rho_i](\mathcal{T}+\mathcal{U}+\beta^{-1}\ln f_0[\rho_i])\} , \tag{A13}$$

where arbitrary densities ρ_i have replaced $\rho_{0,i}$ as the ar-

gument of f_0. With Eq. (A13) one can now define another variational function

$$\Omega[\rho_i]:=\mathcal{F}[\rho_i]+\sum_i \int d^3r\,\rho_i(\mathbf{r})(V_i^{\mathrm{ext}}(\mathbf{r})-\mu_i)\ , \tag{A14}$$

which, in analogy to Eq. (A12), has the property that

$$\Omega_0=\min_{\rho_i}\Omega[\rho_i]\ , \tag{A15}$$

and that those density profiles, which minimize $\Omega[\rho_i]$, represent the equilibrium configurations $\rho_{0,i}(\mathbf{r},T,\mu_A,\mu_B)$.

In the next step one tries to find an explicit expression for $\mathcal{F}[\rho_i]$. For that purpose one starts from

$$\left.\frac{\delta\mathcal{F}[\rho_i]}{\delta w_{ij}(\mathbf{r}_1,\mathbf{r}_2)}\right|_{\rho_i=\rho_{0,i}}=\left.\frac{\delta\Omega[\rho_i]}{\delta w_{ij}(\mathbf{r}_1,\mathbf{r}_2)}\right|_{\rho_i=\rho_{0,i}}=\frac{\delta\Omega_0}{\delta w_{ij}(\mathbf{r}_1,\mathbf{r}_2)}$$
$$=\tfrac{1}{2}\rho_{0,ij}^{(2)}(\mathbf{r}_1,\mathbf{r}_2)\ . \tag{A16}$$

The first equality is due to Eq. (A14), the second one is based on Eq. (A15), and the third one follows from Eq. (A10). $\rho_{0,ij}^{(2)}(\mathbf{r}_1,\mathbf{r}_2)$ is the equilibrium two-particle density (or the pairwise distribution function):

$$\rho_{0,ij}^{(2)}(\mathbf{r}_1,\mathbf{r}_2)=\left\langle \sum_{k=1}^{N_i}\sum_{l=1}^{N_j}{}'\delta(\mathbf{r}_1-\mathbf{r}_{i,k})\delta(\mathbf{r}_2-\mathbf{r}_{j,l})\right\rangle$$
$$=\langle\rho_i(\mathbf{r}_1)\rangle\langle\rho_j(\mathbf{r}_2)\rangle g_{0,ij}^{(2)}(\mathbf{r}_1,\mathbf{r}_2)\ . \tag{A17}$$

The double sum is restricted to $k\neq l$ for $i=j$. The second equality in Eq. (A17) defines the equilibrium two-particle distribution function $g_{0,ij}^{(2)}(\mathbf{r}_1,\mathbf{r}_2)$, which reduces to the radial distribution function in the isotropic case. The two-particle density $\rho^{(2)}$ is related to the density-density correlation function

$$G_{0,ij}(\mathbf{r}_1,\mathbf{r}_2)=\langle(\hat{\rho}_i(\mathbf{r}_1)-\rho_{0,i}(\mathbf{r}_1))(\hat{\rho}_j(\mathbf{r}_2)-\rho_{0,j}(\mathbf{r}_2))\rangle \tag{A18}$$

via

$$G_{0,ij}(\mathbf{r}_1,\mathbf{r}_2)=\rho_{0,ij}^{(2)}(\mathbf{r}_1,\mathbf{r}_2)$$
$$-\rho_{0,i}(\mathbf{r}_1)\rho_{0,j}(\mathbf{r}_2)+\delta_{ij}\delta(\mathbf{r}_1-\mathbf{r}_2)\rho_{0,i}(\mathbf{r}_1)\ . \tag{A19}$$

G contains a δ function, $\rho^{(2)}$ does not. Finally, let us define the pair correlation function

$$h_{0,ij}(\mathbf{r}_1,\mathbf{r}_2)=g_{ij}^{(2)}(\mathbf{r}_1,\mathbf{r}_2)-1\ , \tag{A20}$$

which vanishes for $|\mathbf{r}_1-\mathbf{r}_2|\to\infty$, and the direct correlation function

$$c_{0,ij}^{(2)}(\mathbf{r}_1,\mathbf{r}_2)=[\rho_{0,i}(\mathbf{r}_1)]^{-1}\delta_{ij}\delta(\mathbf{r}_1-\mathbf{r}_2)+G_{0,ij}^{-1}(\mathbf{r}_1,\mathbf{r}_2)\ , \tag{A21}$$

which is given by the (matrix) inverse of the density-density correlation function.

Equation (A16) can now be functionally integrated with respect to the pair potentials along a certain path in function space:[42]

$$\mathcal{F}[\rho_{0,i}]=\mathcal{F}_r[\rho_{0,i}]+\tfrac{1}{2}\sum_{i,j}\int_0^1 d\alpha_{ij}\int d^3r_1\int d^3r_2\rho_{0,ij}^{(2)}(w_{\alpha_{ij}};\mathbf{r}_1,\mathbf{r}_2)(w_{ij}(\mathbf{r}_1,\mathbf{r}_2)-w_{r,ij}(\mathbf{r}_1,\mathbf{r}_2))\ , \tag{A22}$$

with

$$w_{\alpha_{ij}}:=w_{r,ij}(\mathbf{r}_1,\mathbf{r}_2)+\alpha_{ij}(w_{ij}(\mathbf{r}_1,\mathbf{r}_2)-w_{r,ij}(\mathbf{r}_1,\mathbf{r}_2))\ . \tag{A23}$$

$\mathcal{F}_r[\rho_{0,i}]$ corresponds to a reference system in which the particles interact with pair potentials $w_{r,ij}$ and in which the equilibrium densities would be $\rho_{r,i}$; here, however, $\rho_{r,i}$ are replaced by $\rho_{0,i}$ which correspond to the pair potentials w_{ij}.

Putting aside the possibility of three-body interactions the above approach is exact. The whole problem has now been shifted to evaluating $\rho_{0,ij}^{(2)}(w_{\alpha_{ij}};\mathbf{r}_1,\mathbf{r}_2)$ for all interaction potentials in Eq. (A23) with $0\le\alpha_{ij}\le 1$. Here we make now the following approximation:

$$\rho_{0,ij}^{(2)}(w_{\alpha_{ij}};\mathbf{r}_1,\mathbf{r}_2)\simeq\rho_{0,i}(\mathbf{r}_1)\rho_{0,j}(\mathbf{r}_2)\ . \tag{A24}$$

Thus, we replace $\rho^{(2)}$ by its asymptotic value for $|\mathbf{r}_1-\mathbf{r}_2|=\infty$. *Inter alia*, this implies that the critical properties of the fluid are only captured within mean-field theory. Whether the possibility of solidification of the fluid is still captured depends in the ability to evaluate properly $\mathcal{F}_r[\rho_{0,i}]$ for the inhomogeneous reference system (see below and Appendix B). Thus, we obtain

$$\mathcal{F}[\rho_{0,i}]=\mathcal{F}_r[\rho_{0,i}]+\tfrac{1}{2}\sum_{i,j}\int d^3r_1\int d^3r_2\rho_{0,i}(\mathbf{r}_1)\rho_{0,j}(\mathbf{r}_2)\tilde{w}_{ij}(\mathbf{r}_1,\mathbf{r}_2)\ , \tag{A25}$$

where

$$\tilde{w}_{ij}(\mathbf{r}_1,\mathbf{r}_2)=w_{ij}(\mathbf{r}_1,\mathbf{r}_2)-w_{r,ij}(\mathbf{r}_1,\mathbf{r}_2)\ . \tag{A26}$$

Combining Eqs. (A14), (A25), and (A26) and replacing $\rho_{0,i}$ by arbitrary densities ρ_i gives Eq. (2.1), provided one has

$$\mathcal{F}_r[\rho_{0,i}]=\int d^3r\,f_h(\rho_{0,i}(\mathbf{r}),T)\ . \tag{A27}$$

For studies of interfacial wetting V_i^{ext} is omitted and replaced by appropriate boundary conditions.

Equation (A27) states that the Helmholtz free energy of the inhomogeneous reference system [see Eq. (A14)] is

obtained by integrating an appropriate Helmholtz free-energy density of a homogeneous system whose constant densities have been replaced by the actual inhomogeneous densities. This local-density approximation is known to fail in reproducing correctly sharp density variations as they occur in a solid or close to a hard wall. In this paper, however, we deal only with smooth fluid interfaces without density oscillations (see Sec. III B in Ref. 1), so that the local-density approximation is appropriate for the present study.

APPENDIX B: REFERENCE SYSTEM

According to Eq. (A22) we have to determine the reference free energy $\mathcal{F}_r[\rho_{r,i}]$ for an inhomogeneous fluid, whose particles interact via the pair potentials $w_{r,ij}$. In Eq. (A22) $\mathcal{F}_r[\rho_{r,i}]$ enters by replacing the arguments $\rho_{r,i}(\mathbf{r})$ by $\rho_{0,i}(\mathbf{r})$. In order to obtain the reference free energy of the *inhomogeneous* fluid, we apply the local-density approximation:

$$\mathcal{F}_r[\rho_{r,i}]=\int d^3r\, f_r(\rho_{r,i}(\mathbf{r}))\ , \tag{B1}$$

where $f_r(\rho_{r,i})$ is the bulk free-energy density for a *homogeneous* fluid whose particles interact with $w_{r,ij}$. Up to here $w_{r,ij}$ are not yet specified. For Lennard-Jones fluids as considered here it has turned out that the following choice for $w_{r,ij}$ due to Weeks *et al.*[111,112] yields a satisfactory description:[113]

$$w_{r,ij}(r)=\begin{cases}4\epsilon_{ij}[(\sigma_{ij}/r)^{12}-(\sigma_{ij}/r)^6]+\epsilon_{ij} & \text{for } r/\sigma_{ij}\le 2^{1/6},\\ 0 & \text{for } r/\sigma_{ij}\ge 2^{1/6}\ .\end{cases} \tag{B2}$$

With this choice Eq. (2.34) follows from Eqs. (A26) and (B1).

Thus, the reference system is characterized by purely repulsive but smoothly varying interaction potentials. This system is still too difficult to solve analytically. Instead, as a further approximation, $f_r(\rho_{r,i})$ is expressed in terms of free-energy density $f_h(\rho_{h,i})$ of a mixture of hard speres with diameters R_A and R_B, respectively,

$$f_r(\rho_{r,i})\simeq f_h(\rho_{h,i}=\rho_{r,i})\ , \tag{B3}$$

where the densities $\rho_{h,i}$ correspond to a fluid whose particles interact with pair potentials

$$w_{h,ij}(r)=\begin{cases}\infty & \text{for } r\le R_{ij}\ ,\\ 0 & \text{for } r>R_{ij}\ .\end{cases} \tag{B4}$$

Equation (B3) requires that the parameters R_{ij} are known functionals of $w_{r,ij}(r)$. Since Eq. (B3) is valid only approximately there are several ways to implement this relation, which have repercussions on the accuracy of the approximation in Eq. (B3). In order to establish this relation we follow the same procedure as in Appendix A but now for the reference free energy [see Eq. (A16)]:

$$\frac{\delta\mathcal{F}_r[\rho_i]}{\delta w_{r,ij}(\mathbf{r}_1,\mathbf{r}_2)}=\tfrac{1}{2}\rho^{(2)}_{r,ij}(\mathbf{r}_1,\mathbf{r}_2)\ . \tag{B5}$$

It is useful to introduce the smoothly varying and shifted Boltzmann factor [$\beta=(k_BT)^{-1}$],

$$f_{r,ij}(\mathbf{r}_1,\mathbf{r}_2)=\exp(-\beta w_{r,ij}(\mathbf{r}_1,\mathbf{r}_2))-1\ , \tag{B6}$$

which vanishes for $|\mathbf{r}_1-\mathbf{r}_2|\ge 2^{1/6}\sigma_{ij}$; otherwise it is close to -1. With

$$\frac{\delta\mathcal{F}_r[\rho_i]}{\delta f_{r,ij}(\mathbf{r}_1,\mathbf{r}_2)}=\sum_{k,l}\int d^3r_3\int d^3r_4\frac{\delta\mathcal{F}_r[\rho_i]}{\delta w_{r,kl}(\mathbf{r}_3,\mathbf{r}_4)}\times\frac{\delta w_{r,kl}(\mathbf{r}_3,\mathbf{r}_4)}{\delta f_{r,ij}(\mathbf{r}_1,\mathbf{r}_2)} \tag{B7}$$

and

$$f_{\gamma_{ij}}:=f_{h,ij}(\mathbf{r}_1,\mathbf{r}_2)+\gamma_{ij}(f_{r,ij}(\mathbf{r}_1,\mathbf{r}_2)-f_{h,ij}(\mathbf{r}_1,\mathbf{r}_2))\ , \tag{B8}$$

where

$$\begin{aligned}f_{h,ij}(\mathbf{r}_1,\mathbf{r}_2)&=\exp(-\beta w_{h,ij}(\mathbf{r}_1,\mathbf{r}_2))-1\\ &=-1 \quad \text{for } |\mathbf{r}_1-\mathbf{r}_2|\le R_{ij}\\ &=0 \quad \text{for } |\mathbf{r}_1-\mathbf{r}_2|>R_{ij}\ ,\end{aligned} \tag{B9}$$

the integration of the expression in Eq. (B7) taken for arbitrary $f_{ij}(\mathbf{r}_1,\mathbf{r}_2)$ between $f_{h,ij}$ and $f_{r,ij}$ along the path given by Eq. (B8) yields due to Eq. (B5)

$$\mathcal{F}_r[\rho_i]=\mathcal{F}_h[\rho_i]-\frac{1}{2\beta}\sum_{i,j}\int_0^1 d\gamma_{ij}\int d^3r_1\int d^3r_2\rho^{(2)}_{ij}(f_{\gamma_{ij}};\mathbf{r}_1,\mathbf{r}_2)(f_{\gamma_{ij}}(\mathbf{r}_1,\mathbf{r}_2)+1)^{-1}(f_{r,ij}(\mathbf{r}_1,\mathbf{r}_2)-f_{h,ij}(\mathbf{r}_1,\mathbf{r}_2))\ . \tag{B10}$$

In the next step, we expand the pairwise distribution function $\rho^{(2)}(f_{\gamma_{ij}})$ in terms of the blip functions $\Delta f_{ij}=f_{r,ij}-f_{h,ij}$.[113] Keeping only the lowest-order term and by using the analog of Eq. (A17), we obtain (see also Ref. 114)

$$\mathcal{F}_r[\rho_i]=\mathcal{F}_h[\rho_i]-\frac{1}{2\beta}\int d^3r_1\int d^3r_2\sum_{i,j}\rho_i(\mathbf{r}_1)\rho_j(\mathbf{r}_2)y_{h,ij}(\mathbf{r}_1,\mathbf{r}_2)\Delta f_{ij}(\mathbf{r}_1,\mathbf{r}_2)+\cdots\ , \tag{B11}$$

where

$$y_{h,ij}(\mathbf{r}_1,\mathbf{r}_2)=g^{(2)}_{h,ij}(\mathbf{r}_1,\mathbf{r}_2)e^{\beta w_{h,ij}(\mathbf{r}_1,\mathbf{r}_2)} . \tag{B12}$$

In the homogeneous case this reduces to

$$\beta f_r=\beta f_h-((\rho_A+\rho_B)^2/2) \times \sum_{i,j} x_i x_j \int d^3r\, y_{h,ij}(r)\Delta f_{ij}(r)+\cdots , \tag{B13}$$

with $x_i=\rho_i/(\rho_A+\rho_B)$. Following Weeks *et al.*[111,112] one chooses R_{ij} such that the term linear in Δf_{ij} in Eq. (B13) vanishes:[115]

$$\int d^3r\, y_{h,ij}(r)\Delta f_{ij}(r)=0 . \tag{B14}$$

Lee and Levesque[115] solved Eq. (B14) numerically for R_{ij} by using an improved version of the two-particle distribution function $g^{(2)}_{h,ij}$ for a binary mixture of hard spheres derived by Lebowitz,[64] whose solution is the basis of the Percus-Yevick theory in Sec. IV. [For the BEG model (Sec. III) all R_{ij} are equal so that in this case this effective diameter only enters into the absolute values of the number densities, which are unimportant for those wetting phenomena we are studyiing here (see Sec. II).] With negligible error they could represent their data as

$$R_{ij}=R^{\mathrm{BH}}_{ij}(1+\delta_{ij}) , \tag{B15}$$

where

$$R^{\mathrm{BH}}_{ij}=\int_0^\infty dr\{1-\exp[-\beta w_{r,ij}(r)]\} \tag{B16}$$

is the Barker-Henderson (BH) expression for the effective diameter.[116] R^{BH}_{ij} is a decreasing function of temperature which has been tabulated by Verlet and Weis[117] for $w_{r,ij}(r)$ given in Eq. (B2). In the temperature interval $0.65\le k_BT/\epsilon_{ij}\le 5.00$ R^{BH}_{ij} decreases from $1.031\sigma_{ij}$ to $0.947\sigma_{ij}$. δ_{ij} is, in addition, a function of the densities ρ_i. Since $|\delta_{ij}|$ is less than about 0.015 (Ref. 117) we shall ignore it. Furthermore, Eqs. (B15) and (B16) yield $R_{ij}=(R_{ii}+R_{jj})/2$ within an accuracy of 0.3%.[115]

Thus, for the reference system we use a mixture of hard spheres with diameters [Eq. (B16)],

$$R_A=R^{\mathrm{BH}}_{AA},\quad R_B=R^{\mathrm{BH}}_{BB},\quad R_{AB}=(R_A+R_B)/2 , \tag{B17}$$

which depend on $R^{(0)}_A=\sigma_{AA}$, k_BT/ϵ_{AA}, and $R^{(0)}_B=\sigma_{BB}$, k_BT/ϵ_{BB}, respectively. Due to Eq. (B16) the ratio of the diameters is given as

$$r=R_B/R_A=r_0\chi(k_BT/\epsilon_{AA};k_BT/\epsilon_{BB}) \tag{B18}$$

with $r_0=\sigma_{BB}/\sigma_{AA}$ and χ given by the ratio of the integrals in Eq. (B16) in reduced spatial units. [See also the second paragraph after Eq. (D6).]

APPENDIX C: BULK BEG MODEL

Equation (3.8) represents the variational grand canonical free-energy density. At the minimum with respect to $\bar{Q}$ and $\bar{M}$ it gives the grand canonical free energy:

$$G(H,\Delta,T)=T\left[\frac{Q+M}{2}\ln\left[\frac{Q+M}{2}\right]+\frac{Q-M}{2}\ln\left[\frac{Q-M}{2}\right]+(1-Q)\ln(1-Q)\right]-\tfrac{1}{2}(M^2+KQ^2+2CQM)-HM+\Delta Q \tag{C1}$$

with $G=\min_{\bar{Q},\bar{M}}(f2^{-1/2}R_A^3)$. According to the main text, all quantities in Eq. (C1) should carry a bar; in this appendix we omit this additional notation for reasons of clarity, but it should be kept in mind for translating the results of this appendix into unreduced quantities. In Eq. (C1) Q and M are function of H, Δ, and T which are given implicitly by the simultaneous solutions of the following two equations:[48–50]

$$H=\tfrac{1}{2}T\ln((Q+M)/(Q-M))-M-CQ , \tag{C2}$$

$$\Delta=T\ln(2(1-Q))-(T/2)\ln(Q^2-M^2)+CM+KQ . \tag{C3}$$

If Equations (C2) and (C3) are inserted into Eq. (C1) one obtains the function

$$Z(M,Q,T)=T\ln(1-Q)+\tfrac{1}{2}M^2+\tfrac{1}{2}KQ^2+CMQ , \tag{C4}$$

so that

$$G(H,\Delta,T)=Z(M=M(H,\Delta,T),Q=Q(H,\Delta,T),T) , \tag{C5}$$

where $M(H,\Delta,T)$ and $Q(H,\Delta,T)$ are the solutions of Eqs. (C2) and (C3). Critical points are determined most easily from a thermodynamic potential, which involves at least one density variable.[118] Following Ref. 49 we perform therefore a Legendre transform with respect to H:

$$\phi(M,\Delta,T)=G(H=H(M,\Delta,T),\Delta,T)+MH(M,\Delta,T) , \tag{C6}$$

where $H(M,\Delta,T)$ is given implicitly by

$$\partial G(H,\Delta,T)/\partial H=-M(H,\Delta,T)\rightarrow H(M,\Delta,T) . \tag{C7}$$

Note that

$$\partial G(H,\Delta,T)/\partial\Delta=Q(H,\Delta,T) , \tag{C8}$$

$$\partial\phi(M,\Delta,T)/\partial M=H(M,\Delta,T) , \tag{C9}$$

and

$$\partial\phi(M,\Delta,T)/\partial\Delta=Q(H=H(M,\Delta,T),\Delta,T) . \tag{C10}$$

Within the potential ϕ the critical points are given by the vanishing of its second and third derivative with respect to M, i.e.,

$$\partial H(M,\Delta,T)/\partial M=\partial^2 H(M,\Delta,T)/\partial M^2=0\ ,$$
$$\partial^3 H(M,\Delta,T)/\partial M^3>0\ . \tag{C11}$$

Equation (C11) describes the critical points of two phases correctly as long as neither the difference between the densities M in the two phases nor the difference between the densities Q in the two phases, which become critical, happen to vanish by reasons of symmetry. In our model this happens only in the exceptional case $C=0$ for which the values of Q in the two coalescing cases are the same. In this case one has to consider that potential which, in addition, is the Legendre transform with respect to Δ.[118] Since we consider the general case $C\neq 0$, Eq. (C11) remains valid. Equation (C11) involves derivatives of $H(M,\Delta,T)$. These derivatives can be expressed explicitly in terms of the functions $H(M,Q,T)$ and $\Delta(M,Q,T)$ given explicitly in Eqs. (C2) and (C3), respectively. Equation (C3) defines $Q(M,\Delta,T)$ implicitly so that

$$H(M,\Delta,T)=H(M,Q=Q(M,\Delta,T),T)\ , \tag{C12}$$

and

$$\left.\frac{\partial H(M,\Delta,T)}{\partial M}\right|_{\Delta,T}=\left.\frac{\partial H(M,Q,T)}{\partial M}\right|_{T,Q=Q(M,\Delta,T)}+\left.\frac{\partial H(M,Q,T)}{\partial Q}\right|_{T,Q=Q(M,\Delta,T)}\times\left.\frac{\partial Q(M,\Delta,T)}{\partial M}\right|_{\Delta,T}\ . \tag{C13}$$

If one now takes the explicit function $\Delta(M,Q,T)$ in Eq. (C3) one has the identity

$$\Delta=\Delta(M,Q=Q(M,\Delta,T),T)\ .$$

If this equation is differentiated with respect to M by keeping Δ fixed one obtains

$$0=\left.\frac{\partial\Delta(M,Q,T)}{\partial M}\right|_{T,Q=Q(M,\Delta,T)}+\left.\frac{\partial\Delta(M,Q,T)}{\partial Q}\right|_{T,Q(M,\Delta,T)}\times\left.\frac{\partial Q(M,\Delta,T)}{\partial M}\right|_{T,\Delta}\ , \tag{C14}$$

which is an equation for $\partial Q(M,\Delta,T)/\partial M$. The combination of Eqs. (C13) and (C14) finally leads to

$$\partial H(M,\Delta,T)/\partial M=X(M,Q=Q(M,\Delta,T),T) \tag{C15}$$

with $Q(M,\Delta,T)$ given implicitly by Eq. (C3) and with

$$X(M,Q,T)=\frac{\partial H}{\partial M}-\frac{\partial H}{\partial Q}\frac{\partial\Delta}{\partial M}\left[\frac{\partial\Delta}{\partial Q}\right]^{-1}\ , \tag{C16}$$

where $H\equiv H(M,Q,T)$ and $\Delta\equiv\Delta(M,Q,T)$ are given explicitly by Eqs. (C2) and (C3). Along the same lines one finds

$$\partial^2 H(M,\Delta,T)/\partial M^2=Y(M,Q=Q(M,\Delta,T),T) \tag{C17}$$

with

$$Y(M,Q,T)=\frac{\partial^2 H}{\partial M^2}-\frac{\partial^2 H}{\partial M\partial Q}\frac{\partial\Delta}{\partial M}\left[\frac{\partial\Delta}{\partial Q}\right]^{-1}-\frac{\partial H}{\partial Q}\frac{\partial^2\Delta}{\partial M^2}\left[\frac{\partial\Delta}{\partial Q}\right]^{-1}+\frac{\partial H}{\partial Q}\frac{\partial\Delta}{\partial M}\frac{\partial^2\Delta}{\partial Q\partial M}\left[\frac{\partial\Delta}{\partial Q}\right]^{-2}-\frac{\partial^2 H}{\partial M\partial Q}\frac{\partial\Delta}{\partial M}\left[\frac{\partial\Delta}{\partial Q}\right]^{-1}$$
$$-\frac{\partial^2 H}{\partial Q^2}\left[\frac{\partial\Delta}{\partial M}\right]^2\left[\frac{\partial\Delta}{\partial Q}\right]^{-2}+\frac{\partial H}{\partial Q}\frac{\partial\Delta}{\partial M}\frac{\partial^2\Delta}{\partial M\partial Q}\left[\frac{\partial\Delta}{\partial Q}\right]^{-2}-\frac{\partial H}{\partial Q}\frac{\partial^2\Delta}{\partial Q^2}\left[\frac{\partial\Delta}{\partial M}\right]^2\left[\frac{\partial\Delta}{\partial Q}\right]^{-3}\ . \tag{C18}$$

Now it is straightforward, but tedious, to obtain the functions $X(M,Q,T)$ and $Y(M,Q,T)$, whose lengthy expressions we refrain to write down explicitly.

As explained in the main text, we need the densities $M_\alpha(T_{\rm cep})=M_\beta(T_{\rm cep})$, $Q_\alpha(T_{\rm cep})=Q_\beta(T_{\rm cep})$, $M_\gamma(T_{\rm cep})$, and $Q_\gamma(T_{\rm cep})$ at the critical end point $T_{\rm cep}$. At $T_{\rm cep}$ Eq. (C11) must be fulfilled, since it is a critical point, and H,Δ as well as the pressure $p=-G(H,\Delta,T)$ must be the same in both the critical phase $\alpha=\beta$ and the vapor phase γ. Thus, we end up with a system of five coupled nonlinear equations for M_α, Q_α, M_γ, Q_γ, and $T_{\rm cep}$:

$$\begin{aligned}
&X(M_\alpha,Q_\alpha,T_{\rm cep})=0\ ,\\
&Y(M_\alpha,Q_\alpha,T_{\rm cep})=0\ ,\\
&Z(M_\alpha,Q_\alpha,T_{\rm cep})=Z(M_\gamma,Q_\gamma,T_{\rm cep})\ ,\\
&H(M_\alpha,Q_\alpha,T_{\rm cep})=H(M_\gamma,Q_\gamma,T_{\rm cep})\ ,\\
&\Delta(M_\alpha,Q_\alpha,T_{\rm cep})=\Delta(M_\gamma,Q_\gamma,T_{\rm cep})\ .
\end{aligned} \tag{C19}$$

The functions X, Y, Z, H, and Δ are given explicitly by Eqs. (C16), (C18), and (C2)–(C4). We solved Eq. (C19) numerically by iterating suitable initial guesses. Equation (C19) depends on the two dimensionless parameters K and C (recall that they are identical to $\bar{K}=\hat{K}/\hat{J}$ and $\hat{C}=\hat{C}/\hat{J}$, respectively, in the main text). We scanned the solutions of Eq. (C19) within that two-dimensional region in (K,C) space in which the BEG model leads to a simple bulk phase diagram by using a grid with $\delta K=0.1$ and $\delta C=0.1$.

The solutions of Eq. (C19) determine $\lambda_{\beta\gamma}$ [see Eqs. (2.11) and (2.23)]. In order to evaluate E_A and E_B [see Eqs. (2.21) and (2.22)] we also need $\lambda_{\alpha\beta}$ [see Eqs. (2.10) and (2.23)]. Since along the triple line both $M_\alpha-M_\beta$ and $Q_\alpha-Q_\beta$ vanish for $\tau=(T_{\rm cep}-T)/T_{\rm cep}\to 0$, one has

$$M_\alpha-M_\beta=\kappa_M\tau^\beta(1+\delta_M(\tau))\ , \tag{C20}$$

and

$$Q_\alpha - Q_\beta = \kappa_Q \tau^\beta (1+\delta_Q(\tau)) , \tag{C21}$$

where β is the critical exponent of the order parameter and $\delta_M(0)=\delta_Q(0)=0$. Therefore, $\lambda_{\alpha\beta}$ is given by the amplitude ratio

$$\lambda_{\alpha\beta} = \kappa_M / \kappa_Q . \tag{C22}$$

In a straightforward calculation one would have to follow both $M_\alpha - M_\beta$ and $Q_\alpha - Q_\beta$ along the triple line for each value of K and C in order to determine $\lambda_{\alpha\beta}$ by taking the limit $\tilde{\lambda}_{\alpha\beta}(\tau \to 0)$. This would require us to determine a whole piece of the triple line for each of the parameters. In practice this would amount to an enormous numerical effort. Therefore, it is very convenient that $\lambda_{\alpha\beta}$ can be expressed explicitly in terms of $M_\alpha(T_{\rm cep})$, $Q_\alpha(T_{\rm cep})$, and $T_{\rm cep}$ which are already known from the solution of Eq. (C19).

In order to derive this relationship let us consider one fixed critical point T_c on L_2 in Fig. 1, which we approach along an arbitrary path on S_2 (see Fig. 1). The thermodynamic states along this path are characterized uniquely by (M_α, Q_α, T) on the α-phase side of this path and by (M_β, Q_β, T) on the opposite side whereby $M_\kappa \to M_c$, $Q_\kappa \to Q_c$, and $T \to T_c$ for $\kappa = \alpha, \beta$. Since we are at two-phase coexistence we have, along this path [see Eq. (C2)],

$$H(M_\alpha, Q_\alpha, T) = H(M_\beta, Q_\beta, T) . \tag{C23}$$

We can now expand the function $H(M,Q,T)$ around (M_c, Q_c, T_c):

$$H(M_\kappa,Q_\kappa,T) = H(M_c,Q_c,T_c) + \left.\frac{\partial H(M,Q,T)}{\partial M}\right|_{M_c,Q_c,T_c} \times (M_\kappa - M_c) + \left.\frac{\partial H(M,Q,T)}{\partial Q}\right|_{M_c,Q_c,T_c} \times (Q_\kappa - Q_c) + \left.\frac{\partial H(M,Q,T)}{\partial T}\right|_{M_c,Q_c,T_c} \times (T - T_c) + \cdots . \tag{C24}$$

Combining Eqs. (C23) and (C24) we arrive at

$$\lambda_{\alpha\beta} = -\left.\frac{\partial H(M,Q,T)}{\partial Q}\right|_{M_c,Q_c,T_c} \times \left[\left.\frac{\partial H(M,Q,T)}{\partial M}\right|_{M_c,Q_c,T_c}\right]^{-1} = \frac{T_c M_c + C(Q_c^2 - M_c^2)}{T_c Q_c - (Q_c^2 - M_c^2)} . \tag{C25}$$

Equation (C25) shows that $\lambda_{\alpha\beta}$ is independent from the choice for the path approaching the critical point. Thus, we can choose the triple line as a particular path for approaching the particular critical point $T_c = T_{\rm cep}$. For a few values of K and C we also tested Eq. (C25) numerically.

Thus, the numerical solutions of Eq. (C19) determine E_A and E_B which in turn determine $\mathrm{sgn}[a(T \to T_{\rm cep})]$ [see Eqs. (2.17)–(2.22)]. Therefore, we are in the position to check the condition $a(T_{\rm cep}) = 0^+$ throughout the parameter space (K,C). It is sufficient to look at $C > 0$ because the grand canonical free energy is invariant under the transformation $C \to -C$, $K \to K$, $M \to -M$, $Q \to Q$, $H \to -H$, and $\Delta \to \Delta$ [see Eqs. (C2)–(C5)]. Therefore, we have [Eqs. (2.10), (2.11), and (2.23)]

$$\lambda_{\alpha\beta}(K,-C) = -\lambda_{\alpha\beta}(K,C) , \tag{C26}$$

and

$$\lambda_{\beta\gamma}(K,-C) = -\lambda_{\beta\gamma}(K,C) . \tag{C27}$$

As a consequence $|\lambda_{\kappa,\kappa'}(K, C=0)|$ is either zero or infinite.

The grand canonical free energy of the BEG model is not only invariant against interchanging A with B, but also against interchanging B particles with the vacuum. This means that under the transformation

$$\begin{aligned} J &= (J' + K' + 2C')/4 , \\ K &= (9J' + K' - 6C')/4 , \\ C &= (3J' - K' + 2C')/4 , \\ H &= (-J' + K' + H' - \Delta')/2 , \\ \Delta &= (3J' + K' - 4C' - 3H' - \Delta')/2 , \end{aligned} \tag{C28}$$

the densities are transformed according to

$$Q = 1 - (Q' - M')/2, \quad M = -1 + (3Q' + M')/2 . \tag{C29}$$

[The inverse transformation is just given by interchanging the primed and unprimed quantities in Eq. (C28).] Equation (C29) means that $\rho_A = \rho'_A$ and $\rho_B = 1 - (\rho'_A + \rho'_B)$. [The transformation $\rho_B = \rho'_B$ and $\rho_A = 1 - (\rho'_A + \rho'_B)$ gives rise to still another transformation which leaves the free-energy invariant, but which we do not consider here.] It is straightforward to check that under the transformation given in Eq. (C28) the line $\bar{C} = (\bar{K} - 3)/2$ is mapped onto the line $\bar{C}' = 0$. (Here we used $\bar{C} = C/J$, etc.) On the other hand, we have under this transformation

$$\tilde{\lambda}_{\alpha\beta} = \frac{M_\alpha - M_\beta}{Q_\alpha - Q_\beta} = \frac{3(Q'_\alpha - Q'_\beta) + M'_\alpha - M'_\beta}{Q'_\beta - Q'_\alpha + M'_\alpha - M'_\beta} , \tag{C30}$$

where the transformed densities correspond to a system with J', K', C', H', and Δ'. If this system is given by $C' = 0$ one has by symmetry $Q'_\alpha = Q'_\beta$. In this case the last term in Eq. (C30) reduces to 1. This means that

$$\lambda_{\alpha\beta} = 1 \quad \text{for } \bar{C} = (\bar{K} - 3)/2 . \tag{C31}$$

$\overline{A_1D_b}$ in Fig. 7 is a segment of the line $\bar{C}=(\bar{K}-3)/2$, so that there $\lambda_{\alpha\beta}=1$ and, by symmetry, $\lambda_{\alpha\beta}=-1$ on $\overline{A_2D_a}$. This provides a useful check for the numerical calculation of $\lambda_{\alpha\beta}$.

APPENDIX D: BULK PY MODEL

According to Appendix C all quantities of interest to us in the present context [Eq. (C19) and the first equation in (C25)] are obtained from three functions: $H(M,Q,T)$, $\Delta(M,Q,T)$, and $Z(M,Q,T)=-p(M,Q,T)$ [see Eqs. (C2)–(C5), (C16), and (C18)]. Using Eqs. (2.4), (2.5), (3.2), (3.3), (3.9)–(3.11), and (4.5), we find

$$Z(M,Q,T)=-Tp_h(M,Q)+\tfrac{1}{2}M^2+\tfrac{1}{2}KQ^2+CMQ\ , \tag{D1}$$

where

$$p_h(M,Q)=\left[Q(1+d_3+d_3^2)-\frac{\pi}{4\sqrt{2}}\gamma_1^2(Q^2-M^2)(\alpha_1+d_2r)\right](1-d_3)^{-3} \tag{D2}$$

with

$$d_k=\frac{\pi}{6\sqrt{2}}(\alpha_kQ+\gamma_kM) \tag{D3}$$

and ($r=R_B/R_A$),

$$\alpha_k=1+r^k,\quad \gamma_k=1-r^k,\quad k=1,2,3\ . \tag{D4}$$

Equations (D1)–(D3) are written in reduced units so that all quantities therein should carry a bar. For reasons of clarity we omit all bars throughout Appendix D as we did in most of the parts of Appendix C. The corresponding equation for the unreduced quantities can be retrieved from Eqs. (D1)–(D3) by performing the following replacements there: $-Z=p\to 2^{-1/2}R_A^3p/\hat{J}$, $T\to k_BT/\hat{J}$, $K\to\hat{K}/\hat{J}$, $C\to\hat{C}/\hat{J}$, $M\to 2^{-1/2}R_A^3M$, $Q\to 2^{-1/2}R_A^3Q$. Similarly, in the following equations for H and Δ one would have to replace H by $H/\hat{J}$ and Δ by $\Delta/\hat{J}$:

$$H=T\left[\tfrac{1}{2}\ln((Q+M)/(Q-M))-3\gamma_1\gamma_2/\gamma_3+3\left[\gamma_1\gamma_2/\gamma_3+\frac{\pi}{6\sqrt{2}}Q(\gamma_3-\alpha_3\gamma_1\gamma_2/\gamma_3)\right](1-d_3)^{-1}+\tfrac{9}{4}\gamma_2d_2^2(1-d_3)^{-2}+\frac{\pi}{6\sqrt{2}}\gamma_3p_h(M,Q)\right]-M-CQ\ , \tag{D5}$$

$$\Delta=T\left[-\tfrac{1}{2}\ln(Q^2-M^2)+\ln(1-d_3)+3-3\left[1+\frac{\pi}{6\sqrt{2}}Q(\alpha_1\alpha_2-\alpha_3)\right](1-d_3)^{-1}-\tfrac{9}{4}\alpha_2d_2^2(1-d_3)^{-2}-\frac{\pi}{6\sqrt{2}}\alpha_3p_h(M,Q)\right]+CM+KQ\ . \tag{D6}$$

Here we used the relation $\alpha_1\gamma_2+\alpha_2\gamma_1=2\gamma_3$.

The comparison between Eqs. (C2)–(C4) and Eqs. (D1)–(D6) shows that, as it should be, in the low-density limit $Q,M\to 0$ the reference contributions of the functions $Z_{\rm PY}$, $H_{\rm PY}$, and $\Delta_{\rm PY}$ reduce in leading order to their counterparts in $Z_{\rm BEG}$, $H_{\rm BEG}$, and $\Delta_{\rm BEG}$; the contributions from the attractive interactions are identical. This also shows that, as expected, the effect of different sizes of the particles vanishes in the low-density limit. Therefore, our results derived for the BEG model remain reliable as long as the involved densities are not too high. Note that for $r=1$ we have $H_{\rm BEG}=H_{\rm PY}$ so that in this case the two models differ only with respect to Δ and p.

The ratio r of the diameters, which enters into Eqs. (D1), (D5), and (D6) is given by Eq. (B18). It depends on r_0, $k_BT/\hat{J}$, $\hat{K}/\hat{J}$, and at $T_{\rm cep}$ on r_0, $\hat{K}/\hat{J}$, and $\hat{C}/\hat{J}$. Since both R_A and R_B are increasing functions of temperature their ratio r exhibits a weaker dependence on temperature than R_A and R_B themselves. We exploit this fact by approximating r by r_0 but keeping the temperature dependence of R_A. This good approximation eases the scan through the whole parameter space $\hat{K}/\hat{J}$ and $\hat{C}/\hat{J}$ considerably. Thus, in our numerical results presented in Sec. IV, we have identified r with r_0.

Finally, let us note that the solution of the generalized Percus-Yevick equations gives the direct correlation function $c_{ij}^{(2)}(\mathbf{r}_1-\mathbf{r}_2)$ [see Eq. (A21)] or the pair correlation function $h_{ij}(\mathbf{r}_1-\mathbf{r}_2)$ of the reference system. The pressure can be obtained from these functions either by the virial theorem or by the compressibility relation.[64,67] If these functions would be known exactly, the two relations would yield the same result; however, within the Percus-Yevick approximation they do not. The formulas we use in our paper are based on the compressibility relation:[64,67]

$$1-\sum_i\rho_ic_{ij}^{(2)}(\mathbf{q}=0)=\frac{\partial p_h}{\partial\rho_j}/(k_BT)\ ,\qquad \rho_ic_{ij}^{(2)}(\mathbf{q}=0)=\delta_{ij}-\rho_i\frac{\partial\mu_{h,i}}{\partial\rho_j}/(k_BT)\ , \tag{D7}$$

where $c_{ij}^{(2)}(\mathbf{q})$ is the Fourier transform of $c_{ij}^{(2)}(\mathbf{r}_1-\mathbf{r}_2)$. The reference free energy follows from p_h and $\mu_{h,i}$ according to Eq. (4.2). After the elimination of $c_{ij}^{(2)}(\mathbf{q}=0)$ Eq. (D7) provides the following relations between the basic functions Z, H, and Δ [see Eqs. (D1), (D5), and (D6)]:

$$\frac{\partial Z}{\partial Q}=Q\frac{\partial \Delta}{\partial Q}-M\frac{\partial H}{\partial Q}\ ,$$
$$\frac{\partial Z}{\partial M}=Q\frac{\partial \Delta}{\partial M}-M\frac{\partial H}{\partial M}\ . \tag{D8}$$

Equation (D8) provides a useful test for the correctness of the numerical analysis.

---

*Author to whom correspondence should be addressed.

[1]S. Dietrich, in *Phase Transitions and Critical Phenomena,* edited by C. Domb and J. L. Lebowitz (Academic, London, 1988), Vol. 12, p. 1.

[2]J. S. Rowlinson and B. Widom, *Molecular Theory of Capillarity* (Clarendon, Oxford, 1982).

[3]R. Pandit, M. Schick, and M. Wortis, Phys. Rev. B **26**, 5112 (1982).

[4]E. H. Hauge, in *Fundamental Problems in Statistical Mechanics VI,* edited by E. G. D. Cohen (North-Holland, Amsterdam, 1985), p. 65.

[5]M. Wortis, in *Fundamental Problems in Statistical Mechanics VI,* edited by E. G. D. Cohen (North-Holland, Amsterdam, 1985), p. 87.

[6]G. P. de Gennes, Rev. Mod. Phys. **57**, 827 (1985).

[7]D. E. Sullivan and M. M. Telo da Gama, in *Fluid Interfacial Phenomena,* edited by C. A. Croxton (Wiley, New York, 1986), p. 45.

[8]M. Schick, in *Liquids at Interfaces,* Proceedings of the Les Houches Summer School Lectures, Session XLVIII (North-Holland, Amsterdam, 1989).

[9]S. Dietrich and M. Schick, Phys. Rev. B **33**, 4952 (1986).

[10]W. A. Curtin and N. W. Ashcroft, Phys. Rev. Lett. **56**, 2775 (1986).

[11]D. W. Pohl and W. I. Goldburg, Phys. Rev. Lett. **48**, 185 (1982).

[12]D. Beysens and D. Estéve, Phys. Rev. Lett. **54**, 2123 (1985).

[13]L. Sigl and W. Fenzl, Phys. Rev. Lett. **57**, 2191 (1986).

[14]X. Wu, M. Schlossman, and C. Franck, Phys. Rev. B **33**, 402 (1986).

[15]K. Abeysuriya, X. Wu, and C. Franck, Phys. Rev. B **35**, 6771 (1987).

[16]D. J. Durian and C. Franck, Phys. Rev. Lett. **59**, 555 (1987).

[17]D. J. Durian and C. Franck, Phys. Rev. B **36**, 7307 (1987).

[18]D. E. Sullivan, J. Chem. Phys. **77**, 2632 (1982).

[19]M. M. Telo da Gama and R. Evans, Mol. Phys. **48**, 687 (1983).

[20]I. Hadjiagapiou and R. Evans, Mol. Phys. **54**, 383 (1985).

[21]S. Dietrich, M. P. Nightingale, and M. Schick, Phys. Rev. B **32**, 3182 (1985).

[22]R. B. Heady and J. W. Cahn, J. Chem. Phys. **58**, 896 (1973).

[23]M. R. Moldover and J. W. Cahn, Science **207**, 1073 (1980).

[24]O'D. Kwon, D. Beaglehole, W. W. Webb, B. Widom, J. W. Schmidt, J. W. Cahn, M. R. Moldover, and B. Stephenson, Phys. Rev. Lett. **48**, 185 (1982).

[25]D. Beaglehole, J. Phys. Chem. **87**, 4749 (1983).

[26]J. W. Schmidt and M. R. Moldover, J. Chem. Phys. **79**, 379 (1983).

[27]V. Vani, S. Guha, E. S. R. Gopal, and S. M. Rao, Phys. Lett. **99A**, 441 (1983).

[28]M. R. Moldover and J. W. Schmidt, Physica **12D**, 351 (1984).

[29]C. Houessou, P. Guenoun, R. Gastaud, F. Perrot, and D. Beysens, Phys. Rev. A **32**, 1818 (1985).

[30]S. Chatterjee, V. Vani, S. Guha, and E. S. R. Gopal, J. Phys. (Paris) **46**, 1533 (1985).

[31]J. W. Schmidt and M. R. Moldover, J. Chem. Phys. **84**, 4563 (1986).

[32]J. Gracia, C. Guerrero, J. G. Llanes, and A. Robledo, J. Phys. Chem. **90**, 1350 (1986).

[33]F. Guzman and J. W. Schmidt, J. Phys. Chem. **91**, 263 (1987).

[34]J. W. Schmidt, J. Colloid Interface Sci. **122**, 575 (1988).

[35]M. Kahlweit, G. Busse, D. Haase, and J. Jen, Phys. Rev. A **38**, 1395 (1988).

[36]P. Tarazona, M. M. Telo da Gama, and R. Evans, Mol. Phys. **49**, 283 (1983).

[37]P. Tarazona, M. M. Telo da Gama, and R. Evans, Mol. Phys. **49**, 301 (1983).

[38]P. Tarazona, R. Evans, and U. M. B. Marconi, Mol. Phys. **54**, 1357 (1985).

[39]M. M. Telo da Gama and R. Evans, Mol. Phys. **48**, 229 (1983); **48**, 251 (1983).

[40]M. Napiórkowski and S. Dietrich, Phys. Rev. B **34**, 6469 (1986).

[41]We are grateful to Dr. W. Fenzl for pointing out this possibility to us.

[42]R. Evans, Adv. Phys. **28**, 143 (1979).

[43]Here we have changed the notation compared with Refs. 1 and 9, where this quantity has been denoted as $\bar{w}_{ij}$. In *this* paper, in order to have a common notation compared with other quantities, we define $\bar{w}_{ij}=\hat{w}_{ij}/\hat{w}_{AB}$.

[44]J. N. Israelachvili, *Intermolecular and Surface Forces* (Academic, London, 1985).

[45]R. F. Kayser, J. W. Schmidt, and M. R. Moldover, Phys. Rev. Lett. **54**, 707 (1985).

[46]B. M. Law, Phys. Rev. B **32**, 5987 (1985).

[47]B. M. Law, Phys. Rev. B **32**, 5996 (1985).

[48]M. Blume, V. Emery, and R. B. Griffiths, Phys. Rev. A **4**, 1071 (1971).

[49]D. Mukamel and M. Blume, Phys. Rev. A **10**, 610 (1974).

[50]D. Furman, S. Dattagupta, and R. B. Griffiths, Phys. Rev. B **15**, 441 (1977).

[51]W. Selke and J. Yeomans, J. Phys. A **16**, 2789 (1983).

[52]W. Selke, Surf. Sci. **144**, 176 (1984).

[53]W. Selke, in *Lecture Notes in Physics,* edited by A. Pekalski and J. Sznajd (Springer, Berlin, 1984), Vol. 206, p. 191.

[54]W. Selke, in *Phase Transformations in Solids,* edited by T. Tsakalakos (North-Holland, Amsterdam, 1984), p. 3.

[55]W. Selke, D. A. Huse, and D. M. Kroll, J. Phys. A **17**, 3019 (1984).

[56]P. Upton and J. Yeomans, J. Phys. A **20**, 2989 (1987).

[57]J. Bricmont and J. L. Lebowitz, J. Stat. Phys. **46**, 1015 (1987).

[58]J. W. Cahn, J. Chem. Phys. **66**, 3667 (1977).

[59]M. P. Nightingale and J. O. Indekeu, Phys. Rev. B **32**, 3364 (1985).

[60]C. Ebner, W. F. Saam, and A. K. Sen, Phys. Rev. B **32**, 1558 (1985).

[61]C. Ebner and W. F. Saam, Phys. Rev. B **35**, 1822 (1987).

[62]C. Ebner and W. F. Saam, Phys. Rev. Lett. **58**, 587 (1987).

[63]C. Ebner and W. F. Saam, Phys. Rev. B **37**, 5252 (1988).

[64]J. L. Lebowitz, Phys. Rev. **133**, A895 (1964).
[65]J. L. Lebowitz, E. Helfand, and E. Praestgaard, J. Chem. Phys. **43**, 774 (1965).
[66]H. L. Frisch and J. L. Lebowitz, *The Equilibrium Theory of Classical Fluids* (Benjamin, New York, 1964), p. II–300.
[67]J. L. Lebowitz and E. M. Waisman, in *The Liquid State of Matter: Fluids, Simple and Complex*, edited by E. W. Montroll and J. L. Lebowitz (North-Holland, Amsterdam, 1982), p. 1.
[68]R. Lipowsky, Phys. Rev. B **32**, 1731 (1985).
[69]R. F. Kayser, M. R. Moldover, and J. W. Schmidt, J. Chem. Soc., Faraday Trans. II, **82**, 1701 (1986).
[70]C. H. Chen, P. E. Siska, and Y. T. Lee, J. Chem. Phys. **59**, 601 (1973).
[71]C. Y. Ng, Y. T. Lee, and J. A. Barker, J. Chem. Phys. **61**, 1996 (1974).
[72]B. E. F. Fender and G. D. Halsey, J. Chem. Phys. **36**, 1881 (1962).
[73]J. A. Barker, in *Rare Gas Solids*, edited by M. L. Klein and J. A. Venables (Academic, New York, 1976), Vol. 1, Chap. 4.
[74]J. A. Barker and D. Henderson, Rev. Mod. Phys. **48**, 587 (1976).
[75]G. C. Maitland, M. Rigby, E. B. Smith, and W. A. Wakeham, *Intermolecular Forces* (Clarendon, Oxford, 1981).
[76]C. G. Gray and K. E. Gubbbins, *Theory of Molecular Fluids* (Clarendon, Oxford, 1982), Vols. 1 and 2.
[77]N. Bernardes, Phys. Rev. **112**, 1534 (1958).
[78]R. A. Aziz and H. H. Chen, J. Chem. Phys. **67**, 5719 (1977).
[79]R. A. Aziz, Mol. Phys. **38**, 177 (1979).
[80]R. A. Aziz, V. P. S. Nain, J. S. Carley, W. L. Taylor, and G. T. McConville, J. Chem. Phys. **70**, 4330 (1979).
[81]R. A. Aziz, P. W. Riley, U. Buck, G. Maneke, J. Schleusener, G. Scoles, and U. Valbusa, J. Chem. Phys. **71**, 2637 (1979).
[82]R. A. Aziz and A. van Dalen, J. Chem. Phys. **78**, 2402 (1983).
[83]R. A. Aziz and A. van Dalen, J. Chem. Phys. **78**, 2413 (1983).
[84]R. A. Aziz and A. van Dalen, J. Chem. Phys. **81**, 779 (1984).
[85]R. A. Aziz and M. J. Slaman, Mol. Phys. **58**, 679 (1986).
[86]J. S. Rowlinson and F. L. Swinton, *Liquids and Liquid Mixtures* (Butterworth, London, 1982).
[87]J. A. Schouten, A. Deerenberg, and N. J. Trappeniers, Physica **81A**, 151 (1975).
[88]R. L. Scott and P. H. van Konynenburg, Discuss. Faraday Soc. **49**, 87 (1970).
[89]P. H. van Konynenburg and R. L. Scott, Philos. Trans. R. Soc. London, Ser. A **298**, 495 (1980).
[90]J. de Swaan Arons and G. A. M. Diepen, J. Chem. Phys. **44**, 2322 (1966).
[91]W. B. Streett and J. L. E. Hill, J. Chem. Phys. **54**, 5088 (1971).
[92]N. J. Trappeniers and J. A. Schouten, Physica **73**, 539 (1974).
[93]N. J. Trappeniers and J. A. Schouten, Physica **73**, 546 (1974).
[94]A. Deerenberg, J. A. Schouten, and N. J. Trappeniers, Physica **101A**, 459 (1980).
[95]A. Deerenberg, J. A. Schouten, and N. J. Trappeniers, Physica **103A**, 183 (1980).
[96]L. C. van den Bergh, J. A. Schouten, and N. J. Trappeniers, Physica **132A**, 537 (1985).
[97]L. C. van den Bergh, J. A. Schouten, and N. J. Trappeniers, Physica **132A**, 549 (1985).
[98]D. Furman and R. B. Griffiths, Phys. Rev. A **17**, 1139 (1978).
[99]J. I. Frenkel, *Kinetische Theorie der Flüssigkeiten* (Deutscher Verlag der Wissenschaften, Berlin, 1957), Chap. VI.
[100]S. Chatterjee and E. S. R. Gopal, J. Phys. (Paris) **49**, 675 (1988).
[101]L. V. Mikheev, Phys. Lett. A **129**, 245 (1988).
[102]J. L. Harden and R. F. Kayser, J. Colloid Interface Sci. **127**, 548 (1989).
[103]S. Dietrich (unpublished).
[104]M. P. Nightingale, W. F. Saam, and M. Schick, Phys. Rev. Lett. **51**, 1275 (1983).
[105]D. S. Fisher and D. A. Huse, Phys. Rev. B **32**, 274 (1985).
[106]Note, however, that resorting to a solid-on-solid model in order to unfreeze capillary waves and thus to improve the MFT density functional result has been questioned by R. Evans, Mol. Phys. **42**, 1169 (1981), in an analysis of the free interface.
[107]P. Fulde and H. Wagner, Phys. Rev. Lett. **27**, 1280 (1971).
[108]B. H. Wells and S. Wilson, Mol. Phys. **55**, 199 (1985).
[109]B. H. Wells, Mol. Phys. **61**, 1283 (1987).
[110]L. Reatto and M. Tau, J. Chem. Phys. **86**, 6474 (1987).
[111]J. D. Weeks, D. Chandler, and H. C. Anderson, J. Chem. Phys. **54**, 5237 (1971).
[112]H. C. Anderson, J. D. Weeks, and D. Chandler, Phys. Rev. A **4**, 1597 (1971).
[113]J. P. Hansen and I. R. McDonald, *Theory of Simple Liquids* (Academic, London, 1986).
[114]M. M. Telo da Gama and R. Evans, Mol. Phys. **41**, 1091 (1980).
[115]L. L. Lee and D. Levesque, Mol. Phys. **26**, 1351 (1973).
[116]J. A. Barker and D. Henderson, J. Chem. Phys. **47**, 4714 (1967).
[117]L. Verlet and J.-J. Weis, Phys. Rev. A **5**, 939 (1972).
[118]J. T. Bartis, J. Chem. Phys. **59**, 5423 (1973).